

INFLUENCE OF GASEOUS HYDROGEN ON METALS
FINAL REPORT

BY
R. J. WALTER AND
W. T. CHANDLER

ROCKETDYNE
A DIVISION OF ROCKWELL INTERNATIONAL
CANOGA PARK, CALIFORNIA

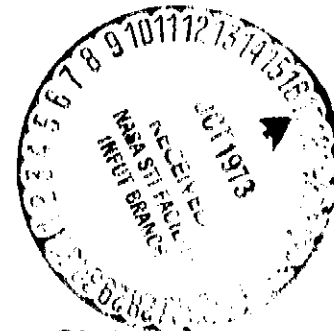
PREPARED FOR

NATIONAL AERONAUTICS AND SPACE ADMINISTRATION
GEORGE C. MARSHALL SPACE FLIGHT CENTER
MARSHALL SPACE FLIGHT CENTER, ALABAMA 35812

(NASA-CR-124410) INFLUENCE OF GASEOUS
HYDROGEN ON METALS Final Report
(Rocketdyne) 169 p HC \$10.50 CSCL 11F

N73-32428

Unclas
G3/17 18352



INFLUENCE OF GASEOUS HYDROGEN
ON METALS

FINAL REPORT

by

R. J. Walter and
W. T. Chandler

Prepared for
George C. Marshall Space Flight Center
Marshall Space Flight Center
Alabama 35812

October 1973

Contract NAS8-25579

Advanced Programs
Rocketdyne
A Division of Rockwell International
Canoga Park, California

PRECEDING PAGE BLANK NOT FILMED

FOREWORD

This final report was prepared by the Advanced Programs Department of Rocketdyne Division of Rockwell International, in compliance with National Aeronautics and Space Administration Contract NAS8-25579, and covers the period from 5 May 1970 through 5 August 1973. The majority of the work was sponsored by the George C. Marshall Space Flight Center, Alabama, with Mr. W. B. McPherson acting as Project Monitor. One phase was sponsored by the Naval Ship Research and Development Center, Annapolis, Maryland, with Mr. John Gudas acting as Project Monitor. Mr. L. P. Combs and Mr. T. A. Coultas were Rocketdyne Program Managers.

Acknowledgement is gratefully given to the following personnel for their contributions to this investigation:

Rocketdyne Division, Rockwell International

E. A. Burowick	Set Up of Acoustic Emission Apparatus
G. E. Dyer	Performance of Most of the Testing
H. G. Hayes	Set Up of K_{TH} Test Apparatus and Performance of Initial Testing
G. L. Heslington	Assistance in Performing Calculations
A. J. Jacobs	Responsible for Acoustic Emission Monitoring of Crack Growth
R. P. Jewett	Helpful Technical Discussions
D. A. Pearson	Assistance with K_{TH} Measurements
J. Testa	Metallography

Space Division, Rockwell International

R. J. Demonet and J. E. Collipriest, Jr.	Compliance Calibration of HY100
---	---------------------------------

B-1 Division, Rockwell International

C. A. Moore	Precracking of Fracture Mechanics Specimen
-------------	--

Science Center, Rockwell International

J. D. Frandsen	Provided Scanning Electron Fractographs of Inconel 718
----------------	--

Ames Research Center, National Aeronautics and Space Administration

D. P. Williams	Provided Scanning Electron Fractographs of Inconel 718
----------------	--

ABSTRACT

Tensile, fracture toughness (K_{IC}), threshold stress intensity for sustained-load crack growth (K_{TH}), and cyclic and sustained load crack growth rate measurements were performed on a number of alloys in high-pressure hydrogen and helium environments. The results of tensile tests performed in 34.5 MN/m^2 (5000 psi) hydrogen indicated that Inconel 625 was considerably embrittled at ambient temperature but was not embrittled at 144 K (-200 F). The tensile properties of AISI 321 stainless steel were slightly reduced at ambient temperature and 144 K (-200 F). The tensile properties of Ti-5Al-2.5 Sn ELI were essentially unaffected by hydrogen at 144 K (-200 F). OFHC copper was not embrittled by hydrogen at ambient temperature or at 144 K (-200 F).

Threshold stress intensity (K_{TH}) measurements were performed on Inconel 718 (in two heat treatment conditions), Inconel 625, AISI 321 stainless steel, A-286 stainless steel, Ti-5Al-2.5 Sn ELI, 2219-T87 Al alloy, and OFHC copper. The tests were performed at ambient temperature and 144 K (-200 F) in 34.5 MN/m^2 (5000 psi) hydrogen and helium environments and were monitored by acoustic emission. Sustained load, hydrogen-induced crack growth occurred in Inconel 718, Ti-5Al-2.5 Sn ELI and in A-286 stainless steel. No influence of hydrogen was noted on crack propagation in 2219-T87 aluminum and in OFHC copper. The acoustic emission data indicated that crack growth occurred discontinuously and at irregular time intervals.

Embrittlement of notched Inconel 718 tensile specimens by 34.5 MN/m^2 (5000 psi) hydrogen at ambient temperature was found to vary considerably with condition. Reduction of notch tensile properties was least for Inconel 718 with a very fine grain size, moderate for a coarse-grained material after a 1325, 1033-922 K (1925, 1400-1200 F) heat treatment and most severe for a coarse-grained material after a 1214, 991-894 K (1725, 1325-1150 F) heat treatment. Embrittlement appeared to correlate with grain size and the presence of a nearly continuous precipitate identified as Ni_3Cb . The weld metal and the heat-affected

zone of Inconel 718 welds were more embrittled by hydrogen than was the parent metal. Fracture mechanics tests gave K_{TH} values for coarse-grained Inconel 718 in 34.5 MN/m^2 (5000 psi) hydrogen at ambient temperatures of approximately $14 \text{ MN/m}^2 \sqrt{\text{m}}$ (13 ksi $\sqrt{\text{in.}}$) for the 1214, 991-894 K (1725, 1325-1150 °F) heat treatment condition; and $42 \text{ MN/m}^2 \sqrt{\text{m}}$ (38 ksi $\sqrt{\text{in.}}$) for the 1325, 1033-922 K (1925, 1400-1200 °F) heat treatment condition.

K_{TH} for sustained load crack growth in Inconel 718 exposed to hydrogen was apparently independent of temperature between ambient and 200 K (-100 °F). The cyclic crack growth rate in Inconel 718 increased with increasing hydrogen pressure, and was a complex function of cyclic rate. The influence of hydrogen on the cyclic crack growth rate of Inconel 718 decreased appreciably from ambient to 200 K (-100 °F).

The ambient temperature cyclic crack growth rates in HY100 and ASTM A-533-B steels were approximately 20 times greater in hydrogen than in helium over a wide range of stress intensities at pressures of 51.7 MN/m^2 (7500 psi) for HY100 and 103.4 MN/m^2 (15,000 psi) for ASTM A-533-B. Hydrogen-induced, sustained load crack growth in ASTM A-533-B was restricted to the inner plane strain region of the specimen.

K_{TH} was measured as a function of hydrogen pressure for AISI 4340 steel and Inconel 718 to determine whether hydrogen-environment embrittlement is caused by adsorbed or absorbed hydrogen. K_{TH} was proportional to $P_{H_2}^{0.076}$ for AISI 4340 for hydrogen pressures between 0.034 MN/m^2 (5 psia) and 34.5 MN/m^2 (5000 psi). The Inconel 718 results indicate that K_{TH} decreased approximately as $\sqrt{P_{H_2}}$ at hydrogen pressures less than 21 MN/m^2 (3000 psi) and was independent of hydrogen pressure above 21 MN/m^2 (3000 psi). The crack growth rate in Inconel 718 was slow when exposed to hydrogen at the lower hydrogen pressures, and it appeared from extrapolation of the crack growth rate data that the stress intensity at crack arrest may be independent of hydrogen pressure. The small effect of hydrogen pressure on K_{TH} of both alloys indicates that hydrogen-environment embrittlement results from a hydrogen adsorption dependency mechanism.

CONTENTS

Nomenclature	
Introduction	1
Phase I. Tensile Properties of Alloys in Hydrogen Environments	1
Phase II. Threshold Stress Intensities of Alloys in Hydrogen Environments	2
Phase III. Acoustic Emission for Monitoring Crack Growth in Hydrogen	2
Phase IV. Variation of Hydrogen-Environment Embrittlement With Material Condition for Inconel 718	2
Phase V. Fracture Characteristics of Inconel 718 in Hydrogen as a Func- tion of Test Variables	3
Phase VI. Fracture Mechanics Properties of a Pressure Vessel Steel in High-Pressure Hydrogen	3
Phase VII. Cyclic Crack Growth in HY100 Steel in High-Pressure Hydrogen	3
Phase VIII. Mechanism of Hydrogen-Environment Embrittlement	4
Experimental Procedures	5
Materials	5
Tensile Property Measurements	5
Fracture Mechanics Properties Measurements With Compact Tension Specimens	14
Fracture Mechanics Properties Measurements With WOL Specimens	18
Fracture Mechanics Properties Measurements With Tapered Double Cantilever Beam (TDCB) Specimen	21
Test Apparatus Used for Performing Fracture Mechanics Measurements	27
Test Environment	32
Acoustic Emission Apparatus	33
Results and Discussion	37
Phase I. Tensile Properties of Alloys in Hydrogen Environments	37
Phase II. Threshold Stress Intensities of Alloys in Hydrogen Environments	43
Inconel 718--1214, 991-894 K (1725, 1325-1150 F) Heat Treatment Condition	48
Inconel 718--1325, 1033-922 K (1925, 1400-1200 F) Heat Treatment Condition	50
Inconel 625	52
AISI 321 Stainless Steel	53

A-286 Stainless Steel	54
Ti-5Al-2.5 Sn ELI	56
2219-T87 Al Alloy	57
OFHC Copper	58
Sustained-Load Crack Propagation in Hydrogen	59
Phase III. Acoustic Emission Monitoring of Crack Growth in Hydrogen . .	61
Phase IV. Variation of Hydrogen-Environment Embrittlement of Inconel 718	
With Material Condition	63
Tensile Tests of Notched Inconel 718 Specimens	63
Metallography of Inconel 718	66
Phase V. Fracture Characteristics of Inconel 718 in Hydrogen as a	
Function of Test Variables	92
Phase VI. Fracture Mechanics Properties of a Pressure Vessel Steel	
in High-Pressure Hydrogen	105
Phase VII. Cyclic Crack Growth in HY100 Steel in High-Pressure Hydrogen.	109
Phase VIII. Mechanism of Hydrogen-Environment Embrittlement	114
AISI 4340	115
Inconel 718	121
Discussion and Summary	128
Inconel 718	128
ASTM A-533-B	131
HY100	132
Inconel 625	133
AISI 321 Stainless Steel	134
A-286 Stainless Steel	134
Ti-5 Al-2.5 Sn ELI	135
2219-T87 Aluminum Alloy	136
OFHC Copper	136
Acoustic Emission Monitoring of Crack Growth	136
Mechanism of Hydrogen-Environment Embrittlement	137
References	138
<u>Appendix A</u>	
Measurement Units and Conversion to International Systems	
of Units (SI) and SI Prefixes Used	A-1

Appendix B

Phase I Data B-1

Appendix C

Phase IV Data Tabulations C-1

ILLUSTRATIONS

1. Weld Design for Gas Tungsten Arc Welding of Inconel 718 With Inconel 718 Filler Metal	12
2. Compact Tension Specimen	15
3. Modified WOL Specimen With Straight EDM Notch	19
4. Tapered Double Cantilever Beam Specimen Design	22
5. Compliance at the Load Centerline Versus Crack Length for an HY100 TDCB Specimen	24
6. Compliance at the Specimen Mouth [0.0127m (0.5 in.) from Load Centerline] Versus Crack Length for an HY100 TDCB Specimen	25
7. Vessel Used for Performing Fracture Mechanics Tests on Compact Tension, WOL, and TDCB Specimens in Ambient-Temperature Environments at Pressures up to 103.4 MN/m ² (15,000 psi)	28
8. Pressure Vessel Used to Perform Tests on Modified WOL Specimens in High Pressure Hydrogen	29
9. Apparatus for Performing Threshold Stress Intensity Measurements in High Pressure Environments	31
10. Block Diagram of Acoustic Emission Apparatus	35
11. Inconel 625 Unnotched Specimen Tested in 34.5 MN/m ² (5000 psi) Hydrogen at Room Temperature	39
12. AISI 321 Stainless Steel Unnotched Specimen Tested in 34.5 MN/m ² (5000 psi) Hydrogen at Room Temperature	41
13. AISI 321 Stainless Steel Unnotched Specimen Tested in 34.5 MN/m ² (5000 psi) Hydrogen at 144 K (-200 F)	42
14. Changes in Acoustic Emission and Applied Load With Time During a KTH Test Conducted on A-286 Steel in 34.5 MN/m ² (5000 psi), Ambient Temperature Hydrogen	62
15. Photomicrographs of Inconel 718 Rolled Bar in the 1228 K (1750 F) Solution Annealed As-Received Condition. Etchant: 92 HCl, 3 HNO ₃ , 1/2 H ₂ SO ₄	67
16. Photomicrographs of Transverse Sections of Inconel 718 Forging and Plate in 1228 K (1750 F) Solution Annealed, As-Received Condition. Etchant: 92 HCl, 3 HNO ₃ , 1/2 H ₂ SO ₄	68

17.	Photomicrographs of Transverse Sections of Inconel 718 in the A Heat Treatment Condition. Etchant: 92 HCl, 3 HNO ₃ , 1/2 H ₂ SO ₄	69
18.	Photomicrographs of Inconel 718 Rolled Bar in the B Heat Treatment Condition. Etchant: 92 HCl, 3 HNO ₃ , 1/2 H ₂ SO ₄	70
19.	Photomicrographs of Transverse Sections of Inconel 718 Forging and Plate in the B Heat Treatment Condition. Etchant: 92 HCl, 3 HNO ₃ , 1/2 H ₂ SO ₄	71
20.	Photomicrographs of Transverse Sections of Inconel 718 in the C Heat Treatment Condition. Etchant: 92 HCl, 3 HNO ₃ , 1/2 H ₂ SO ₄ (200X)	73
21.	Electron Micrographs of Inconel 718 in the 1228 K (1750 F) Annealed, As-Received Condition. Etchant: 92 HCl, 3 HNO ₃ , 1/2 H ₂ SO ₄ (3000 X)	74
22.	Electron Micrographs of Inconel 718 in the A Heat Treatment Condition. Etchant: 92 HCl, 3 HNO ₃ , 1/2 H ₂ SO ₄ (3000X)	75
23.	Electron Micrographs of Inconel 718 in the B Heat Treatment Condition. Etchants: 92 HCl, 3 HNO ₃ , 1/2 H ₂ SO ₄ (3000X)	76
24.	Electron Micrographs of Inconel 718 in the C Heat Treatment Condition. Etchant: 92 HCl, 3 HNO ₃ , 1/2 H ₂ SO ₄	77
25.	Optical and Electron Micrographs of Inconel 718 Rolled Bar in the 1297 K (1875 F) Solution Annealed Condition (Heat Treatment D). Etchant: 92 HCl, 3 HNO ₃ , 1/2 H ₂ SO ₄	80
26.	Optical and Electron Micrographs of Inconel 718 Rolled Bar in the E Heat Treatment Condition. Etchant: 92 HCl, 3 HNO ₃ , 1/2 H ₂ SO ₄	81
27.	Optical and Electron Micrographs of Inconel 718 Forging in the E Heat Treatment Condition. Etchant: 92 HCl, 3 HNO ₃ , 1/2 H ₂ SO ₄	82
28.	Optical and Electron Micrographs of Inconel 718 Plate in the E Heat Treatment Condition. Etchant: 92 HCl, 3 HNO ₃ , 1/2 H ₂ SO ₄	83
29.	Optical and Electron Micrographs of Welded Inconel 718 Plate in the A Heat Treatment Condition. Etchant: 92 HCl, 3 HNO ₃ , 1/2 H ₂ SO ₄	84
30.	Optical and Electron Micrographs of Welded Inconel 718 Plate in the B Heat Treatment Condition. Etchant: 92 HCl, 3 HNO ₃ , 1/2 H ₂ SO ₄	85

31. Optical and Electron Micrographs of Welded Inconel 718 Plate in the C Heat Treatment Condition. Etchant: 92 HCl, 3 HNO ₃ , 1/2 H ₂ SO ₄	86
32. Scanning Electron Fractography of an Inconel 718 WOL Specimen Tested in 34.5 MN/m ² (5000 psi) Hydrogen in the A Heat Treatment Condition	88
33. Scanning Electron Fractograph of Inconel 718 WOL Specimen Tested in 68.9 MN/m ² (10,000 psi) Hydrogen in the F Heat Treatment Condition	89
34. Scanning Electron Fractography of an Inconel 718 WOL Specimen Tested in 0.069 MN/m ² (10 psi) Hydrogen	
35. Cyclic Crack Growth Rate as a Function of Stress Intensity Range for Inconel 718 Exposed to 34.5 MN/m ² (5000 psi) Helium and 68.9 MN/m ² (10,000 psi) Hydrogen Ambient-Temperature Environments	
36. Cyclic Crack Growth Rate as a Function of Stress Intensity Range for Inconel 718 Exposed to 34.5 MN/m ² (5000 psi) Helium and 34.5 MN/m ² (5000 psi) Hydrogen Ambient-Temperature Environments	
37. Cyclic Crack Growth Rate as a Function of Stress Intensity Range for Inconel 718 Exposed to 34.5 MN/m ² (5000 psi) Helium and 0.069 MN/m ² (10 psi) Hydrogen Ambient-Temperature Environments	
38. Cyclic Crack Growth Rate as a Function of Stress Intensity Range for Inconel 718 Exposed to 34.5 MN/m ² (5000 psi) Helium and 0.069 MN/m ² (10 psi), 34.5 MN/m ² (5000 psi) and 68.9 MN/m ² (10,000 psi) Hydrogen Ambient-Temperature Environments	
39. Ambient-Temperature Cyclic Crack Growth Rate as a Function of Cyclic Rate for Inconel 718 Specimen No. 6 Exposed to 68.9 MN/m ² (10,000 psi) Hydrogen at Stress Intensity Range of 54.7 MN/m ² \sqrt{m} (49.7 ksi $\sqrt{in.}$)	
40. Cyclic Crack Growth Rate as a Function of Stress Intensity Range for Inconel 718 Exposed to 34.5 MN/m ² (5000 psi) Hydrogen at 200 K (-100 F)	
41. Cyclic Crack Growth Rate as a Function of Stress Intensity for ASTM A-533-B Exposed to 103.4 MN/m ² (15,000 psi) Helium and 103.4 MN/m ² (15,000 psi) Hydrogen Ambient-Temperature Environments	
42. Cyclic Crack Growth Rate as a Function of Stress Intensity Range for HY100 Exposed to 51.7 MN/m ² (7500 psi) Helium and 51.7 MN/m ² (7500 psi) Hydrogen Ambient-Temperature Environments	

43. Ambient-Temperature Cyclic Crack Growth Rate as a Function of Hydrogen Pressure for HY100 at Stress Intensity Range of $54.7 \text{ MN/m}^2 \sqrt{\text{m}}$ ($49.7 \text{ ksi } \sqrt{\text{in.}}$) (Cycle Rate: 1.0 cycles/sec)
44. Stress Intensity at Crack Arrest for AISI 4340 WOL Specimens at Ambient Temperature as a Function of Hydrogen Pressure
45. Sustained Load Crack Growth Rate in AISI 4340 WOL Specimen No. 14 as a Function of Stress Intensity at Various Hydrogen Pressures
46. Stress Intensity at Crack Arrest for Inconel 718 at Ambient Temperature as a Function of Hydrogen Pressure
47. Stress Intensity at Crack Arrest for Inconel 718 at Ambient Temperature as a Function of Square Root of Hydrogen Pressure
48. Sustained Load Crack Growth Rate in Inconel 718 TDCB Specimens as a Function of Stress Intensity at Various Hydrogen Pressures

TABLES

1. Chemical Composition (Weight Percent) of Test Materials	6
2. Heat Treatment of Materials as Received	7
3. Mechanical Properties of Test Materials As-Received	8
4. Suppliers of Inconel 718 Test Materials	9
5. Heat Treatment of Materials Performed at Rocketdyne	10
6. Tensile Properties of Heat Treated Unnotched Inconel 718 Specimens Tested in Air at 0.1 MN/m^2 (1-Atmosphere Pressure).	11
7. Average Tensile Properties of Alloys in Various Environments	38
8. Results of Fracture Mechanics Property Measurements on Modified WOL Specimens of Various Alloys in 0.1 MN/m^2 (1-atm Pressure) Air and in 34.5 MN/m^2 (5000 psi) H_2 and He	44
9. Average K_{IC} and K_{TH} Values for Various Metals in 34.5 MN/m^2 (5000 psi) Hydrogen and Helium Environments	46
10. Yield Strengths and Maximum Stress Intensities at Which Plane Strain Exists for the 0.0254 m (1.0 in.) Thick WOL Specimen Used for These Tests	47
11. Effect of 34.5 MN/m^2 (5000 psi) Hydrogen at Room Temperature on the Average Properties of Notched Specimens of Inconel 718 in Various Conditions	64
12. Average Notched Tensile Properties of Inconel 718 in 34.5 MN/m^2 (5000 psi) H_2 and He	91
13. Results of Ambient-Temperature Fracture Mechanics Measurements on Inconel 718 Compact Tension Specimens	93
14. Results of Fracture Mechanics Measurement on Inconel 718 WOL Specimens Tested in 34.5 MN/m^2 (5000 psi) H_2 and He at 200 K (-100 F)	95
15. Tensile Properties of ASTM A-533-B (ASTM A-302 Gr B, Nickel Modified) Steel in 103.4 MN/m^2 (15,000 psi) Hydrogen and Helium Environments	106
16. Results of Ambient-Temperature Fracture Mechanics Measurements on ASTM A-533-B Compact Tension Specimens	107
17. Results of Crack Arrest Measurements on AISI 4340 WOL Specimens Tested in Hydrogen at Ambient Temperature at Various Pressures	116
18. Results of Crack Arrest Measurements on Inconel 718 WOL and TDCB Spec- imens Tested in Hydrogen at Room Temperature at Various Pressures	

NOMENCLATURE AND UNITS OF MEASUREMENTS

a	= crack length, inch
B	= specimen thickness, inch
B _n	= net specimen thickness, inch
C	= compliance, in./lb
COD	= crack opening displacement, inch
E	= Young's modulus, psi
K	= stress intensity, ksi√in.
K _{IC}	= plane strain critical stress intensity factor or plane strain fracture toughness, ksi√in.
K _{max}	= maximum stress intensity reached prior to specimen failure, ksi√in.
K _Q	= conditional value of fracture toughness from test data, ksi√in.
K _{TH}	= plane strain threshold stress intensity, ksi√in.
N	= number of cycles or total number of surface sites available for gas adsorption
P	= applied load, pounds
P _{max}	= maximum applied load obtained prior to specimen failure, pounds
R	= ratio of minimum to maximum stress during a cycle
R _{SC}	= ratio of nominal stress at K _{max} to yield strength
T	= time, hours or minutes
W	= specimen dimension, inch
μ	= Poisson's ratio
σ _{YS}	= uniaxial tensile yield strength of the material, psi
σ _{nominal}	= nominal stress in compact tension-type specimens, psi

INTRODUCTION

Advanced, high-performance rocket engines for the propulsion of space vehicles use high-pressure hydrogen and oxygen as propellants and, in one instance, the Space Shuttle main engine (SSME), the hydrogen pressures will be higher than in any previous production engine. It has been shown (Ref. 1 through 11) that high-pressure hydrogen can seriously degrade the mechanical properties of many of the commonly used engineering alloys, particularly the higher-strength alloys. However, data are lacking on the effects of high-pressure hydrogen on specific candidate materials, at appropriate temperatures and pressures, and on certain properties such as fracture mechanics properties. Thus, this program was conducted to develop information on the mechanical properties of candidate structural alloys in high-pressure hydrogen under simulated operating conditions to assist in the selection of alloys and to provide design data and safe operating parameters for rocket engine components and test facilities. In addition, one phase was conducted at the request of the Naval Ship Research and Development Center to provide data relative to high-pressure hydrogen storage bottles for deep-submergence vessels.

The program was divided into eight phases which are outlined below. Throughout this report, the phases have been ordered for logical development and are not in chronological order.

PHASE I. TENSILE PROPERTIES OF ALLOYS IN HYDROGEN ENVIRONMENTS

Candidate materials for regions exposed to high-pressure hydrogen in the SSME included Inconel 625, AISI 321 stainless steel, Ti-5Al-2.5Sn ELI and OFHC copper (or copper alloy). On the basis of previous work (Ref. 1 and 4), Ti-5Al-2.5Sn ELI was categorized as severely embrittled and AISI 321 stainless steel as slightly embrittled by 68.9 MN/m² (10,000 psi) hydrogen at ambient temperature. Inconel 625, being a nickel-base alloy, was expected to be embrittled when

exposed to high-pressure hydrogen environments. Water and Chandler (Ref. 1 and 4) found that OFHC copper was not embrittled by exposure to 10,000-psi hydrogen, but investigations by Vennett and Ansell (Ref. 11) indicated some reduction of ductility of unnotched specimens of OFHC copper in 68.9 MN/m² (10,000 psi) hydrogen at ambient temperature.

In this phase, the effect of 34.5 MN/m² (5000 psi) hydrogen on the tensile properties of the alloys listed above was determined at ambient temperature and 144 K (-200 F).

PHASE II. THRESHOLD STRESS INTENSITIES OF ALLOYS IN HYDROGEN ENVIRONMENTS

At the initiation of this program, almost no data existed on the effect of high-pressure hydrogen environments on fracture mechanics properties. The effect of 34.5 MN/m² (5000 psi) hydrogen at ambient temperature and 144 K (-200 F) on the threshold stress intensity was determined for the alloys listed in Phase I and, in addition, the 2219-T87 aluminum alloy.

PHASE III. ACOUSTIC EMISSION FOR MONITORING CRACK GROWTH IN HYDROGEN

An acoustic emission technique was developed for monitoring crack growth in threshold stress intensity tests in gaseous hydrogen environments.

PHASE IV. VARIATION OF HYDROGEN-ENVIRONMENT EMBRITTLEMENT WITH MATERIAL CONDITION FOR INCONEL 718

Inconel 718 has many attractive properties and is being designed extensively into the SSME. In previous work (Ref. 1 and 4), it was found to be extremely embrittled by high-pressure hydrogen. However, the degree of embrittlement was found (Ref. 10) to vary significantly with the heat treatment and/or heat of Inconel 718 tested. Also, few data (Ref. 9) were available on the hydrogen-environment embrittlement of Inconel 718 weldments.

Tensile tests on notched specimens were used to determine the effect of material form (i.e., plate, bar, or forging), heat treatment, and welding on the hydrogen-environment embrittlement of Inconel 718 in 34.5 MN/m^2 (5000 psi) hydrogen at ambient temperature.

PHASE V. FRACTURE CHARACTERISTICS OF INCONEL 718 IN HYDROGEN AS A FUNCTION OF TEST VARIABLES

The effect of hydrogen environments on the fracture mechanics properties of Inconel 718 was determined for hydrogen pressures from 0.0689 MN/m^2 (10 psi) to 68.9 MN/m^2 (10,000 psi) at ambient temperature and 200 K (-100 F).

PHASE VI. FRACTURE MECHANICS PROPERTIES OF A PRESSURE VESSEL STEEL IN HIGH-PRESSURE HYDROGEN

The SSME test facility at Rocketdyne requires the storage of hydrogen at pressures near 103.4 MN/m^2 (15,000 psi). The available storage vessels were constructed of ASTM A-533-B (previously designated A-302-B Ni modified), a low-alloy steel that had been found previously (Ref. 4) to be considerably embrittled by 68.9 MN/m^2 (10,000 psi) hydrogen. To provide additional information on the storage of hydrogen in these vessels, tests were performed to determine the effect of 103.4 MN/m^2 (15,000 psi) hydrogen on tensile properties, fracture toughness (K_{IC}), threshold stress intensity (K_{TH}), and cyclic flaw growth rates (da/dN vs K_{Ii}) for the ASTM A-533-B steel.

PHASE VII. CYCLIC CRACK GROWTH IN HY100 STEEL IN HIGH-PRESSURE HYDROGEN

The effect of 51.7 MN/m^2 (7500 psi) hydrogen on cyclic crack growth rates in HY100 steel was determined to provide data pertinent to the use of that steel in high-pressure hydrogen storage bottles on naval deep-submergence vessels.

PHASE VIII. MECHANISM OF HYDROGEN-ENVIRONMENT EMBRITTLEMENT

The mechanism by which hydrogen environments embrittle metals has not been established, although several have been postulated (Ref. 12). To clarify the mechanism of hydrogen-environment embrittlement, measurements were made of equilibrium crack extension (crack arrest) as a function of hydrogen pressure for Inconel 718 and ASTM 4340 steel.

EXPERIMENTAL PROCEDURES

MATERIALS

The chemical compositions, heat treatments, and mechanical properties of the test materials in the as-received conditions are listed in Tables 1 through 3, respectively. The Inconel 718 was purchased in four forms from the suppliers listed in Table 4. The Inconel 718 and AISI 4340 were further heat treated at Rocketdyne, and these heat treatments are listed in Table 5. The mechanical properties of the Inconel 718 materials in the various heat treatment conditions are listed in Table 6.

The hardness of the AISI 4340 material after heat treatment was Rockwell C 47, which corresponds to a yield strength of approximately 1380 MN/m^2 (200 ksi).

Inconel 718 weldments were made using the 0.013 m (1/2 inch) thick plate with a joint design shown in Fig. 1. The weldments were made by gas tungsten arc welding with Inconel 718 filler metal, and with the weld perpendicular to the plate rolling direction. After each weld pass, the weld was die penetrant inspected and, after the weldments were completed, the welded plates were X-rayed. No defects were found during these inspections.

TENSILE PROPERTY MEASUREMENTS

The tensile specimens were fabricated with the longitudinal axis parallel to the materials longitudinal rolling direction. The test specimens were 0.0077 m (0.306 in.) in diameter, 0.23 m (9 in.) long, were threaded on each end, and had a 16-rms surface finish. For the unnotched specimens, a 0.032 m (1.25 in.) long, 0.0064 m (0.25 in.) diameter gage section was used. The notched specimens had a 60 degree V-notch at the midpoint, with a specimen diameter at the root of the notch of 0.0038 m (0.150 in.). A root radius of $2.4 \times 10^{-5} \text{ m}$ (0.00095 in.) was used to obtain an elastic stress concentration factor (K_t) of approximately 8.4. The stress concentration factor was calculated according to Peterson (Ref. 13).

TABLE 1. CHEMICAL COMPOSITION (WEIGHT PERCENT) OF TEST MATERIALS
(SUPPLIER CERTIFICATION)

Material	C	S	Mn	Si	Cr	Mo	Ti	Al	Fe	Cu	Ni	P	Cb + Ta	Miscellaneous
<u>Inconel 718</u>														
0.032 x 0.07 m (1-1/4 x 2-3/4 in.) Rolled Bar	0.073	0.024	0.096	0.17	18.82	2.98	0.98	0.49	Bal.	0.03	51.68	0.008	5.02	0.46 Co; 0.005 B
0.038 m (1-1/2 in.) Forging	0.05	0.003	1.10	0.10	17.8	3.00	1.00	0.57	18.5	0.10	Bal.	0.01	5.59	0.10 Co; 0.005 B
0.013 m (1/2 in.) Plate	0.06	0.009	0.12	0.10	17.92	3.10	1.01	0.52	Bal.	0.01	52.77	0.002	5.10	0.39 Co; 0.004 B
0.041 m (1-5/8 in.) Forging	0.04	0.005	0.010	0.010	18.2	3.00	0.99	0.51	17.7	0.10	54.1	0.01	5.51	0.10 Co; 0.004 B
<u>Inconel 625</u>														
0.032 x 0.07 m (1-1/4 x 2-3/4 in.) Rolled Bar	0.047	0.003	0.05	0.20	21.14	8.97	0.11	0.20	2.55	--	Bal.	0.008	3.73 0.04	0.97 Co
<u>A-286 Stainless Steel</u>														
0.032 m (1-1/4 in.) Forging	0.048	0.010	1.20	0.63	14.15	1.25	2.21	0.16	Bal.	--	24.88	0.016	--	0.47 B; 0.01 Zn; 0.22 V
<u>AISI 321 Stainless Steel</u>														
0.032 m (1-1/4 in.) Plate	0.060	0.015	1.46	0.58	17.80	0.24	0.51	--	Bal.	0.12	10.45	0.026	--	
<u>Ti-5Al-2.5 Sn ELI</u>														
0.032 m (1-1/4 in.) Plate	0.022	--	0.001	--	--	--	Bal.	5.1	0.19	--	--	--	--	0.012 Nb; 0.010 Hf; 0.080 O ₂ ; 2.4 Sn
<u>2219-T87 Al Alloy</u>														
0.032 m (1-1/4 in.) Plate	--	--	0.20- 0.40	0.20- Max	--	--	--	Bal.	0.30- Max	5.8- 6.8	--	--	--	0.10-0.25 Zn; 0.05- 0.15 V; 0.10 max Zn; 0.02 max Vg
<u>OFHC Copper</u>														
0.032 m (1-1/4 in.) Plate														
<u>ASTM A-531-B</u>														
0.089 m (5 1/2 in.) Plate	0.24	0.020	1.19	0.29		0.49			Bal.		0.58	0.012		
<u>AISI 4340</u>														
0.038 m (1 1/2 in.) Plate	0.59	0.017	0.65	0.27	0.82	0.22			Bal.		1.8	0.003		
<u>W100</u>														
0.038 m (1 1/2 in.) Plate	0.16	0.019	0.31	0.20	1.4	0.41	0.003		Bal.	0.15	0.86	0.012		0.003

*Cu-99.99 min; S-0.0018 max; P-0.003 max;
Zn, Mn, As, Sb, Bi, Te, Sn, Se, Pb, O₂-0.001 max each;
Hg, Cd-0.001 max each

*From Rocketdyne Specification RB0173-047, no supplier certification

TABLE 2. HEAT TREATMENT OF MATERIALS AS RECEIVED

Material	Heat Treatment
<u>Inconel 718</u>	
0.032 x 0.07 m (1-1/4 x 2-3/4 in.) Rolled Bar	1228 K (1750 F), 3.6 ksec (1 hour), air cooled
0.038 m (1-1/2 in.) Forging	1228 K (1750 F), 3.6 ksec (1 hour), air cooled
0.013 m (1/2 in.) Plate	1228 K (1750 F), 1.8 ksec (1/2 hour), spray quenched
0.041 m (1 5/8 in.) Forging	1228 K (1750 F), 3.6 ksec (1 hour) air cooled; 991 K (1325 F), 28.8 ksec (8 hours), furnace cooled at 0.01 K/sec (75 F/hr); to 894 K (1150 F) and held at 894 K (1150 F) for 28.8 ksec (8 hours) air cooled
<u>Inconel 625</u>	
0.032 x 0.07 m (1-1/4 x 2-3/4 in.) Rolled Bar	1200 K (1700 F), 3.6 ksec (1 hour), air cooled
<u>A-286 Stainless Steel</u>	
0.032 m (1-1/4 in.) Plate	Solution treated 1255 K (1800 F), 3.6 ksec (1 hour), oil cooled, aged 991 K (1325 K), 57.6 ksec (16 hours), air cooled
<u>AISI 321 Stainless Steel</u>	
0.032 (1-1/4 in.) Plate	Hot rolled, annealed, and descaled
<u>Ti-5Al-2.5 Sn ELI</u>	
0.032 m (1-1/4 in.) Plate	Final anneal cycle 978 K (1300 F) - 1033 K (1400 F), 7.2 to 28.8 ksec (2 to 8 hours), air cooled
<u>2219-T87 Al Alloy</u>	
0.032 m (1-1/4 in.) Plate	Solution annealed 808 K (995 F), cold water quench, approx- imately 8 percent cold work, age 86.4 ksec (24 hours) at 436 K (325 F).
<u>OFHC Copper</u>	
0.032 m (1-1/4 in.) Plate	Annealed
<u>ASTM A-533-B</u>	
0.089 m (3 1/2 in.) Plate	1172 K (1650 F), 10.8 ksec (3 hours) water quenched 936 K (1225 F), 18.0 ksec (5 hours) air cooled 866 K (1100 F), 12.6 ksec (3-1/2 hours), air cooled
<u>AISI 4340</u>	
0.038 m (1 1/2 in.) Plate	Not Supplied
<u>HY-100</u>	
0.038 m (1 1/2 in.) Plate	Not Supplied

TABLE 3. MECHANICAL PROPERTIES OF TEST MATERIALS AS-RECEIVED
(SUPPLIER CERTIFICATION)

Material	Temp.		Yield Stre. ksi MM/m ²	Tensile Strength ksi MM/m ²		Reduction of Area, %	Elongation, %	Stress Rupture Properties**
	K	F						
<u>Inconel 718</u> 0.032 x 0.07 m (1-1/4 x 2-3/4 in.) Rolled Bar 0.038 m (1-1/2 in.) Forging	RT	RT	1140	166	1380	200	44	234 ksec (64.9 hours) at 758 MM/m ² (110 ksi) 5.6% El, 10% RA
	922	1200	970	140	1140	165	43	216 ksec (59.8 hours) at 772 MM/m ² (112 ksi) 5.5% El
	RT	RT	1180	171	1370	199	36	151 ksec (42 hours) at 758 MM/m ² (110 ksi) 12% El
	922	1200	1010	146	1090	158	36	
	RT	RT	1140	165	1430	208	--	
	922	1200	1010	147	1170	170	--	
<u>Inconel 625</u> 0.032 x 0.07 m (1-1/4 x 2-3/4 in.) Rolled Bar A-286 Stainless Steel 0.032 m (1-1/4 in.) Forging	RT	RT	1140	165	1440	209	31	136 ksec (37.7 hours) at 758 MM/m ² (110 ksi) 18.0% El
	922	1200	1050	145	1180	171	57	121 ksec (33.8 hours) at 758 MM/m ² (110 ksi) 16.9% El
	RT	RT	1090	158	1370	199	31	
	922	1200	958	139	1151	167	24	
	RT	RT	630	91	1040	143	54	64.8 ksec (18 hours) at 136 MM/m ² (18 ksi) and 1089 K (14500 F), 64% El, 51% RA
	RT	RT	780	113	1050	150	33	
<u>SI 321 Stainless Steel</u> 0.032 m (1-1/4 in.) Plate TI-SAL-2.5 Sm E11 0.032 m (1-1/4 in.) Plate	RT	RT	340	49	610	89	66	
	RT	RT	720	112	770	112	28.5	17
	RT	RT	820*	119*	860*	124*	39.5*	16.5*
	RT	RT	390	57	480	70	18	
	RT	RT	640	93	760	110	64.7	21
	RT	RT	620*	30*	740*	107*	56*	21*
<u>2219-T87 Al Alloy</u> 0.032 m (1-1/4 in.) Plate CPMC Copper 0.032 m (1-1/4 in.) Plate ASTM A-533-2 0.089 m (3-1/2 in.) Plate AISI 434F 0.038 m (1-1/2 in.) Plate RT100 0.038 m (1-1/2 in.) Plate	NONE SUPPLIED							
	NOT SUPPLIED BY VENDOR							
	RT	RT	758	111	855	124	70	25
	RT	RT	744	108*	834*	121*	64*	22*
	RT	RT						
	RT	RT						

*Transverse Properties
**Stress Rupture properties determined at 922 K (1200 F) in AWS 5596C aged condition for Inconel 718 materials.
The AWS 5596C aging treatment is 991 K (1325 F) for 28.8 ksec (8 hours), furnace cooled to 894 K (1150 F) for a total aging time of 64.8 ksec (18 hours).

TABLE 4. SUPPLIERS OF INCONEL 718 TEST MATERIALS

Material	Supplier
0.032 x 0.07 m (1-1/4 x 2 3/4 in.) Rolled Bar	AllVac Division of Teledyne Carlton Forge Works from a Special Metals Corporation ingot Stellite Division of Cabot Corporation Reisner Metals, Inc., from a Special Metals Corporation ingot
0.038 m (1-1/2 in.) Forging	
0.013 m (1/2 in.) Plate	
0.041 m (1-5/8 in.) Forging	

TABLE 5. HEAT TREATMENT OF MATERIALS PERFORMED AT ROCKETDYNE

Material	Heat Treatment	Solution Treatment*										Aging Treatment										Total Aging Time	
		Temperature			Time		First Aging					Cooling to Second Aging		Second Aging									
		K	F	ksec	min	Temperature		ksec	hours	K	F	ksec	hours	K	F	ksec	hours						
																			ksec	hours			
Inconel 718	A	1214	1725	3.6	60			991	1325	28.8	8	10.8 - 14.4	3 to 4	894	1150	21.6	6 to 7-1/2	64.8	18 to 18-1/2				
	B	1214	1725	3.6	60			1089	1500	36	10	3.6 - 14.4	1 to 4	922	1200	27.0	6 to 8-1/2	66.0	20 to 21				
	C	1325	1925	1.2**	20**			1033	1400	36	10	7.2 - 16.2	2 to 4-1/2	922	1200	30.6	6 to 8	75.6	20 to 20-1/2				
	D	1297	1875	0.6	10			--	--	--	--	--	--	--	--	--	--	--	--				
	E	1297	1875	0.6	10			1033	1400	34.2	9-1/2	6.3	1-3/4	922	1200	32.4	9	72.9	20-1/4				
	F	1311	1900	6.3	105			1033	1400	37.8	10-1/2	10.5	3	922	1200	26.1	7-1/4	74.8	20-3/4				
AISI 4340		1089	1500	3.6	60			644	700	7.2	2												

*Inconel 718 was air cooled following the solution heat treatment

AISI 4340 was oil quenched following the solution heat treatment

**The Inconel 718 welded specimens were solution annealed 3.6 ksec (1 hour) at 1325 K (1925 F) instead of the usual 1.2 ksec (20 minutes).

TABLE 6. TENSILE PROPERTIES OF HEAT TREATED UNNOTCHED INCONEL 718 SPECIMENS
TESTED IN AIR AT 0.1 MN/m² (1-ATMOSPHERE PRESSURE)

Material	Heat Treatment	Tensile Properties					Percent Elongation in 0.032 m (1-1/4 in.) Reduced Section
		Yield Strength		Ultimate Strength		Percent Reduction of Area	
		MN/m ²	ksi	MN/m ²	ksi		
0.032 x 0.007 m (1-1/4 x 2-3/4 in.) Rolled Bar	A	1120	163	1390	202	35	23
	B	876	127	1250	182	32	24
	C	1110	161	1340	195	37	26
	E	1150	167	1380	200	42	23
0.038 m (1-1/2 in.) Forging	A	1100	159	1370	198	31	22
	B	855	124	1230	178	35	25
	C	1170	169	1370	198	41	26
	E	1170	169	1380	202	38	22
0.013 m (1/2 in.) Plate	A	1170	159	1410	205	36	23
	B	917	133	1300	189	35	23
	C	1150	167	1400	204	38	25
	E	1170	170	1430	207	40	22
Weldment in "C" 0.013 m (1/2 in.) Plate	A	1030	150	1190	173	12	4.4*
	B	869	126	1140	166	15	7.3*
	C	1140	165	1370	199	23	13*

*Reduced section 0.017 m (0.65 in.) long

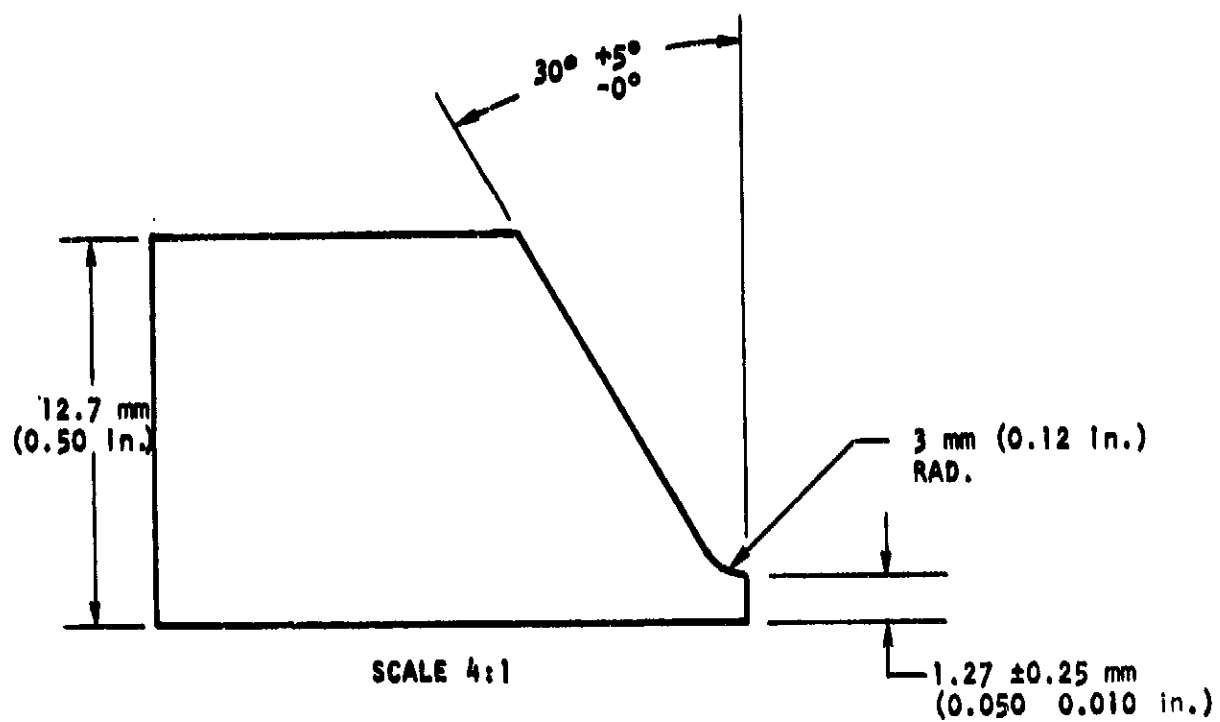


Figure 1. Weld Design for Gas Tungsten Arc Welding of Inconel 718
With Inconel 718 Filler Metal

Notched welded specimens were fabricated with the longitudinal specimen axis parallel to the rolling direction and with the notches located in either the weld or in the heat-affected zone. In addition, the unnotched tensile properties of the Inconel 718 weldments were determined in air. The reduced sections of these specimens were 0.016 m (0.65 in.) long bridging the approximately 0.006 m (1/4 in.) long weldment.

The apparatus used for performing the tensile tests has been described elsewhere (Ref. 4). Briefly, the tensile specimens were enclosed in a small pressure vessel with the ends of the specimens extending outside the vessel through sliding seals. The load was applied to the specimen by a hydraulic ram. The unnotched specimens were crosshead paced at 2.1×10^{-6} m/sec (0.005 in./min). Notched specimens were load paced at a loading rate that corresponds to 1.2×10^{-5} /sec (0.0007/min) strain rate.

Tests with this apparatus were conducted at ambient and cryogenic temperatures. For the cryogenic tests, the pressure vessel was surrounded by a dewar filled with cold nitrogen. The nitrogen was cooled by passing through copper coils immersed in liquid nitrogen, and was fed into the dewar at a rate sufficient to maintain the desired specimen temperature.

Calculation of the actual tensile load for test specimens required that the friction from the sliding seals and the tensile load from the high-pressure gas be considered. The following equation was used to calculate the ultimate load of the unnotched specimens:

$$\begin{aligned} \text{Ultimate Load} = & \text{Applied Load} - \text{Friction} + \text{Pressure} \\ & \times (\text{Specimen Area at Sliding Seal} - \\ & \text{Specimen Area Prior to Necking}) \end{aligned} \quad (1)$$

The maximum combined tensile load was assumed to occur prior to necking. For notched specimens, the original area at the base of the notch was used in place of the "area prior to necking" in the above equation.

The percent elongation of the unnotched specimens was measured between punch marks placed 0.0508 m (2 in.) apart outside and bridging the reduced section. The reduction of area of notched specimens was determined by using an optical comparator to measure the cross section in the notch before and after testing.

FRACTURE MECHANICS PROPERTIES MEASUREMENTS WITH COMPACT TENSION SPECIMENS

K_{IC} and K_{TH} measurements were performed on 0.0254 m (1 in.) thick compact tension specimens designed according to ASTM specifications (Ref. 14) and shown in Fig. 2. The tests were performed and the data analyzed in accordance with ASTM E399-72. The ASTM equation is

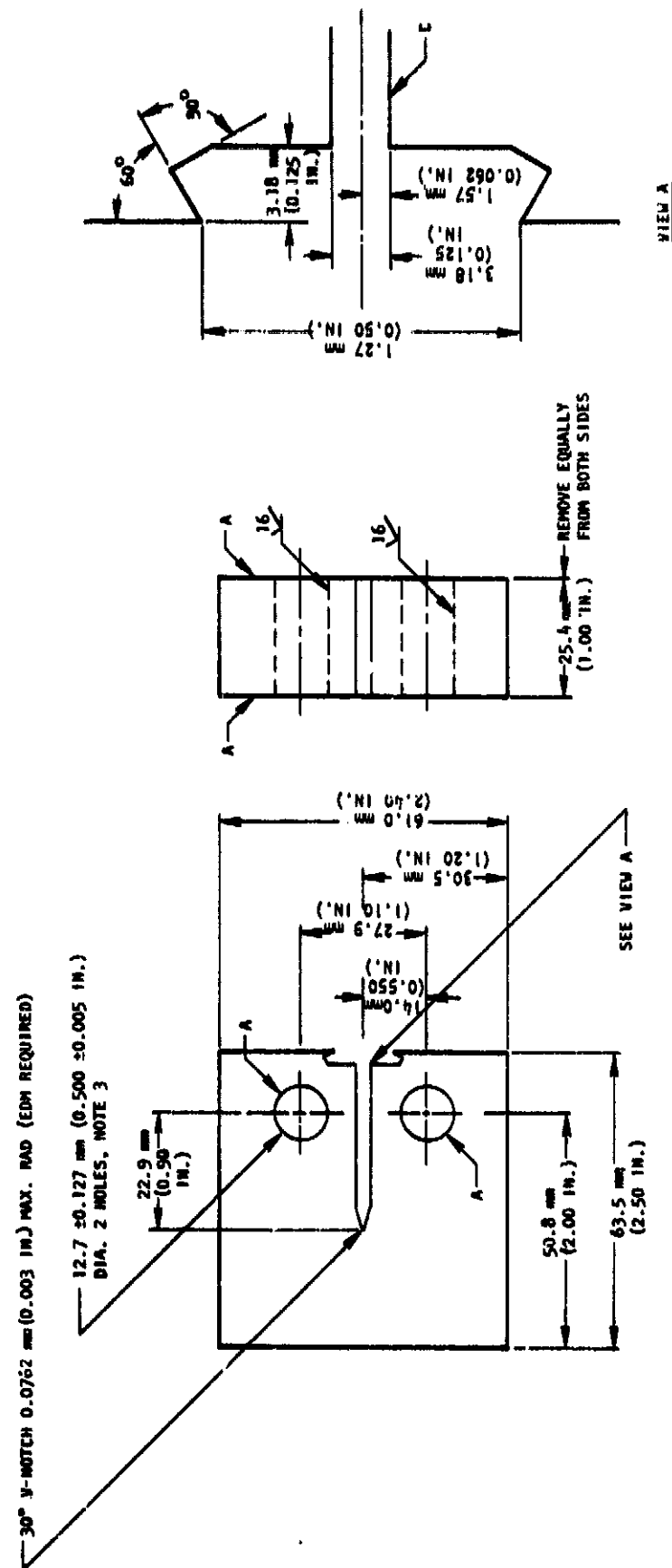
$$K = \frac{P}{BW^{1/2}} \left[29.6 \left(\frac{a}{W} \right)^{1/2} - 185.5 \left(\frac{a}{W} \right)^{3/2} + 655.7 \left(\frac{a}{W} \right)^{5/2} - 1017.0 \left(\frac{a}{W} \right)^{7/2} + 638.9 \left(\frac{a}{W} \right)^{9/2} \right] \quad (2)$$

where

- K = stress intensity, psi $\sqrt{\text{in.}}$
- P = applied load, pounds
- B = specimen thickness, inch
- W = specimen width, inch
- a = crack length, inch

The specimens were loaded to a maximum "failure" load which occurred when further increase of ram travel resulted in reduction of applied load.

ASTM E399 requires that the strength ratio R_{SC} be computed for tests that do not meet the plane strain fracture toughness requirements. The strength ratio is the



1. ALL FINISHES ³²UNLESS OTHERWISE SPECIFIED
2. TOLERANCES NOT SPECIFIED, ±0.127 mm (±0.005 IN.)
3. A AND C SURFACES ARE TO BE PERPENDICULAR AND PARALLEL AS APPLICABLE TO WITHIN 0.05 mm (0.002 IN.) TIR

Figure 2. Compact Tension Specimen

ratio of the nominal stress at K_{max} to the materials yield strength, and can be used as a guide for estimating the relative fracture toughness of the material.

$$R_{SC} = \frac{2 P_{max}}{\sigma_{YS}} \frac{2 W + a}{B(W-a)^2} \quad (3)$$

After the maximum load was reached, each specimen was held under crack opening displacement (COD) control and the crack was allowed to propagate until arrested.

The crack extension at crack arrest generally exceeded the 0.45 to 0.55 a/W range of the ASTM equation (Eq. 2). A compact tension specimen compliance calibration was performed at the Rockwell International Space Division, and the equations derived are accurate along the entire specimen length. Thus, the Space Division compliance calibration was used for calculating the stress intensities at K final. Equation 4 is the Space Division load line compliance equation. Equation 5 is the crack mouth compliance equation, and it was used for predicting crack lengths from crack mouth compliance measurements performed during the tests.

$$\begin{aligned} \ln CEB = & -0.08044612 + 17.91260 \left(\frac{a}{W}\right) - 54.91747 \left(\frac{a}{W}\right)^2 \\ & + 116.1447 \left(\frac{a}{W}\right)^3 - 125.0872 \left(\frac{a}{W}\right)^4 + 55.96971 \left(\frac{a}{W}\right)^5 \end{aligned} \quad (4)$$

$$\begin{aligned} \ln CEB = & 2.250949 + 4.680582 \left(\frac{a}{W}\right) - 15.97384 \left(\frac{a}{W}\right)^2 \\ & + 57.2322 \left(\frac{a}{W}\right)^3 - 81.13585 \left(\frac{a}{W}\right)^4 + 43.08261 \left(\frac{a}{W}\right)^5 \end{aligned} \quad (5)$$

where

$C = \text{compliance} = \frac{COD}{Load}$, $\frac{in.}{lb}$

$E = \text{Young's modulus, psi}$

The stress intensity was obtained by differentiating the compliance with crack length in accordance with the Irwin-Kies relationship for plane strain conditions (Eq. 6).

$$K = \frac{P}{BW^{1/2}} \left(\frac{1}{2} \frac{d(CEB)}{d(a/W)} \right)^{1/2} \left(\frac{1}{1-\mu^2} \right)^{1/2} \quad (6)$$

where

μ = Poison's ratio

Thus, a numerical differentiation of Eq. 4 was performed for each stress intensity measurement.

Linear elastic fracture mechanics assumes that gross yielding is not taking place. Recently, Vroman et al. (Ref. 15) derived an equation (Eq. 7) that can be used to qualitatively predict gross yielding in front of a crack in compact tension and wedge open loaded (WOL) specimens. Equation 7 was derived on the basis of two beams pivoting around the centroid of the material remaining ahead of the crack.

$$\sigma_{\text{nominal}} = \frac{P}{B_n w \left(1 - \frac{a}{w}\right)} \left[1 + 3 \frac{\left(1 + \frac{a}{w}\right)}{\left(1 - \frac{a}{w}\right)} \right] \quad (7)$$

Gross yielding ahead of the crack is assumed when σ_{nominal} is greater than σ_{yield} .

Equation 7 was computed for all stress intensity measurements made on compact tension and WOL specimens and the nominal stress (σ_{nominal}) value obtained was compared to the materials' yield strength to determine whether gross yielding had occurred. As would be expected, the computed $\sigma_{\text{nominal}}/\sigma_{\text{yield}}$ values were virtually the same as R_{SC} computed from Eq. 3.

FRACTURE MECHANICS PROPERTIES MEASUREMENTS WITH WOL SPECIMENS

Wedge open loaded (WOL) specimens were used principally for performing measurements of threshold stress intensity (K_{TH}) in high-pressure hydrogen and helium.

Figure 3 shows the WOL specimen used for these measurements. The design follows that of Novak and Rolfe (Ref. 16) and their experimentally determined stress intensity equation for this specimen design is given below:

$$K = \frac{P C_3 \left(\frac{a}{w}\right)}{\sqrt{B B_n a}}, \text{ ksi } \sqrt{\text{in.}} \quad (8)$$

where

- P = applied load, kip
- $C_3 \left(\frac{a}{w}\right) = 30.96 \left(\frac{a}{w}\right) - 195.8 \left(\frac{a}{w}\right)^2 + 730.6 \left(\frac{a}{w}\right)^3 - 1186.3 \left(\frac{a}{w}\right)^4 + 754.6 \left(\frac{a}{w}\right)^5$
- a = measured crack length, in.
- w = specimen dimension, in. (2.55 in., 0.065 m)
- B = specimen thickness, in. (1 in., 0.0254 m)
- B_n = net specimen thickness, in. (0.90 in., 0.0223 m)

The measured crack length was determined from the following relationship:

$$a = \frac{a_1 + a_5 + 2(a_2 + a_3 + a_4)}{8} \quad (9)$$

where

- a_1 and a_5 = crack length measured at points 3.8×10^{-4} m (0.015 in.) in from the face notches along the two sides. The intersection of the crack at the face notches was difficult to accurately determine and thus a distance slightly in from the sides was chosen.
- a_3 = crack length at the center thickness
- a_2 = crack length midway between a_1 and a_3
- a_4 = crack length midway between a_3 and a_5

Crack lengths were also determined on all of the specimens from the compliance at the beginning of the test (initial crack length) and at the end of the test (final crack length). The compliance versus crack length relationship (Eq. 10) was obtained by Novak and Rolfe (Ref. 16) for the side-grooved specimen shown in Fig. 3.

$$\frac{E}{B} \left(\frac{v}{P} \right) = C_6 \left(\frac{a}{W} \right) \quad (10)$$

$$C_6 \left(\frac{a}{W} \right) = \exp \left[3.453 - 18.097 \left(\frac{a}{W} \right) + 42.314 \left(\frac{a}{W} \right)^2 - 64.677 \left(\frac{a}{W} \right)^3 + 36.845 \left(\frac{a}{W} \right)^4 \right]$$

where

- v = crack opening displacement at knife edge groove 0.0155 m (0.6 in.) from the load center line
- P = load, pounds
- E = Young's modulus, psi

The displacement gage calibration was made at the knife edge, 0.0165 m (0.65 in.), from the load centerline rather than at the knife-edge groove 0.0155 m (0.6 in.) from the load centerline as used by Novak and Rolfe for deriving Eq. 10. For predicting crack lengths, v/P in Eq. 10 was increased by $(0.65 + a)/(0.60 + a)$.

The method selected for measuring K_{TH} was patterned after one developed by Novak and Rolfe (Ref. 16). The technique involves maintaining a constant crack opening displacement and allowing the load, and thus the stress intensity, to decrease as the crack extends. The test apparatus for performing these measurements will be described in a subsequent section.

The load and COD were monitored during the threshold stress intensity measurements and, therefore, K_{IC} -type measurements were also obtainable. The K_{TH} measurements were performed during the period ASTM E399-70T (Ref. 17) for plane-strain fracture toughness measurements was in effect. For most of the K_{TH} measurements, the

specimens were loaded to somewhat above the 5-percent secant offset, but were rarely loaded to the failure load, as required for obtaining valid K_{IC} data in the subsequent ASTM standard E399-72 (Ref. 14). The stress intensity at the 5-percent secant offset (K_Q) was designated K_{IC} according to E399-70T if the E399-70T plane strain requirements were met.

The 5-percent secant intercept corresponds to 1.7- to 2.4-percent increase of crack length in the ASTM standard compact tension (CT) and bend specimen design. For the WOL specimen (Fig. 3), the 5-percent secant intercept corresponds to about 2.8-percent increase of crack length. Thus, the resulting K_{IC} stress intensity measured by the 5-percent secant offset on WOL specimens would be slightly higher than the stress intensity measured on CT specimens using the 5-percent secant intercept method, but the difference would not be significant.

FRACTURE MECHANICS PROPERTIES MEASUREMENTS WITH TAPERED DOUBLE CANTILEVER BEAM (TDCB) SPECIMEN

Nearly all of the cyclic load crack growth measurements and many of the Phase VIII crack arrest measurements were performed with (TDCB) specimens. The particular advantage of this specimen is that, over a considerable portion of the specimen, the applied stress intensity is virtually independent of crack length, and dependent only on the applied load. Thus, for cyclic load crack growth measurements, the specimen can be load-cycled at a constant stress intensity for a sufficient distance to accurately establish the cyclic load crack growth rate at that stress intensity. The TDCB specimen design also is advantageous for crack arrest-type K_{TH} measurements. This is because the stress intensity decreases considerably more rapidly during crack extension at constant COD than it does with the compact tension or WOL specimens in which K increases with crack length for a given load.

The TDCB test specimen design is shown in Fig. 4. Mostovoy et al. (Ref. 18) designed the specimen and showed that the compliance was linear (constant K) for crack lengths of approximately 0.0254 m (1.0 in.) to 0.0762 m (3.0 in.). Since

Mostovoy et al. performed their tests on an aluminum alloy, it was deemed desirable to perform a compliance calibration on one of the materials tested in this program.

The compliance calibration was performed (Ref. 19) at Rockwell International's Space Division on an HY100 TDCB specimen. The specimen was tension-tension cyclic loaded ($R = 0.1$) to extend the crack. Cycles with a maximum load of 17,800 newtons (4000 pounds) were applied for 20,000 cycles to extend the crack, and the maximum cyclic load was then reduced to 10,700 newtons (2400 pounds) for 20,000 cycles to produce a visible marker band to delineate the crack position. The compliance measurements were then performed before and after marking. This process of growing, marking, and making compliance measurements was continued for the length of the specimen. At each change of cyclic load, a test record of the load versus COD was made at the load centerline and at knife edges 12.7 mm (0.50 in.) from the load centerline. After the specimen was broken, the crack length (a) to each marker band was measured. This crack length was matched to its appropriate load versus COD record and a plot of (a) versus B (COD/load), where B is the specimen thickness, was generated. These data were then put into a Hewlett Packard Model 9100 programmable calculator with plotter which, with a regression analysis program, determined the best fit polynomial equations for the data points. Equations were derived relating: (1) compliance to crack length, and (2) load and crack length to stress intensity.

Figures 5 and 6 show the results of the compliance calibrations performed on the TDCB HY100 specimen. Included in Fig. 5 and 6 are the data point plots, best fit curves, and the equation for these curves. The variables in the equations are:

$$X = a \quad \text{and} \quad Y = B \left(\frac{\text{COD}}{P} \right)$$

where

- B = specimen thickness, inch
- COD = crack opening displacement, microinches
- P = load, pounds
- a = crack length from load centerline, inch

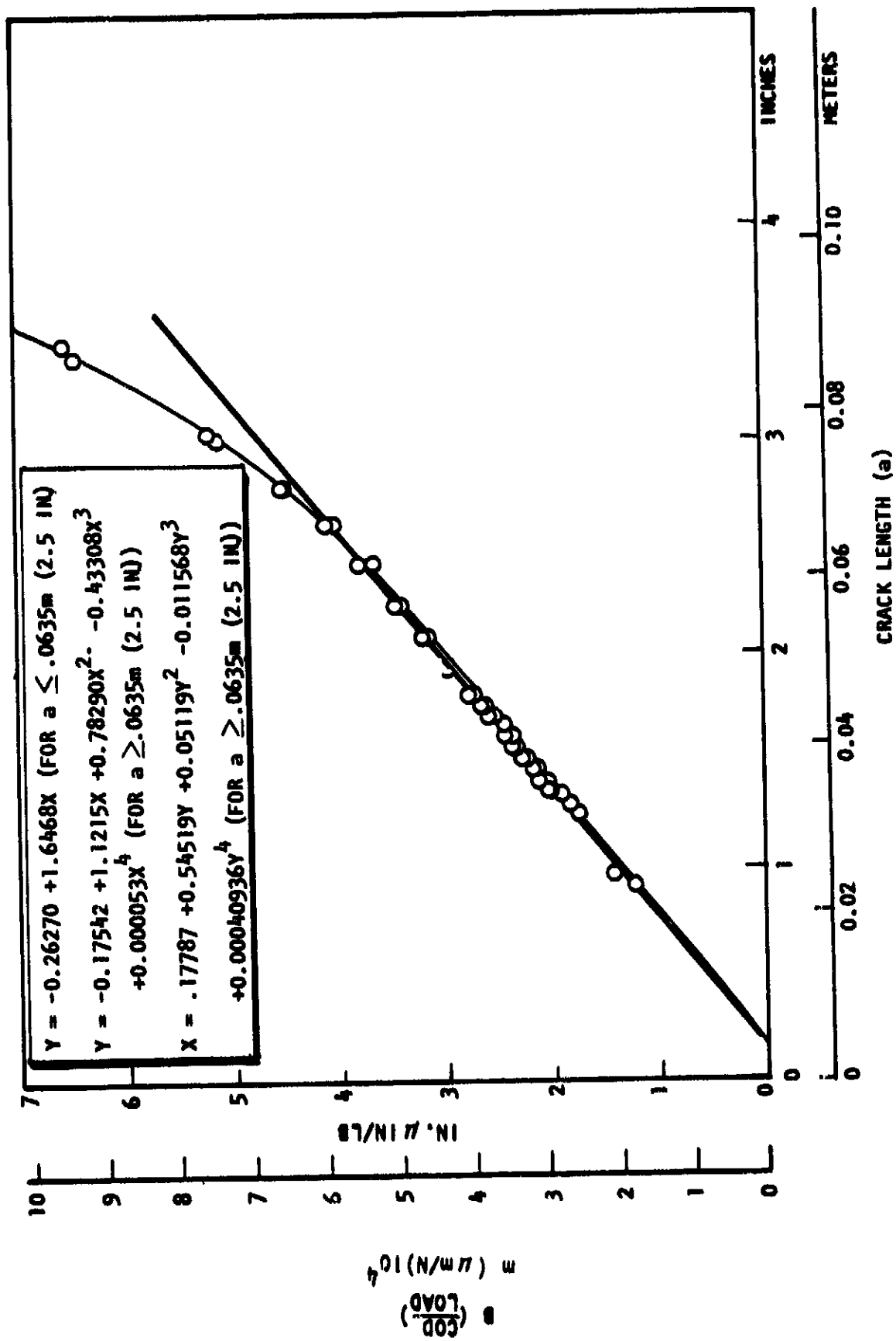


Figure 5. Compliance at the Load Centerline Versus Crack Length for an HY100 TDCB Specimen

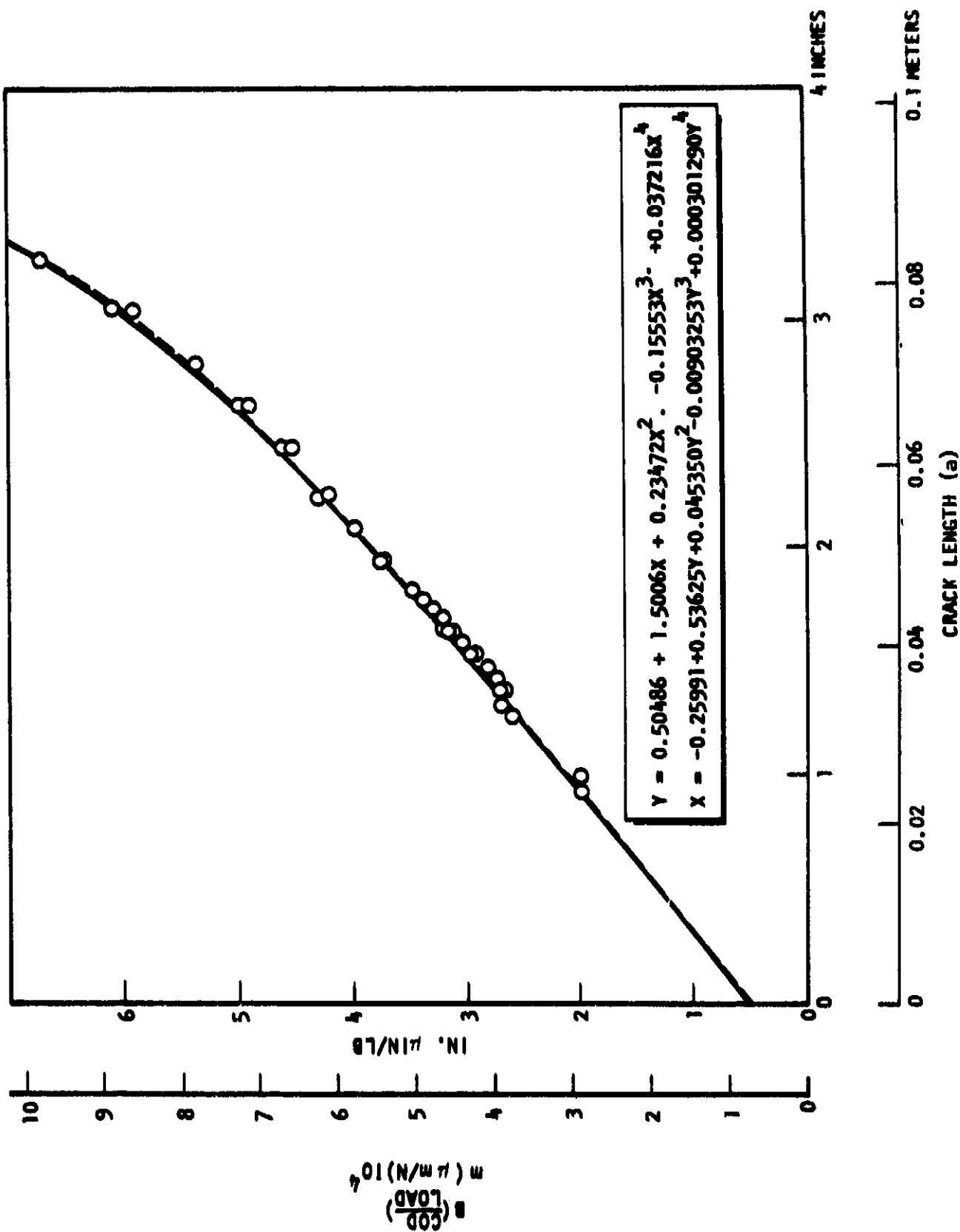


Figure 6. Compliance at the Specimen Mouth [0.0127m (0.5 in.) from Load Centerline] Versus Crack Length for an HY100 TDCB Specimen

Stress intensity equations were derived from the compliance data at the load centerline. The stress intensity is independent of crack length for crack lengths between 0.0254 m (1 in.) and 0.0635 m (2.5 in.). The following are the stress intensity equations.

$$K = P \sqrt{\frac{30 \times 10^6 \times 1.6468 \times 10^{-6}}{2 B \cdot B_n (1-\mu^2)}} \quad \text{for } 0.0254 \text{ m (1.0 in.)} \leq a \leq 0.0635 \text{ m (2.5 in.)} \quad (11)$$

$$K = P \sqrt{\frac{30 \times 10^6 (1.1215 + 1.5658a - 1.3a^2 + 0.32a^3) 10^{-6}}{2 \cdot B \cdot B_n (1-\mu^2)}} \quad \text{for } a \geq 0.0635 \text{ m (2.5 in.)} \quad (12)$$

where

- K = stress intensity, $\text{psi} \sqrt{\text{in.}}$
- P = load, pounds
- B = Specimen thickness, inch
- B_n = Net specimen thickness at bottom of side grooves, inch
- a = crack length, inch
- μ = Poisson's ratio

Modulus of elasticity of 30×10^6 was assumed for HY100 steel, and the same modulus was assumed for calculating the stress intensities for Inconel 718 specimens. These results, when normalized to specimen thickness and modulus, compare closely with those obtained by Mostovoy and co-workers (Ref. 18) for specimens fabricated from an aluminum alloy.

The compliance calibrations also were performed at the specimen mouth (Fig. 6), and the crack length as a function of specimen mouth compliance is given in

Eq. 13. Equation 13 was used to calculate the crack length during the cyclic and sustained load crack growth measurements.

$$a = -25991 + 0.53625Y + 0.045350Y^2 - 0.00903253Y^3 + 0.000301290Y^4 \quad (13)$$

The cyclic load crack growth rate measurements were performed at 1 cycle/sec at a load amplitude of $R = \text{Minimum Load/Maximum Load} = 0.1$. Several data points were usually obtained at each stress intensity, and only the average values of the cyclic crack growth rates were plotted.

The sustained load K_{TH} measurements were performed by loading the specimen to a stress intensity above K_{TH} and allowing the crack to propagate while holding the COD constant.

Test Apparatus Used for Performing Fracture Mechanics Measurements

Two test vessels were used for performing the fracture mechanics measurements. One vessel is 0.15 m (6 in.) in diameter and 0.41 m (16 in.) long. The vessel is rated at 103.4 MN/m² (15,000 psi), and is designed for ambient-temperature service only. For the fracture mechanics tests, the vessel contained the specimen, loading grips or clevis, load cell, and displacement transducer as is shown schematically in Fig. 7. The specimens were loaded by means of a 290,000 newton (65,000 pound) loading ram that extended into the side (top of the picture) of the vessel through sliding seals. The electrohydraulic loading column was controlled from the load cell signal for the K_{IC} and cyclic load crack growth rate measurements, and from the signal from the COD transducer for the K_{TH} measurements.

The second vessel is of 0.15 m (6 in.) diameter and 0.25 m (10 in.) long, and is rated at 41.3 MN/m² (6000 psi) at ambient and cryogenic temperatures. This vessel was used for performing K_{TH} measurements at ambient and cryogenic temperatures on WOL specimens, and cyclic load crack extension measurements at cryogenic temperatures on WOL specimens. The vessel is shown in Fig. 8.

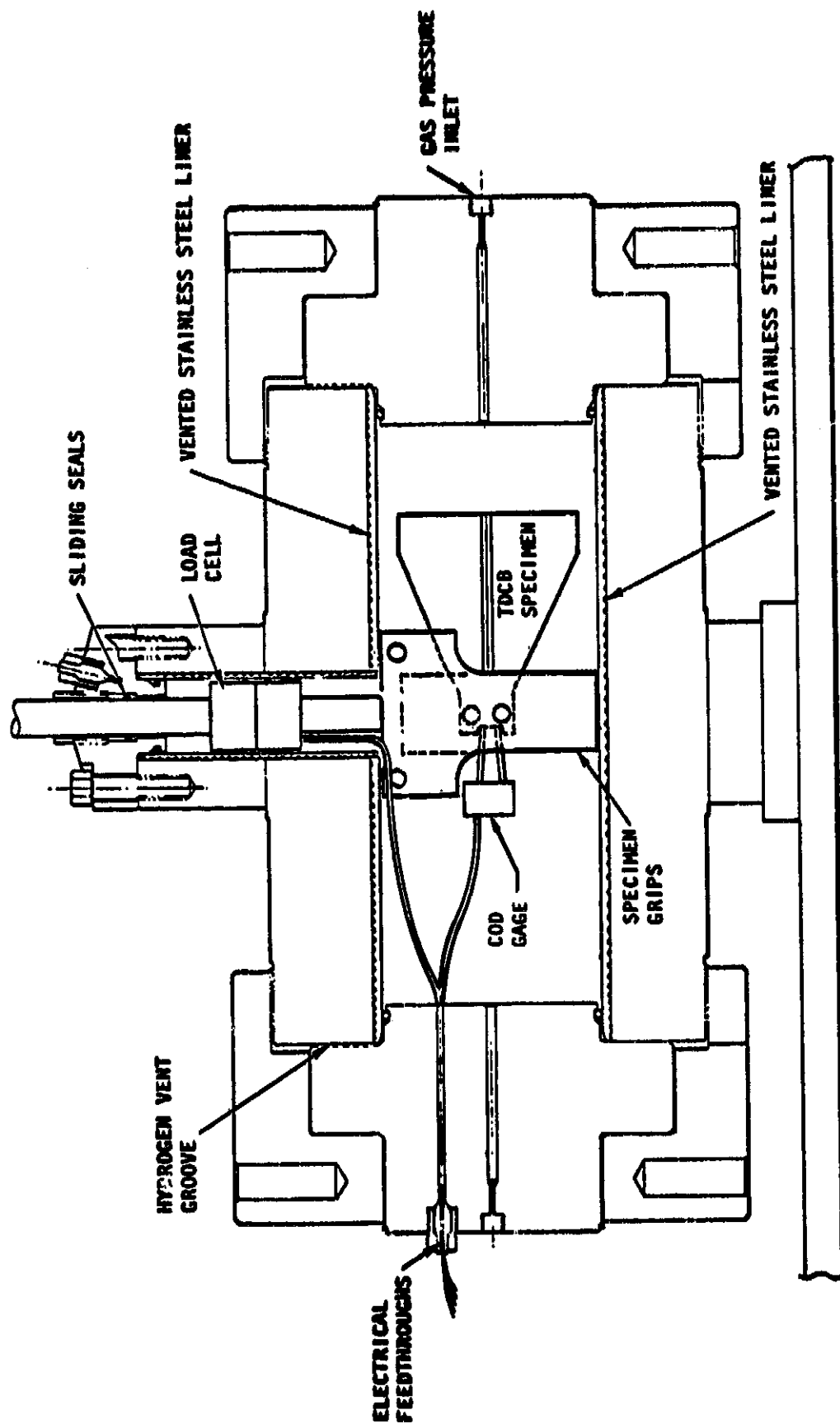


Figure 7. Vessel Used for Performing Fracture Mechanics Tests on Compact Tension, WOL, and TDCB Specimens in Ambient-Temperature Environments at Pressures up to 103.4 MN/m² (15,000 psi)

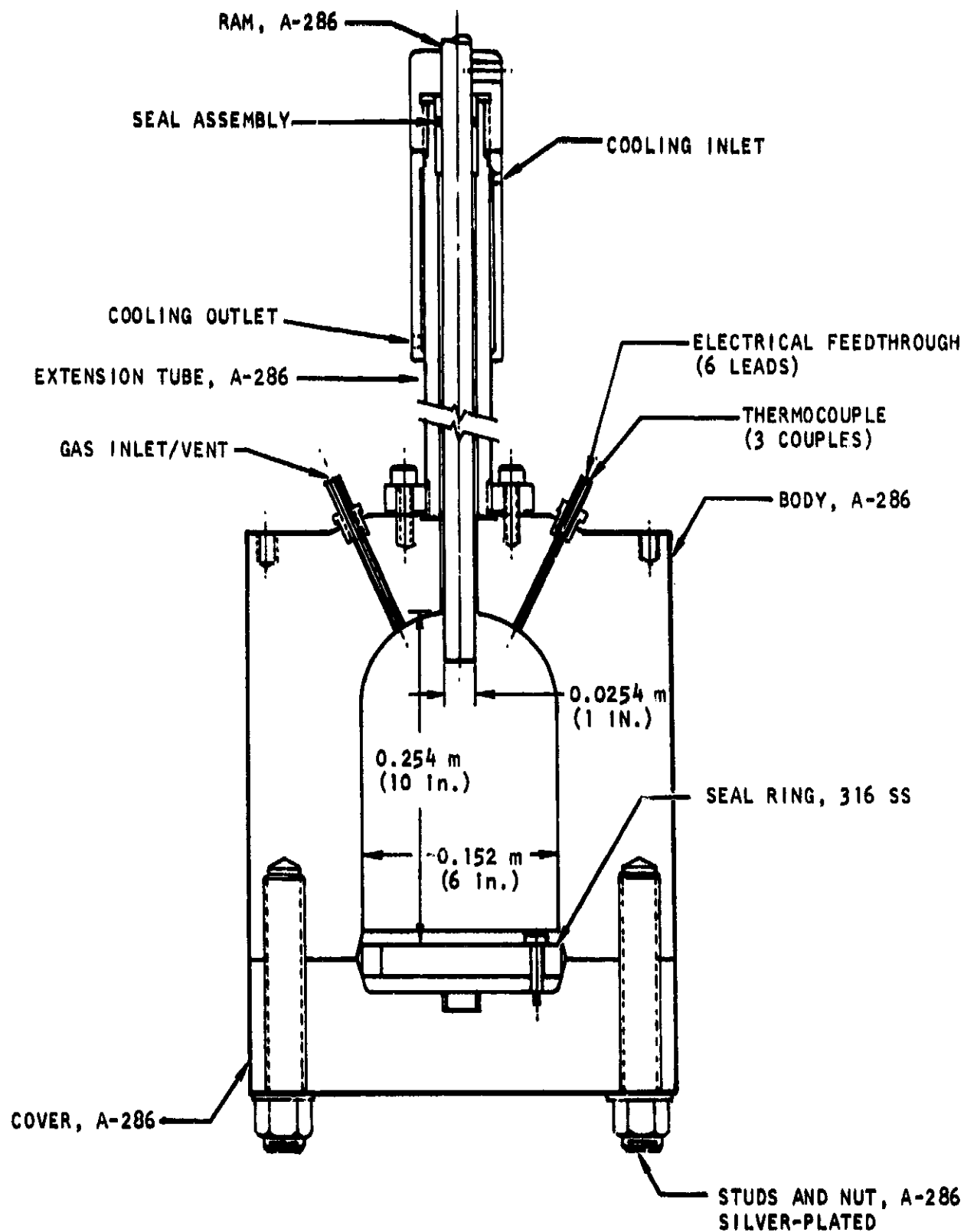


Figure 8. Pressure Vessel Used to Perform Tests on Modified WOL Specimens in High Pressure Hydrogen

A special loading column was developed for performing the K_{TH} measurements in high-pressure environments, and the loading apparatus is shown schematically in Fig. 9. A load was exerted on the specimen by rotating the torque shaft that extends through a sliding seal located above the vessel. By rotating the loading ram, a compressive force was exerted across the load cells, and this force in turn acts as a tension load across the specimen. The specimen was held from turning by the two bolts at the bottom of the apparatus. When the vessel is pressurized, the pressure acts to push the loading ram through the sliding seals out of the vessel. To ensure that this pressure load was not transmitted to the specimen, the loading ram was held in place by means of a spacer located between the torque shaft coupler and the inside vessel top. The two bolts at the bottom of the vessel were loosened so that the spacer takes the entire pressure load.

The displacement was monitored during the test by means of NASA-type clip-on gage positioned on the specimen in the usual manner.

During the latter part of the program, the loading column was modified to increase its stiffness and thus increase the rate of stress intensity decrease with increasing crack length. The modification consisted basically of inverting the test specimen to essentially eliminate the stub shaft and increase the size of the loading bridge.

The specimens were loaded hydraulically for the cryogenic-temperature, cyclic load, crack growth measurements. For these tests, the spacer coupler and stub shaft were removed and the torque shaft was screwed directly into the specimen. An adapter was placed between the loading bridge and the top of the vessel so that a compression load was exerted across the dual load cells while the specimen was loaded in tension. The vessel was placed in a test frame and the torque shaft was connected to the hydraulic cylinder.

Tests were performed at ambient temperature and at temperatures as low as 144 K (-200 F). For the cryogenic tests, heat exchanger openings were machined into the pressure vessel, and a heat exchanger in the form of a coil was installed

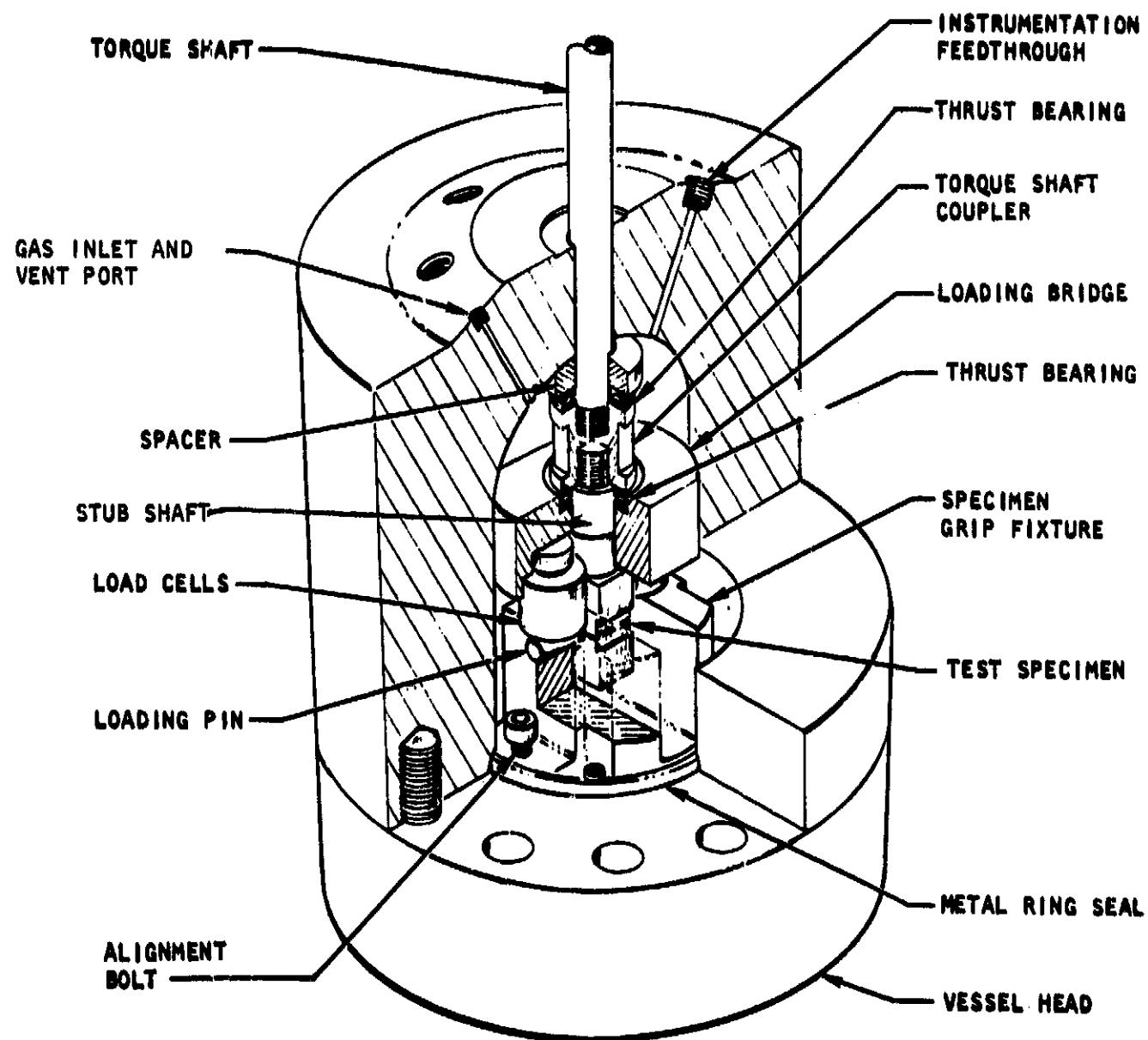


Figure 9. Apparatus for Performing Threshold Stress Intensity Measurements in High Pressure Environments

around the inside wall of the vessel. Liquid nitrogen was circulated through the heat exchanger on demand from a temperature controller that regulates the LN_2 flow through a solenoid valve. The pressure vessel was also surrounded by a dewar filled with cold GN_2 and the temperature maintained in the dewar by inflow of LN_2 controlled by means of a temperature controller.

There were three thermocouples inside the vessel. One of the thermocouples was located at the inside vessel wall, and its signal was sensed by the temperature controller controlling the LN_2 flow through the heat exchanger inside the vessel. The other two thermocouples were used to measure and record the test temperature. A thermocouple, spot welded to the outside vessel wall, was used for controlling the temperature in the dewar surrounding the pressure vessel. The temperature was controlled within ± 5.5 K (10 F) during the cryogenic-temperature tests. During most of the test period, the temperature deviation was, however, considerably less than 5.5 K (10 F).

TEST ENVIRONMENT

Considerable care was taken that the hydrogen test environment for the tensile and fracture mechanics measurements was of high purity. High-purity bottled hydrogen was further purified by passing through an Engelhard DeOxo unit, BaO desiccant, and a mixture of activated charcoal and activated alumina maintained at boiling nitrogen temperature. The hydrogen was then pressurized by means of a diaphragm compressor or a nonlubricated air-driven compressor encased in a box purged with argon. The hydrogen was then further purified by passing through a vessel containing activated charcoal and a molecular sieve, while the vessel was maintained at boiling nitrogen temperature.

Purity of the purified, high-pressure hydrogen was analyzed to be <0.9 ppm N_2 , ~ 0.2 ppm O_2 , and ~ 1.3 ppm H_2O , with no measurable CO or CO_2 . Bottled helium with typical impurity contents of 3 ppm O_2 , 1 ppm H_2O , and 6 to 7 ppm N_2 was used for comparison tests.

To remove air from the pressure vessels used for performing the tensile tests, the vessels were evacuated to <20 microns and backfilled to 0.69 MN/m^2 (100 psi) with hydrogen three times. This was then followed by five hydrogen pressurization-depressurization cycles between a pressure equal to the final test pressure and about 0.34 MN/m^2 (50 psi) hydrogen before the final pressurization to the test pressure. The pressure vessels used for performing the fracture mechanics measurements were evacuated to <20 microns and backfilled three times to 6.89 MN/m^2 (1000 psi). This was followed by three hydrogen pressurization-depressurization cycles from the test pressure to about 1.38 MN/m^2 (200 psi) before final pressurization to the test pressure. For tests conducted at less than 6.89 MN/m^2 (1000 psi), the pressure vessels were purged seven times between <20 microns and the test pressure prior to final test vessel pressurization.

ACOUSTIC EMISSION APPARATUS

Crack growth during testing of the WOL specimens was monitored by acoustic emission. It has been well established during recent years that stress-induced slip, twinning, and fracture can emit a low-level sound, a phenomenon known as acoustic emission. The test method employs a piezoelectric crystal detector that is in direct or indirect contact with the specimen. When deformation or cracking occurs, the crystal produces signals that may be amplified and recorded on tape together with the load or may be used to drive a loud speaker. The acoustic method is extremely sensitive to small crack extensions, and may give definite indications of crack movement before either an electrical potential or a displacement gage gives a discernible output. Another advantage of this method is its relative simplicity and adaptability to a variety of specimen types and testing situations.

Acoustic emission can be utilized for detecting crack growth during threshold measurements conducted on modified WOL specimens in high-pressure hydrogen environments. To perform these measurements, the specimens are deflected until crack growth occurs. The crack opening displacement is then held constant until the crack ceases to propagate. Thus initiation and termination of crack growth can be detected by acoustic emission if the emissions from extraneous sounds (e.g., those from loading) can be filtered out.

While the amplitudes of the acoustic signals seem to increase with the amount of material involved in a given increment of crack movement, there is no technique at present for relating the emission to the extent of crack growth. For this reason, the acoustic technique is best used in conjunction with either potential measurements or displacement gages.

The acoustic emission circuitry was designed and set up on a prior IR&D program conducted at Rocketdyne. A block diagram of the apparatus is shown in Fig. 10. The circuitry includes an Endevco 2217 accelerometer having a resonant frequency of 30 kHz. The accelerometer output is amplified and filtered* before being processed, i.e., integrated and rectified. An amplification of 200,000 is imposed on the preprocessed signal. The final signal is recorded simultaneously on a strip-chart recorder for analog output and in a counter-printout system. The final signal is a shaped pulse that is produced for every incoming signal burst above a preset voltage level. The duration and height of the pulse are determined by the time constant of the RC integrator. In the tests described below, the time constant was approximately 20 milliseconds. The counter/printout system is controlled by a preset counter, and records total count in predetermined time intervals. Total count and count rate (slope of total count versus time plot) are the only parameters having quantitative significance at the present time. However, pulse height and pulse energy, and emission frequencies have unique features as characterizing parameters to distinguish such things as deformation versus fracture. Further development work is required before these parameters can be used. The final signal is also fed into an oscilloscope for data viewing (Fig.10).

The effort assigned to the acoustic emission phase was limited, and thus only a small fraction of the K_{TH} tests were monitored by acoustic emission. Moreover, the circuitry design was new and not completely "de-bugged." There were several persistent problems. One of these, which was concerned with extraneous emissions from the flow of LN_2 and from a solenoid valve in the nitrogen line, prevented the

*Frequencies up to 20 kHz are removed by filtering.

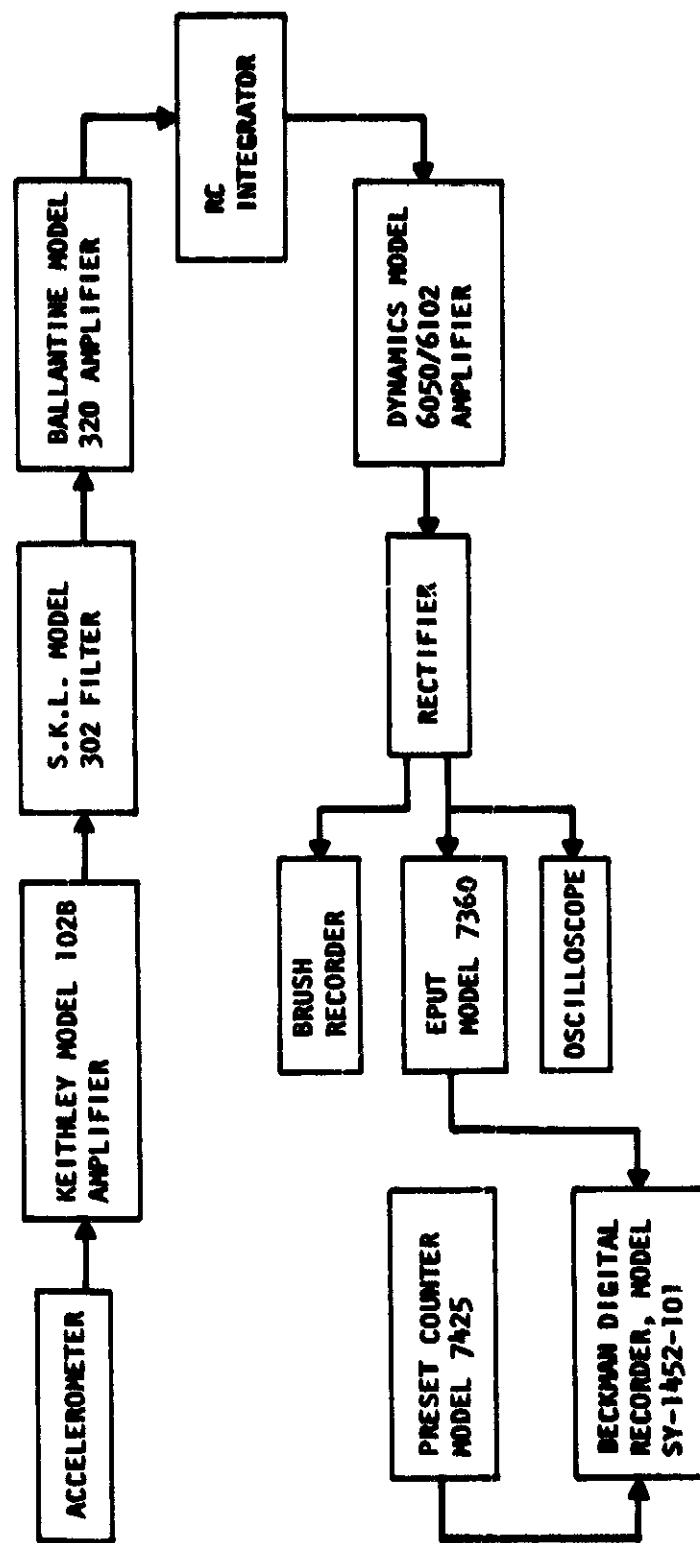


Figure 10. Block Diagram of Acoustic Emission Apparatus

successful conduct of any cryogenic test. An auxiliary bucking circuit was designed to eliminate these unwanted emissions. Emissions from the LN_2 flow were eliminated but not those from the solenoid valve. In all tests, the accelerometer was attached via a stud to a collar around the loading column. Despite this remote location external to the test chamber, the accelerometer performed satisfactorily, with no detectable loss in sensitivity to crack-induced emissions from the test specimen.

RESULTS AND DISCUSSION

PHASE I. TENSILE PROPERTIES OF ALLOYS IN HYDROGEN ENVIRONMENTS

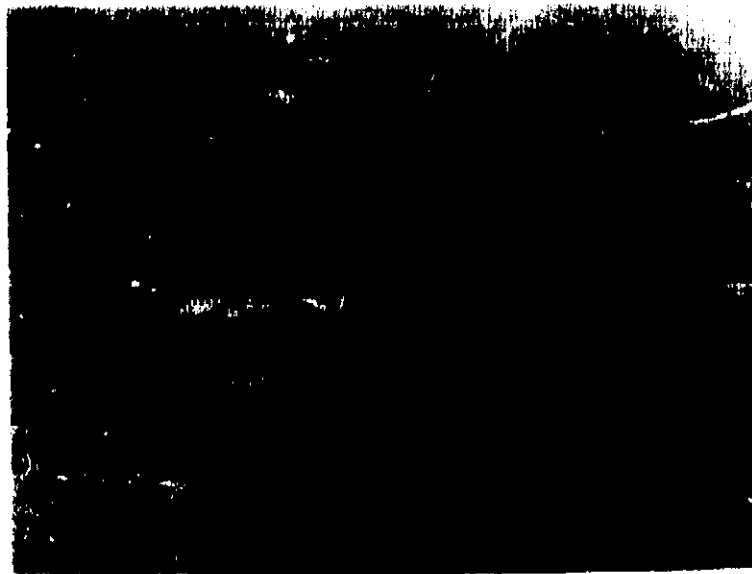
Under this phase, the effects of hydrogen environments on tensile properties were determined for Inconel 625, AISI Type 321 stainless steel, Ti-5Al-2.5 Sn ELI, and OFHC copper. Unnotched specimens were tested in air under ambient conditions and unnotched and notched specimens were tested in 34.5 MN/m^2 (5000 psi) hydrogen environments at ambient temperature and 144 K (-200 F). The average tensile properties are given in Table 7, and the data for individual specimens are presented in Appendix B. As has been found in previous programs for other materials, none of the materials tested experienced any decrease in yield strength due to the hydrogen environment.

For Inconel 625, the ductility of unnotched specimens was considerably reduced and the strength and ductility of notched specimens was moderately reduced in 34.5 MN/m^2 (5000 psi) hydrogen compared to 34.5 MN/m^2 (5000 psi) helium at room temperature. Even the ultimate strength of the unnotched specimens was somewhat reduced in hydrogen at room temperature. The reduction of notch strength of Inconel 625 by 34.5 MN/m^2 (5000 psi) hydrogen is similar to that found for the more moderately embrittled conditions of Inconel 718 although Inconel 625 is not as strong an alloy. Generally, for similar materials, it has been found previously (Ref. 4), that the stronger the alloy, the greater the susceptibility to hydrogen environment embrittlement. The reduction of ductility of Inconel 625 by hydrogen at room temperature was quite severe although considerable ductility was still present. The unnotched Inconel 625 specimens tested in hydrogen at room temperature contained surface cracks in the necked-down region, which were rather large and deep (Fig. 11) and are similar to those that have been observed on steels such as ASTM A-302. The effect of 34.5 MN/m^2 (5000 psi) hydrogen on the tensile properties of Inconel 625 at 144 K (-200 F) was insignificant and no surface cracking was observed at this temperature.

TABLE 7. AVERAGE TENSILE PROPERTIES OF ALLOYS IN VARIOUS ENVIRONMENTS

Material	Specimen Type*	Environment			Test Results								
		Temperature		Type	Pressure		Strength			Ductility			
		K	F		MN/m ²	psig	ksi	MN/m ²	ksi				
Inconel 625	UN	Rn	Rn	Air	0	0	648	94	993	144	--	54	50
	UN	Rn	Rn	He	34.5	5000	634	92	993	144	--	50	55
	UN	Rn	Rn	H ₂	→	→	600	87	889	129	0.90	18	20
	N	Rn	Rn	He	→	→	--	--	1430	208	--	9.4	--
	N	Rn	Rn	H ₂	→	→	--	--	1090	156	0.76	4.6	--
	UN	144	-200	He	→	→	710	103	1130	164	--	52	45
	UN	144	-200	H ₂	→	→	696	101	1120	162	--	48	43
	N	144	-200	He	→	→	--	--	1460	212	--	8.1	--
	N	144	-200	H ₂	→	→	--	--	1520	221	--	6.9	--
AISI 321	UN	Rn	Rn	Air	0	0	221	32	600	87	--	71	77
	UN	Rn	Rn	He	34.5	5000	200	29	579	84	--	66	63
	UN	Rn	Rn	H ₂	→	→	255	37	593	86	--	60	64
	N	Rn	Rn	He	→	→	--	--	779	113	--	6.4	--
	N	Rn	Rn	H ₂	→	→	--	--	683	99	0.88	2.3	--
	UN	144	-200	He	→	→	--	--	855	124	--	67	48
	UN	144	-200	H ₂	→	→	--	--	841	122	--	56	43
	N	144	-200	He	→	→	--	--	986	143	--	12	--
	N	144	-200	H ₂	→	→	--	--	972	141	--	12	--
Ti-5 Al-2.5 Sn ELI	UN	Rn	Rn	Air	0	0	786	114	820	119	--	31	18
	UN	144	-200	He	34.5	5000	--	--	1040	151	--	26	14
	UN	144	-200	H ₂	34.5	5000	738	107	1030	149	--	30	9
	N	144	-200	He	34.5	5000	--	--	1570	228	--	1.7	--
	N	144	-200	H ₂	34.5	5000	--	--	1570	227	--	1.3	--
	UN	Rn	Rn	Air	0	0	117	17	193	28	--	84	5
	UN	Rn	Rn	He	34.5	5000	83	12	193	28	--	85	63
	UN	Rn	Rn	H ₂	34.5	5000	76	11	186	27	--	84	65
	N	Rn	Rn	He	34.5	5000	--	--	296	43	--	25	--
OFHC Copper	N	Rn	Rn	H ₂	34.5	5000	--	--	290	42	--	25	--
	N	144	-200	He	34.5	5000	--	--	283	41	--	29	--
	N	144	-200	H ₂	34.5	5000	--	--	303	44	--	24	--
	UN	Rn	Rn	Air	0	0	--	--	--	--	--	--	--
	UN	Rn	Rn	He	34.5	5000	--	--	--	--	--	--	--
	UN	Rn	Rn	H ₂	34.5	5000	--	--	--	--	--	--	--
	N	Rn	Rn	He	34.5	5000	--	--	--	--	--	--	--
	N	Rn	Rn	H ₂	34.5	5000	--	--	--	--	--	--	--
	N	144	-200	He	34.5	5000	--	--	--	--	--	--	--

^aUN = unnotched, N = notched, K_t = 8.7 for all notched specimens



Photomacrograph 5x



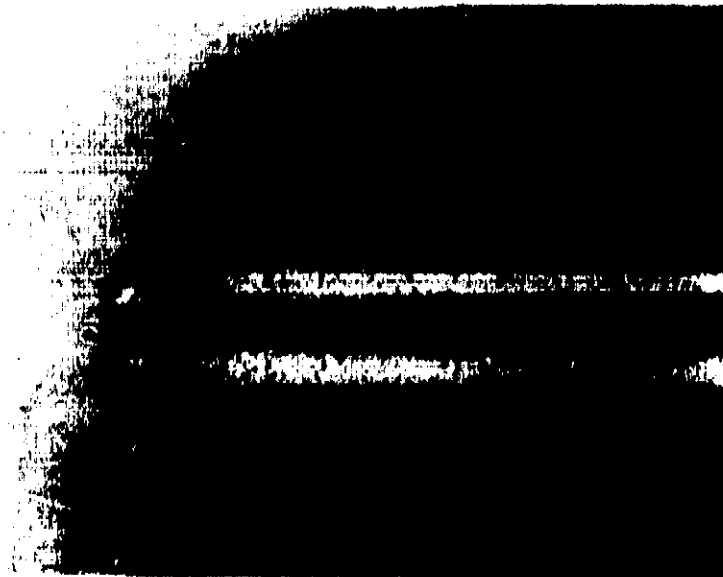
Photomicrograph 100x

Figure 11. Inconel 625 Unnotched Specimen Tested
in 34.5 MN/m^2 (5000 psi) Hydrogen at
Room Temperature

For AISI 321 stainless steel, the strength and ductility of notched specimens was slightly reduced by 34.5 MN/m^2 (5000 psi) hydrogen compared to 34.5 MN/m^2 (5000 psi) helium at room temperature. At 144 K (-200 F), the properties of notched AISI 321 stainless-steel specimens were essentially unaffected by hydrogen. For unnotched AISI 321 stainless-steel specimens, the reduction of area was decreased very slightly by hydrogen at room temperature but to a somewhat greater extent at 144 K (-200 F). The unnotched AISI 321 stainless-steel specimens tested in hydrogen contained surface cracks. At room temperature, numerous, small, very shallow, blunt surface cracks (Fig. 12) formed over the entire reduced section. At 144 K (-200 F), the surface cracks (Fig. 13) were larger, considerably sharper, and deeper, but were restricted mainly to the necked-down region. The larger cracks formed at 144 K (-200 F) would account for the somewhat greater decrease in the reduction of area by hydrogen at 144 K (-200 F) than at room temperature. The behavior of the AISI 321 stainless steel in hydrogen is similar to that observed for other stainless steels (e.g., AISI 304), which tend to form martensite during deformation. The effects of hydrogen environments on these stainless steels have been attributed to cracking in the martensite in the hydrogen environment (Ref. 4 and 5). At -200 F, the amount of plastic deformation needed to form martensite is less than at room temperature.

In a previous program (Ref. 4), it was found that the $N_{\text{H}_2}/N_{\text{He}}$ ratio for the Ti-5Al-2.5Sn ELI alloy was approximately 0.8 for pressures of 68.9 MN/m^2 (10,000 psi). However, tests were performed only at room temperature. The results in Table 7 show that this alloy was essentially unaffected by 34.5 MN/m^2 (5000 psi) hydrogen at 144 K (-200 F). No surface cracks were observed in specimens tested in hydrogen.

The results in Table 7 show that OFHC copper was essentially unaffected by 34.5 MN/m^2 (5000 psi) hydrogen both at room temperature and 144 K (-200 F). No surface cracks were formed.

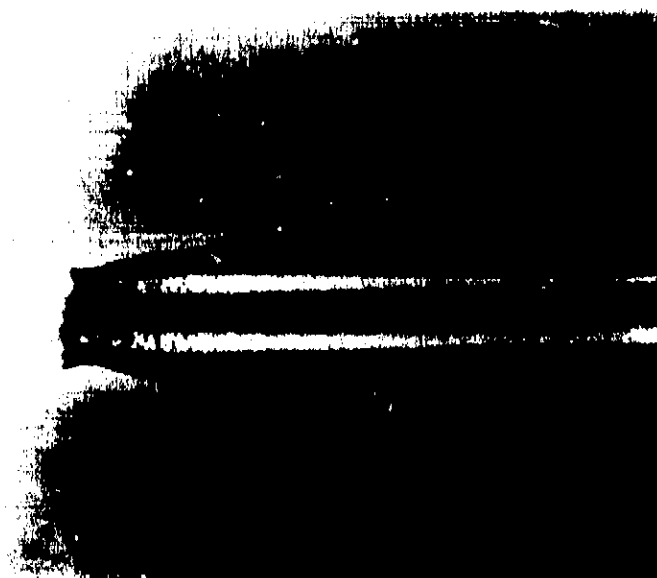


Photomacrograph 5x

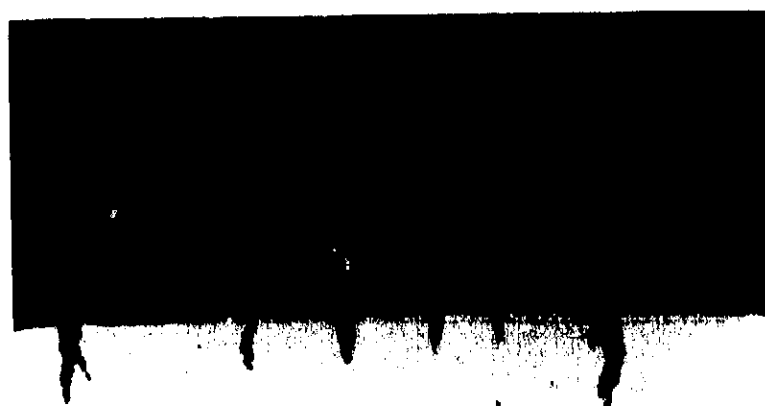


Photomicrograph 100x

**Figure 12. AISI 321 Stainless Steel Unnotched Specimen
Tested in 34.5 MN/m^2 (5000 psi) Hydrogen
at Room Temperature**



Photomacrograph 5x



Photomicrograph 100x

Figure 13. AISI 321 Stainless Steel Unnotched Specimen
Tested in 34.5 MN/m^2 (5000 psi) Hydrogen
at 144 K (-200 F)

PHASE II. THRESHOLD STRESS INTENSITIES OF ALLOYS IN HYDROGEN ENVIRONMENTS

The threshold stress intensity (K_{TH}) was determined for various alloys when exposed to 34.5 MN/m^2 (5000 psi) helium and 34.5 MN/m^2 (5000 psi) hydrogen environments at ambient and at 144 K (-200 F). The alloys tested were Inconel 718 in the A and C heat treatment conditions (Table 5), Inconel 625, AISI 321 stainless steel, A-286 stainless steel, Ti-5Al-2.5Sn ELI, 2219-T87 aluminum alloy, and OFHC copper. All tests were performed on WOL specimens using the loading column shown in Fig. 8. The WOL specimens were fabricated from the same materials as were the tensile specimens for which the test results are given in Table 7. The Inconel 718 WOL specimens were fabricated from the Inconel 718 rolled bar (Table 1).

As described in the Procedures section, the method used for performing the K_{TH} measurements also yielded fracture toughness (K_{IC}) values for many of the conditions tested.

The results of the fracture mechanics properties measurements are tabulated in Table 8 and the average K_{IC} and K_{TH} values are summarized in Table 9. Table 10 lists the yield strengths and maximum stress intensities that meet the $2.5 (K_I/\sigma_{YS})$ requirements for the WOL specimen dimensions used for these tests.

Table 8 contains the K_{IC} fracture toughness and the stress intensity, K_{max} , at which loading was stopped and the crack allowed to propagate until arrested at K_{TH} . The K_{max} stress intensity was computed from the maximum load and the initial crack length. This frequently resulted in an underestimation of K_{max} because of crack growth prior to obtaining the maximum load.

For each stress intensity, Table 8 also indicates for the K_{IC} and K_{TH} stress intensities whether plane strain fracture toughness requirements according to ASTM E399-70T (Ref. 17) were met. For a K_{IC} value to be valid, the following test requirements must be met: (1) the load rate must be such that the rate of increase

TABLE 8. RESULTS OF FRACTURE MECHANICS PROPERTY ME
VARIOUS ALLOYS IN 0.1 MN/m² (1-ATM PRESSURE) AIR A

Material	Specimen No.	Test Environment		K _{IS}							K _{max}				K Final				Time sec x 10 ³
		Type	Tempera- ture		K _Q		Meets ASTM Requirements			Nominal Stress Less than σ _{ys}	MN m ² √m		Nominal Stress Less than σ _{ys}	MN m ² √m		KSI √in.			
			K	F	MN m ² √m	KSI √in.	2.5 K (K/σ _{ys}) ²	0.8 K _Q Require- ment	Crack Uniformity										
Inconel 718 heat treated at 1214K, 991 to 894K (1725F, 1325 to 1150F)	A7	Air (1 atm)	295	70	82	75	yes	yes	yes	yes	82	75	yes	79(c)	72(c)	6.3			
	A2	He	↓	↓	75	68	yes	yes	yes	↓	75	68	↓	60	55	23			
	A9	He	↓	↓	80	73	yes	yes	yes	↓	80	73	↓	55(c)	50(c)	18			
	A3	H ₂	↓	↓	--	--	--	--	yes	↓	36	32	↓	--	--	--			
	A4	H ₂	↓	↓	--	--	--	--	no	↓	27	25	↓	--	--	--			
	A5	H ₂	↓	↓	--	--	--	--	yes	↓	26	24	↓	22	20(c)	2.1			
	A13	H ₂	↓	↓	--	--	--	--	yes	↓	23	21	↓	14	13	--			
	A1	He	144	-200	98	89	yes	yes	no	↓	98	89	↓	--	--	--			
	A12	He	↓	↓	--	--	↓	↓	yes	↓	81(c)	73(c)	↓	81(c)	74(c)	7.1			
	A10	H ₂	↓	↓	--	--	↓	↓	yes	↓	79(c)	71	↓	80(c)	72(c)	2.1			
	A11	H ₂	↓	↓	--	--	↓	↓	yes	↓	76	69	↓	63(c)	57(c)	32			
Inconel 718 Heat treated at 1325K, 1033 to 922K (1925F, 1400 to 1200F)	B2	He	295	70	116	105	margin.	no	yes	↓	N.O.	112	↓	111(c)	101(c)	6.1			
	B6	He	↓	↓	122	111	no	yes	yes	↓	N.O.	N.O.	↓	112	102	7.0			
	B3	H ₂	↓	↓	--	--	--	--	yes	↓	70	64	↓	55	50	2.6			
	B9	H ₂	↓	↓	110	100	yes	--	yes	↓	110	100	↓	N.O.	N.O.	9.1			
	B10	H ₂	↓	↓	N.O.	N.O.	--	--	yes	↓	56	51	↓	42	38	2.4			
	B7	He	144	-200	128	117	no	yes	no	↓	N.O.	N.O.	↓	139(c)	126(c)	6.5			
	B8	He	↓	↓	118	108	yes	no	--	↓	N.O.	N.O.	↓	139(c)	126(c)	7.2			
	B11	He	↓	↓	120	109	yes	yes	yes	↓	N.O.	N.O.	↓	140(c)	127(c)	6.1			
	B12	H ₂	↓	↓	120	109	yes	no	yes	↓	N.O.	N.O.	↓	127(c)	116(c)	5.8			
	B13	H ₂	↓	↓	122	111	yes	yes	no	↓	N.O.	N.O.	↓	119(c)	108(c)	5.9			
	B14	H ₂	↓	↓	119	109	yes	yes	yes	↓	N.O.	N.O.	↓	125(c)	113(c)	6.3			
Inconel 625	2	He	295	70	69	63	no	yes	no	↓	76	70	↓	76	70	6.5			
	3	He	↓	↓	99	90	no	yes	yes	↓	99	90	↓	99	90	14			
	1	H ₂	↓	↓	54	49	yes	yes	yes	↓	62	56	↓	67	56	6.1			
	7	H ₂	↓	↓	81	73	no	no	yes	↓	105(c)	96(c)	↓	105(c)	96(c)	26			
	4	He	144	-200	107(c)	97(c)	↓	yes	--	↓	131(c)	119(c)	↓	130(c)	118(c)	-0.7			
	5	He	↓	↓	108	108	↓	yes	yes	↓	160	145	↓	156	142	5.9			
	6	He	↓	↓	108	98	↓	yes	no	yes	172(c)	157(c)	↓	166(c)	151(c)	7.0			
	9	H ₂	↓	↓	104	94	↓	no	yes	yes	115	105	↓	123	112	6.5			
	8	H ₂	↓	↓	118	107	↓	yes	no	no	156	141	↓	150	137	25			
AISI 321 Stainless Steel	1	He	295	70	33	30	↓	yes	no	no	43(c)	39(c)	↓	43(c)	39(c)	6.1			
	6	He	↓	↓	40	36	↓	--	no	no	47(c)	43(c)	↓	44(c)	40(c)	6.8			
	3	H ₂	↓	↓	28(c)	25(c)	↓	yes	yes	yes	37(c)	34(c)	↓	32(c)	29(c)	0.5			
	3	H ₂	↓	↓	--	--	↓	--	--	--	111(c)	101(c)	↓	111(c)	101(c)	1.6			
	5	H ₂	↓	↓	40	37	no	yes	yes	no	47	42	↓	43	39	10.0			
	4	He	144	-200	30	27	↓	yes	no	yes	91(c)	83(c)	↓	86(c)	79(c)	1.1			
	8	He	↓	↓	38	35	↓	yes	yes	no	47	42	↓	38	35	8.8			
	7	H ₂	↓	↓	38	35	↓	yes	no	no	34(c)	49(c)	↓	41(c)	37(c)	5.9			
	9	H ₂	↓	↓	24	22	yes	no	yes	yes	31	29	↓	31	28	6.1			
A-286 Stainless Steel	4	He	295	70	139	126	no	no	yes	no	159	145	↓	159	145	7.0			
	8	He	↓	↓	153	140	↓	yes	yes	no	181	165	↓	180	163	6.3			
	3	H ₂	↓	↓	89(c)	81(c)	↓	no	yes	yes	120	109	↓	120	109	6.8			
	5	H ₂	↓	↓	79	72	↓	no	yes	yes	170(c)	154(c)	↓	140(c)	127(c)	33			
	10	H ₂	↓	↓	133(c)	121(c)	↓	yes	yes	no	165(c)	150(c)	↓	113(c)	103(c)	285			
	4	He	144	-200	164	149	↓	yes	yes	no	196	178	↓	194	177	8.3			
	7	He	↓	↓	112	102	↓	no	yes	no	204	185	↓	196	179	5.8			
	9	H ₂	↓	↓	152	138	↓	yes	yes	no	199	181	↓	199	181	7.6			

FOLDOUT FRAME

MECHANICS PROPERTY MEASUREMENTS ON MODIFIED WOL SPECIMENS OF
(ATM PRESSURE) AIR AND IN 34.5 MN/m² (5000 PSI) H₂ AND He

al less ys	K _{TH}							Test Description
	K Final		Time Under Load		Meets. ASTM Requirements		Nominal Stress Less than σ_{ys}	
	$\frac{MN}{m^2}$	\sqrt{m} KSI $\sqrt{in.}$	seconds $\times 10^{-4}$	Hours	$\left(\frac{K_{TH}}{\sigma_{ys}}\right)^2$	Crack Uniformity		
	79(c)	72(c)	6.8	19	yes	--	yes	
	60	55	23	64	↓	yes		
	55(c)	50(c)	18	50	↓	no		
	--	--	--	--	--	--		Specimen failed during hold period
	--	--	--	--	--	--		Specimen failed during hold period
	22	20(c)	2.7	7.5	yes	no		Crack arrest determined by backing off of load
	14	13	--	--	yes	yes		
	--	--	--	--	--	--		Crack extended nearly entire length of specimen during pop-in
	81(c)	74(c)	7.2	2.0	yes	--		
	80(c)	72(c)	2.3	6.5	↓	no		H ₂ pressure ranged between 17.6 MN/m ² (2550 psi) and 34.5 MN/m ² (5000 psi) during test
	63(c)	57(c)	32	89	↓	no		
	111(c)	101(c)	6.1	17	marginal	--		
	112	102	7.0	19.5	marginal	yes		
	55	50	2.9	8	yes	5.5		Crack arrest determined by backing off of load
	N.O.	N.O.	9.2	25.5	--	--		Crack extended nearly entire length of specimen
	42	38	2.4	67	yes	yes		
	139(c)	126(c)	6.5	17.5	no	no		
	139(c)	126(c)	7.2	20	no	--		Second loading of specimen; first loading was at room temperature above
	140(c)	127(c)	6.1	17	no	no		
	127(c)	116(c)	5.8	16	marginal	↓		
	119(c)	108(c)	5.9	16.5	yes	↓		
	125(c)	113(c)	6.3	17.5	yes	↓		
	76	70	6.5	18	no	yes	yes	
	99	90	14	40	no	yes	no	
	67	56	6.1	17	no	--	no	Crack branched and did not propagate
	105(c)	96(c)	26	72	marginal	no	no	
	130(c)	118(c)	-0.7	-2	no	--	yes	
	156	142	5.9	16.5	↓	yes	no	
	166(c)	151(c)	7.0	19.5	↓	no	no	
	123	112	6.5	18	↓	yes	yes	
	150	137	25	70	↓	yes	no	
	43(c)	39(c)	6.1	17	↓	--		
	44(c)	40(c)	6.8	19	↓	no		First loading of specimen
	32(c)	29(c)	0.5	1.5	↓	--		Second time specimen was tested
	111(c)	101(c)	1.6	4.5	↓	no		
	43	39	10.0	28	↓	yes		
	86(c)	79(c)	1.1	3	↓	no		
	38	35	8.8	24.5	↓	yes		
	41(c)	37(c)	5.9	16.5	↓	no	yes	
	31	28	6.1	17	↓	yes	yes	
	154	145	7.0	19.5	↓	yes	no	
	181	163	6.3	17.5	↓	yes	no	
	120	109	6.8	19	↓	yes	marginal	
	140(c)	127(c)	33	91	↓	no	no	Hydrogen environment induced crack extension which did not arrest after 792 hours
	113(c)	103(c)	285	792	↓	↓	↓	
	194	177	8.3	23	↓	yes	↓	
	196	179	8.8	16	↓	yes	↓	4 hours at 34.5 MN/m ² (5000 psi); 17 hours between 1.4 MN/m ² (200 psi) and 34.5 MN/m ² (5000 psi)
	199	181	7.6	21	↓	yes	↓	

FOLDOUT FRAME

2

TABLE 8. (CONCLUDE

Material	Specimen No.	Test Environment		K _{IC}							K _{max}				K Final		Time
		Type	Temperature		K _Q		Meets ASTM Requirements			Nominal Stress Less than σ _{ys}	MN/m ² √m	KSI √in.	Nominal Stress Less than σ _{ys}	MN/m ² √m	KSI √in.	seconds x 10 ⁻⁴	
			K	F	MN/m ² √m	KSI √in.	(2.5 K/σ _{ys}) ²	0.8 K _Q Requirement	Crack Uniformity								
Titanium Alloy (Ti-5Al-2.5 Sn) E.L.I.	2	He	295	70	84	76	Marg	yes	yes	yes	yes	84	76	yes	70(c)	64(c)	23
	6	He	↓	↓	71	65	yes	yes	yes	↓	↓	77	70	↓	67(c)	61(c)	7.4
	3	H ₂	↓	↓	N.O.	N.O.	--	--	--	↓	↓	56	51	↓	33(c)	30(c)	14
	9	H ₂	↓	↓	N.O.	N.O.	--	--	--	↓	↓	49	45	↓	34(c)	31(c)	18
	4	He	144	-200	86(c)	79(c)	no	yes	no	yes	↓	86(c)	79(c)	↓	56(c)	51(c)	6.1
	5	He	↓	↓	N.O.	N.O.	--	--	yes	↓	↓	71	64	↓	64(c)	58(c)	5.8
	7	H ₂	↓	↓	N.O.	N.O.	--	--	no	↓	↓	63	58	↓	57(c)	51(c)	5.8
	8	H ₂	↓	↓	N.O.	N.O.	--	--	yes	↓	↓	69	62	↓	60(c)	55(c)	23
2219 T87 Aluminum	3	He	295	70	28(c)	26(c)	yes	yes	yes	↓	↓	28(c)	26(c)	yes	--(c)	--	--
	10	He	↓	↓	37	34	↓	no	no	↓	↓	40	37	↓	32(c)	29(c)	9.2
	4	H ₂	↓	↓	25	23	↓	yes	no	↓	↓	29	27	↓	34(c)	31(c)	23
	6	H ₂	↓	↓	30	27	↓	yes	yes	↓	↓	31	28	↓	31(c)	28(c)	5.4
	11	H ₂	↓	↓	32	29	↓	↓	yes	↓	↓	32	29	↓	32(c)	30(c)	3.6
	7	He	144	-200	40	36	↓	↓	no	yes	↓	45	41	↓	42(c)	38(c)	8.3
	8	He	↓	↓	42	38	↓	↓	no	↓	↓	43	39	↓	36(c)	33(c)	4.9
	9	H ₂	↓	↓	39	36	↓	↓	yes	↓	↓	39	36	↓	40(c)	36(c)	5.8
	12	H ₂	↓	↓	34	31	↓	↓	yes	↓	↓	35	33	↓	38(c)	35(c)	6.5
ORHC Copper	2	He	295	70	22	20	no	yes	yes	no	↓	24	22	no	20	18	6.5
	4	He	↓	↓	18	16	↓	↓	yes	no	↓	19	17	↓	16	15	5.4
	3	H ₂	↓	↓	19	17	↓	↓	yes	no	↓	20	18	↓	20	18	6.5
	9	H ₂	↓	↓	17	15	↓	↓	no	yes	↓	21	19	↓	20	19	6.1
	5	He	144	-200	15	14	yes	↓	yes	↓	↓	29	27	↓	23(c)	21(c)	6.7
	6	He	↓	↓	19	17	↓	↓	yes	↓	↓	33	30	↓	30(c)	27(c)	6.8
	7	H ₂	↓	↓	21	19	↓	↓	yes	↓	↓	29	27	↓	26(c)	23(c)	6.2
	8	H ₂	↓	↓	15	14	yes	no	no	↓	↓	19	17	yes	18(c)	17(c)	6.5

NOTES:

- (c) = specimen compliance, in./lb
 K_{IC} = plane strain critical stress intensity factor or plane strain fracture toughness
 K_Q = conditional value of fracture toughness from test data
 K_{TH} = plane strain threshold fracture toughness
 N.O. = Not obtained
 σ_{ys} = uniaxial tensile yield strength of the material

FOLDOUT FRAME

TABLE 8. (CONCLUDED)

		K _{TH}						Test Description		
		K Final		Time Under Load		Meets. ASTM Requirements				
Nominal Stress Less than σ _{ys}		MN m ²	√n	KSI √in.	seconds x 10 ⁻⁴	Hours	($\frac{K_{TH}}{\sigma_{ys}}$) ²		Crack Uniformity	Nominal Stress Less than σ _{ys}
(c)	yes ↓	70(c) 67(c) 33(c) 34(c) 56(c) 64(c) 57(c) 60(c)	64(c) 61(c) 30(c) 31(c) 31(c) 58(c) 51(c) 55(c)	23 7.4 14 18 6.1 5.8 5.8 23	65 20.5 40 49 17 16 16 64	yes ↓ ↓ ↓ ↓ ↓ ↓ ↓	no ↓ ↓ ↓ ↓ ↓ ↓ ↓	yes ↓ ↓ ↓ ↓ ↓ ↓ ↓	Crack arrest determined by backing off of load	
(c)	yes ↓ yes ↓	-- 32(c) 34(c) 31(c) 32(c) 42(c) 36(c) 40(c) 38(c)	-- 29(c) 31(c) 28(c) 30(c) 38(c) 33(c) 36(c) 35(c)	-- 9.2 23 5.4 3.6 8.3 4.9 5.8 6.5	-- 25.5 64 15 10 23 13.5 16 18	-- marg. yes ↓ ↓ ↓ ↓ ↓ ↓	-- no ↓ ↓ ↓ ↓ ↓ ↓ ↓	-- yes ↓ ↓ ↓ ↓ ↓ ↓ ↓	Specimen Failed During Loading	
	no ↓ yes	20 16 20 20 23(c) 30(c) 26(c) 18(c)	18 15 18 19 21(c) 27(c) 23(c) 17(c)	6.5 5.4 6.5 6.1 6.7 6.8 6.2 6.5	18 15 18 17 18.5 19 17.3 18	no ↓ ↓ no ↓ ↓ ↓ ↓	yes ↓ ↓ no ↓ ↓ ↓ ↓	no ↓ ↓ yes no yes yes yes	No crack growth; plastic deformation only No crack growth; plastic deformation only No crack growth; plastic deformation only	

FOLDOUT FRAME

2

TABLE 9. AVERAGE K_{IC} AND K_{TH} VALUES FOR VARIOUS METALS IN 34.5 MN/m² (5000 PSI) HYDROGEN AND HELIUM ENVIRONMENTS

Material	Environment	295 K (70 F)				144 K (-200 F)				K_{TH}/K_{IC}	
		K_{IC}		K_{TH}		K_{IC}		K_{TH}		295 K (70 F)	144 K (-200 F)
		MN/m ² √	KSI √in.	MN/m ² √	KSI √in.	MN/m ² √	KSI √in.	MN/m ² √	KSI √in.		
Inconel 718 1214, 991 - 894 K (1725, 1325 - 1150 F)	He	78	71	58	53	98	89	81	74	0.73	0.83
	H ₂	--	--	~14	~13	--	--	63	57	0.18	0.65
Inconel 718 1325, 1033 - 922 K (1925, 1400 - 1200 F)	He	119*	108*	112	102	122	111	139	126	0.94	1.13
	H ₂	110	100	38	35	121	110	123	112	0.33	1.01
Inconel 625	He	84*	76*	--	--	110*	100*	--	--	--	--
	H ₂	67*	61*	--	--	108*	98*	--	--	--	--
AISI 321 Stainless Steel	He	36*	33*	--	--	34	31	38**	35**	--	1.13
	H ₂	34*	31*	--	--	32	29	36	33	--	1.07
A-286 Stainless Steel	He	145*	132*	--	--	138	126*	--	--	--	--
	H ₂	100*	91*	<113**	<103**	152	138*	--	--	<0.78	--
Ti-5Al-2.5 Sn ELI	He	79	72	69	63	87	79	60	55	0.88	0.70
	H ₂	--	--	34	31	--	--	58	53	0.43	0.67
2219 T87 Aluminum	He	33	30	32	29	41	37	40	36	0.97	0.97
	H ₂	29	26	33	30	37	34	40	36	1.00	0.97
OFHC Copper	He	20*	18*	--	--	18*	16*	--	--	--	--
	H ₂	17*	16*	--	--	19*	17*	--	--	--	--

*Not valid K_{IC} according to ASTM 399

**Stress at $K_{TH} > \sigma_y$

TABLE 10. YIELD STRENGTHS AND MAXIMUM STRESS INTENSITIES AT WHICH PLANE STRAIN EXISTS FOR THE 0.0254 m (1.0 IN.) THICK WOL SPECIMEN USED FOR THESE TESTS

Material	Yield Strength		$K_{I \text{ (max)}}$ For Plane Strain			
	295 K (70 F)		144 K (-200 F)		295 K (70 F)	
	MN/m ²	ksi	MN/m ²	ksi	MN/m ² \sqrt{m}	ksi $\sqrt{in.}$
Inconel 718	1120	162	1240	180	110	100
Inconel 625	650	94	760	110	64	58
AISI 321 Stainless Steel	220	32	260	38	22	20
A-285 Stainless Steel	780	113	879	126	77	70
T-5A1-2.5 Sn ELI	820	119	1040	151	80	73
2219-T87 Al Alloy	390	57	430	63	38	35
OFHC Copper	120	17	160	23	11	10
					125	114
					77	70
					25	23
					88	80
					105	96
					44	40
					17	15

of the stress intensity is between 0.55 and $2.7 \text{ MN/m}^2 \sqrt{\text{m/sec}}$ (30 and $150 \text{ ksi} \sqrt{\text{in./min}}$), (2) the change from linearity of the load versus deflection curve must be sufficiently sharp in the region between 0.8 and 1.0 of the 5-percent secant offset, (3) the specimen thickness and crack length must be greater than $2.5 (K_{IC}/\sigma_{YS})$, and (4) the maximum deviation of the crack length must be within 5 percent of the average crack length and the crack length along the specimen edges cannot be shorter than 90 percent of the average crack length. Requirement 4 is designated as crack uniformity in Table 8 for the initial crack at K_{IC} and the final crack at K_{final} .

The stress intensities were calculated from the measured crack lengths except when the cracks (initial or final) were not sufficiently uniform to meet ASTM requirements. In those cases, the crack lengths as computed from compliance were considered more accurate and were used for the stress intensity calculations.

No special effort was made to load the specimens at a rate within the range required for a K_{IC} value; however, most of the tests in air and helium environments met this requirement. On the other hand, the rate of loading in hydrogen was frequently very slow so that the minimum stresses at which crack growth occurs would not be greatly exceeded.

Inconel 718--1214, 991 - 894 K (1725, 1325 - 1150 F)

Heat Treatment Condition

Pop-in (sudden load decrease during loading) occurred in the air and helium environments during tests conducted at ambient temperature and at 144 K (-200 F) on Inconel 718 in the 1214, 991 - 894 K (1725, 1325 - 1150 F) heat treatment condition (A condition, Table 5.) For the first specimen (A1, Table 8) tested in helium at 144 K (-200 F), the crack extended nearly the entire length of the specimen during pop-in and, consequently, the threshold stress intensity was not measured on this specimen. For all subsequent tests at 144 K (-200 F), the specimen was loaded very slowly and further loading was halted when sustained-load crack growth was indicated. Thus,

only one K_{IC} measurement was made at 144 K (-200 F). K_{IC} was $78 \text{ MN/m}^2 \sqrt{\text{m}}$ (71 ksi $\sqrt{\text{in.}}$) at ambient temperature and $98 \text{ MN/m}^2 \sqrt{\text{m}}$ (89 ksi $\sqrt{\text{in.}}$) at 144 K (-200 F).

Sustained-load crack growth was quite pronounced in both helium and hydrogen environments at ambient temperature and 144 K (-200 F) in this material. The threshold stress intensity in helium was $58 \text{ MN/m}^2 \sqrt{\text{m}}$ (53 ksi $\sqrt{\text{in.}}$) at ambient temperature and $81 \text{ MN/m}^2 \sqrt{\text{m}}$ (74 ksi $\sqrt{\text{in.}}$) at 144 K (-200 F). It is of interest that a specimen (A7, Table 8) tested in air at ambient temperature had about the same K_{IC} value as did specimens tested in helium, but K_{TH} in air was just slightly less than K_{IC} in air and significantly higher than K_{TH} in helium. It would appear, therefore, that air at ambient temperature and pressure inhibits sustained-load crack growth of Inconel 718 in this heat treatment condition.

The ambient temperature threshold stress intensity in hydrogen of Inconel 718 in the A heat treatment condition was very low. Initial tests conducted in hydrogen resulted in complete fracture of the specimens although the maximum stress intensities to which the specimens were loaded were comparatively low.

Two threshold values were obtained at ambient temperature in 34.5 MN/m^2 (5000 psi) hydrogen. A threshold value of $22 \text{ MN/m}^2 \sqrt{\text{m}}$ (20 ksi $\sqrt{\text{in.}}$) was obtained on specimen A5 (Table 8) by bracketing the load at which crack growth was noted rather than by crack arrest. A subsequent test, specimen A13 (Table 8) was loaded to $23 \text{ MN/m}^2 \sqrt{\text{m}}$ (21 ksi $\sqrt{\text{in.}}$) and the crack extended most of the distance across the specimen before the test was terminated at $14 \text{ MN/m}^2 \sqrt{\text{m}}$ (13 ksi $\sqrt{\text{in.}}$). The crack had not completely arrested, but the crack growth rate at this point was over an order of magnitude slower than occurred at stress intensities above $16.5 \text{ MN/m}^2 \sqrt{\text{m}}$ (15 ksi $\sqrt{\text{in.}}$) as determined from compliances. The final crack length was very uniform and met ASTM's requirements but was quite long with $a = 0.065 \text{ m}$ (2.257 in.) corresponding to $\frac{a}{W} = 0.885$. Novak and Rolfe (Ref. 16) performed the compliance calibration on this specimen to $\frac{a}{W} = 0.875$, and at $\frac{a}{W} = 0.87$, the accuracy of Eq. 8 is within 2 to 3 percent. Therefore, although the crack was slightly longer than the calibration range, the stress intensity value obtained is considered reasonably accurate.

The K_{TH} value obtained by crack arrest is judged more accurate than the higher one obtained by bracketing. Thus, the best estimate of K_{TH} for Inconel 718 in the A heat treatment condition when exposed to 34.5 MN/m^2 (5000 psi) hydrogen is $14 \text{ MN/m}^2 \sqrt{\text{m}}$ (13 ksi $\sqrt{\text{in.}}$). This is the lowest value of K_{TH} obtained for any of the materials (including copper and aluminum) tested in this program. In comparison, Lorenz (Ref. 9) obtained a K_{TH} value of $24 \text{ MN/m}^2 \sqrt{\text{m}}$ (22 ksi $\sqrt{\text{in.}}$) on Inconel 718 plate in the same heat treatment condition when tested in 35.9 MN/m^2 (5200 psi) hydrogen.

A test conducted at 144 K (-200 F) on specimen A11 (Table 8) indicates a lower value of K_{TH} of this material in hydrogen than obtained in helium at this temperature. Crack growth was comparatively slow and it took 32×10^4 seconds (89 hours) for the crack to arrest at $63 \text{ MN/m}^2 \sqrt{\text{m}}$ (57 ksi $\sqrt{\text{in.}}$). The duplicate test, specimen A10 (Table 8), had to be aborted after 2.3×10^4 seconds (6.5 hours) because of excessive pressure vessel leakage.

Gross yielding in front of the crack did not occur during any of the tests.

Inconel 718--1325, 1033 - 922 K (1925, 1400 - 1200 F)

Heat Treatment Condition

The fracture toughness (K_{IC}) and threshold stress intensity (K_{TH}) of Inconel 718 in the 1325, 1033 - 922 K (1925, 1400 - 1200 F) heat treatment condition (C condition, Table 5) was significantly higher than in the A condition. Pop-in occurred during loading at or slightly above the 5-percent secant intercept for the room-temperature tests in helium. A pop-in type phenomenon also occurred at 144 K (-200 F) in both hydrogen and helium environments, but only after significant sustained load crack growth had occurred at a load slightly above the 5-percent secant intercept load. The stress intensity was increasing as the crack extended under constant load prior to the pop-in phenomenon, but the crack length immediately before pop-in was not determined. Therefore, the maximum stress intensities could not be obtained.

The K_{IC} data on this material was very consistent and appeared to be basically independent of temperature and environment. K_{IC} was about $121 \text{ MN/m}^2 \sqrt{\text{m}}$ (110 ksi $\sqrt{\text{in.}}$) at ambient temperatures and 144 K (-200 F). At room temperature, this stress intensity was $11 \text{ MN/m}^2 \sqrt{\text{m}}$ (10 ksi $\sqrt{\text{in.}}$) above the stress intensity allowed by ASTM criteria for this specimen thickness. Only one value, $110 \text{ MN/m}^2 \sqrt{\text{m}}$ (100 ksi $\sqrt{\text{in.}}$) was obtained in hydrogen at ambient temperature because of hydrogen-induced sustained-load crack growth. The lower value in hydrogen compared to helium is probably the result of environmentally induced sustained-load crack growth during loading.

The threshold stress intensity data in helium was extremely consistent, varying within $1 \text{ MN/m}^2 \sqrt{\text{m}}$ (1 ksi $\sqrt{\text{in.}}$) for the two tests conducted at room temperature and within the same amount for the three tests conducted at 144 K (-200 F). K_{TH} at room temperature was $112 \text{ MN/m}^2 \sqrt{\text{m}}$ (102 ksi $\sqrt{\text{in.}}$) and at 144 K (-200 F) K_{TH} was $139 \text{ MN/m}^2 \sqrt{\text{m}}$ (126 ksi $\sqrt{\text{in.}}$).

Two K_{TH} values were obtained in hydrogen at room temperature. A value of $55 \text{ MN/m}^2 \sqrt{\text{m}}$ (50 ksi $\sqrt{\text{in.}}$) was obtained by bracketing, and $42 \text{ MN/m}^2 \sqrt{\text{m}}$ (38 ksi $\sqrt{\text{in.}}$) was obtained later by crack arrest. The value obtained by crack arrest is deemed most accurate. The average K_{TH} of three tests conducted in hydrogen at 144 K (-200 F) was $123 \text{ MN/m}^2 \sqrt{\text{m}}$ (112 ksi $\sqrt{\text{in.}}$). This is significantly below the value obtained in helium, and because of the consistency of the K_{TH} data, there is indication of environmentally induced crack growth at this cryogenic temperature.

In Phase V, K_{TH} measurements were performed on Inconel 718 specimens in the C heat treatment condition exposed to 34.5 MN/m^2 (5000 psi) hydrogen at 200 K (-100 F). The results obtained in that phase indicate that the rate of crack growth decreases with decreasing temperature but K_{TH} at 200 K (-100 F) was about the same as at ambient temperature. Therefore, as is suggested in Phase V, the real value of K_{TH} at 144 K (-200 F) may be lower than $123 \text{ MN/m}^2 \sqrt{\text{m}}$ (112 ksi $\sqrt{\text{in.}}$), but the very slow crack growth rate prevented attainment of the true K_{TH} value.

Gross yielding in front of the crack did not occur during any of the tests.

Inconel 625

There was considerable variation of K_{IC} obtained from the ambient-temperature tests on Inconel 625 specimens. The average fracture toughness was $84 \text{ MN/m}^2 \sqrt{\text{m}}$ ($76 \text{ ksi } \sqrt{\text{in.}}$) in helium and $67 \text{ MN/m}^2 \sqrt{\text{m}}$ ($61 \text{ ksi } \sqrt{\text{in.}}$) in hydrogen. The lower value in hydrogen was due to subcritical crack growth during loading. Both values were above $64 \text{ MN/m}^2 \sqrt{\text{m}}$ ($58 \text{ ksi } \sqrt{\text{in.}}$), which is the maximum stress intensity that will meet plane strain requirements for Inconel 625 with this specimen thickness.

K_{IC} was essentially the same in hydrogen as in helium at 144 K (-200 F), the average value for both environments was about $110 \text{ MN/m}^2 \sqrt{\text{m}}$ ($100 \text{ ksi } \sqrt{\text{in.}}$). This value was also considerably above the allowable stress intensity for plane strain for the specimen thickness.

Sustained-load crack growth did not occur in the two Inconel 625 specimens tested in helium at ambient temperature, but measurable crack growth was observed at 144 K (-200 F) in both helium and hydrogen environments. True K_{TH} values were not, however, obtained because the arrest stress intensity appeared to be only a function of the maximum load rather than an intrinsic value. That is, crack arrest occurred at higher stress intensities for those specimens loaded initially to the higher values and vice versa.

At room temperature, a hydrogen embrittling phenomenon was evident in the two Inconel 625 specimens tested in hydrogen at ambient temperature. Specimen No. 1 (Table 8) was held at $67 \text{ MN/m}^2 \sqrt{\text{m}}$ ($56 \text{ ksi } \sqrt{\text{in.}}$) for 6.1×10^4 seconds (17 hours) without any crack extension. The specimen was then unloaded, exposed to air, replaced in 34.5 MN/m^2 (5000 psi) hydrogen and reloaded in increments up to a stress intensity of $139 \text{ MN/m}^2 \sqrt{\text{m}}$ ($126 \text{ ksi } \sqrt{\text{in.}}$). With each loading increment above approximately $88 \text{ MN/m}^2 \sqrt{\text{m}}$ ($80 \text{ ksi } \sqrt{\text{in.}}$) stress intensity, there was a small indication of crack extension, but significant crack growth did not occur even at the highest stress intensity. Posttest examination showed crack branching at an angle to the plane of the crack and, therefore, no meaningful crack arrest data were obtained.

Crack branching was not observed on specimen No. 7 (Table 8), also tested in ambient temperature hydrogen. Posttest examination showed measurable crack extension with most of it occurring at the sides of the specimen rather than inside the specimen. Preferred crack growth along the sides is very unusual and it represents a surface cracking-type phenomenon rather than normal crack growth.

From the results of the two tests conducted in hydrogen at ambient temperature, hydrogen-induced crack growth followed by blunting and/or branching is indicated.

The stress exceeded the specimens yield strength at K_{final} for most of the Inconel 625 specimens.

AISI 321 Stainless Steel

Plane strain conditions were not obtained with the AISI 321 stainless-steel specimens at ambient temperature or 144 K (-200 F) in either hydrogen or helium environments. To meet plane strain conditions, a considerably thicker specimen would be required. Secondly, gross yielding in front of the crack occurred in five of the eight specimens at the 5-percent secant intercept. Despite these two factors, an average K_{IC} value of about $35 \text{ MN/m}^2 \sqrt{\text{m}}$ ($32 \text{ ksi } \sqrt{\text{in.}}$) was obtained for all of the conditions tested; this value may be reasonably close to the true plane strain fracture toughness of this material.

The results of the crack arrest experiments were similar to those for Inconel 625. Incremental crack growth, followed by blunting, occurred when the specimens were loaded above their apparent K_{IC} value. Blunting was in the form of smooth rounding of the crack front rather than branching as observed in Inconel 625.

Specimen No. 3 (Table 8) was tested twice in hydrogen at ambient temperature. In the first test, the specimen was loaded to a stress intensity of $28 \text{ MN/m}^2 \sqrt{\text{m}}$ ($25 \text{ ksi } \sqrt{\text{in.}}$) and held for 5×10^3 seconds (1-1/2 hours). There was an immediate small indication of crack growth after reaching the maximum load. After the first test, the specimen was exposed to air and then retested in hydrogen. The second test consisted of loading in increments up to $111 \text{ MN/m}^2 \sqrt{\text{m}}$ ($101 \text{ ksi } \sqrt{\text{in.}}$). Crack

extension occurred after each loading increment and the crack arrested each time within a few minutes, although the loads had not decreased to the previous arrest values. Posttest examination showed that the specimen had deformed plastically (over 0.005 m (0.2 in.) increase of crack opening displacement) and the crack front appeared rounded. There was considerable surface cracking along the side grooves just ahead of the precrack. The crack had extended 0.003 m (0.121 in.) during the test and the sustained-load crack growth region was very smooth with an almost polished appearance and contained no branching as observed on one of the Inconel 625 specimens tested in hydrogen. It was, therefore, evident that the crack extended a certain amount with each load increase and then blunted by rounding of the crack front without secondary cracking or branching. This crack rounding is the same as observed (Ref. 3) during metallographic examination of surface cracks in AISI 321 stainless-steel tensile specimens tested in hydrogen.

Normal-type crack extension occurred during tests that were moderately loaded at 144 K (-200 F). The degree of sustained-load crack growth appeared essentially proportional to the maximum stress intensity, and crack arrest occurred at about the apparent K_{IC} value. Incrementally loading a specimen (No. 4, Table 8) to a very high stress intensity of $91 \text{ MN/m}^2 \sqrt{\text{m}}$ ($83 \text{ ksi} \sqrt{\text{in.}}$) in helium at 144 K (-200 F) resulted in step-type crack extension with each load increase, but the load did not decrease to the previous arrest value. Therefore, it is questionable whether a true threshold stress intensity value was obtained on any of the tests on 321 stainless steel conducted at 144 K (-200 F). A conservative estimate of K_{TH} at 144 K (-200 F) would be the same as the apparent K_{IC} value of about $33 \text{ MN/m}^2 \sqrt{\text{m}}$ ($30 \text{ ksi} \sqrt{\text{in.}}$). There appeared to be no hydrogen environment effect on crack extension at the cryogenic temperature.

A-286 Stainless Steel

A-286 stainless steel has the highest fracture toughness of the alloys tested in this program. In fact, it was necessary to extend the crack by fatigue an additional 0.0063 m (0.25 in.) to test the specimens because of the 13,300 N (30,000 pounds) limitation of the loading column. Valid K_{IC} data were not obtained at

either ambient temperature or 144 K (-200 F) because of the high fracture toughness and high stress required for crack extension. The average calculated ambient temperature K_Q value was $145 \text{ MN/m}^2\sqrt{\text{m}}$ ($132 \text{ ksi}\sqrt{\text{in.}}$) in helium and $100 \text{ MN/m}^2\sqrt{\text{m}}$ ($91 \text{ ksi}\sqrt{\text{in.}}$) in hydrogen. It is not known whether this difference is due to a hydrogen environment effect or from an unusually high scatter of the results. There was somewhat less scatter of K_Q at 144 K (-200 F), and the average values in hydrogen and helium at 144 K (-200 F) were about the same as K_Q obtained in helium at ambient temperature.

The initial test (specimen No. 3, Table 8) conducted in hydrogen at ambient temperature showed no crack growth after being held for 6.8×10^4 seconds (16 hours) at $120 \text{ MN/m}^2\sqrt{\text{m}}$ ($109 \text{ ksi}\sqrt{\text{in.}}$). The stress during the hold period was about equal to the yield strength of the specimen. Two tests conducted at about $165 \text{ MN/m}^2\sqrt{\text{m}}$ ($150 \text{ ksi}\sqrt{\text{in.}}$) in ambient-temperature helium also showed no crack extension; it was believed that crack growth could not be developed in A-286 stainless steel.

Subsequently, two ambient-temperature hydrogen environmental tests were performed in which the specimens were loaded to about the same values as were the specimens tested in helium. Slow sustained-load crack growth occurred in both of these specimens. An apparent crack arrest of $140 \text{ MN/m}^2\sqrt{\text{m}}$ ($127 \text{ ksi}\sqrt{\text{in.}}$) was obtained in specimen No. 5 (Table 8) after 33×10^4 seconds (91 hours) by backing off of the load.

A subsequent test (specimen No. 10, Table 8) showed that backing off of the load can effect an apparent crack arrest, but crack growth reinitiates after a hold period. Sustained-load crack extension continued on this specimen for 2.85×10^6 seconds (33 days), at which time the stress intensity had declined from $165 \text{ MN/m}^2\sqrt{\text{m}}$ ($150 \text{ ksi}\sqrt{\text{in.}}$) to $113 \text{ MN/m}^2\sqrt{\text{m}}$ ($103 \text{ ksi}\sqrt{\text{in.}}$) with 0.012 m (0.475 in.) crack extension. At this point, the specimen was unloaded in hydrogen to measure crack length by compliance and then reloaded to the same value without removing it from the environment. No further crack growth was noted after 6.9×10^7 seconds (8 days). The crack was still growing before unloading for compliance, and thus the unloading and reloading evidently effected a change in crack extension (e.g., intergranular to transgranular) sufficient to temporarily prevent further crack extension. Therefore, the threshold stress intensity of A-286 stainless steel in hydrogen at ambient temperature was not established, but it is below $113 \text{ MN/m}^2\sqrt{\text{m}}$ ($103 \text{ ksi}\sqrt{\text{in.}}$).

There is evidence that crack growth in A-286 in hydrogen requires gross yielding in the environment because a specimen loaded initially to a somewhat higher value than the above stress intensity did not show crack extension. However, the hold period may have been insufficient. The very slow crack extension and high stress required to start crack growth in hydrogen explains the apparent lack of embrittlement of A-286 stainless steel when tensile or even low-cycle fatigue tested in high-pressure hydrogen. It may be possible to obtain a true K_{TH} stress intensity for A-286 in ambient temperature hydrogen by extending the crack in hydrogen by fatigue, and then loading the specimen to a stress intensity value below that at which gross yielding occurs.

There was almost no measurable crack extension in the specimens tested in hydrogen and helium environments at 144 K (-200 F) although the specimens were loaded to about $198 \text{ MN/m}^2 \sqrt{\text{m}}$ ($180 \text{ ksi} \sqrt{\text{in.}}$) stress intensity.

Ti-5Al-2.5 Sn ELI

Quantitative K_{IC} and K_{TH} fracture toughness data were obtained on Ti-5Al-2.5 Sn ELI. Pop-in occurred at K_Q at ambient temperature and at 144 K (-200 F) with practically no deviation from linearity of the load-crack opening displacement record. The K_{IC} fracture toughness in helium was $79 \text{ MN/m}^2 \sqrt{\text{m}}$ ($72 \text{ ksi} \sqrt{\text{in.}}$) at room temperature and $87 \text{ MN/m}^2 \sqrt{\text{m}}$ ($79 \text{ ksi} \sqrt{\text{in.}}$) at 144 K (-200 F). The maximum stress intensities were less than K_{IC} for the tests conducted in hydrogen to minimize the crack extension required for crack arrest.

The threshold stress intensity of Ti-5Al-2.5 Sn ELI at ambient temperature in helium was $69 \text{ MN/m}^2 \sqrt{\text{m}}$ ($63 \text{ ksi} \sqrt{\text{in.}}$). The threshold stress intensity at ambient temperature in hydrogen was $34 \text{ MN/m}^2 \sqrt{\text{m}}$ ($31 \text{ ksi} \sqrt{\text{in.}}$). Crack arrest was determined by the bracketing method on specimen No. 3 (Table 8) and by crack arrest on specimen No. 9 (Table 8) and virtually the same K_{TH} value was obtained by both methods. This value is higher than the threshold stress intensity of $24 \text{ MN/m}^2 \sqrt{\text{m}}$ ($21.5 \text{ ksi} \sqrt{\text{in.}}$) obtained by Bixler (Ref. 20) for Ti-5Al-2.5 Sn ELI from measurements conducted at ambient temperature in 9.6 MN/m^2 (1400 psi) hydrogen.

The hydrogen affected region of the fracture surface of specimens tested in hydrogen was very dark and in some regions almost black. This dark texture is usually indicative of extensive secondary cracking.

The average threshold stress intensity at 144 K (-200 F) was $60 \text{ MN/m}^2 \sqrt{\text{m}}$ (55 ksi $\sqrt{\text{in.}}$) in helium and $58 \text{ MN/m}^2 \sqrt{\text{m}}$ (53 ksi $\sqrt{\text{in.}}$) in hydrogen. Therefore, there does not appear to be a hydrogen environmental influence on K_{TH} for Ti-5Al-2.5 Sn ELI at 144 K (-200 F).

The yield strength was not exceeded during any of the tests conducted on Ti-5Al-2.5 Sn ELI specimens.

2219-T87 Al Alloy

Quantitative K_{IC} and K_{TH} fracture mechanics data were also obtained on 2219-T87 Al alloy at ambient temperature and at 144 K (-200 F). Pop-in occurred for all of the tests at a stress intensity somewhat above K_Q . The average K_{IC} fracture toughness at ambient temperature was $33 \text{ MN/m}^2 \sqrt{\text{m}}$ (30 ksi $\sqrt{\text{in.}}$) in helium and $29 \text{ MN/m}^2 \sqrt{\text{m}}$ (26 ksi $\sqrt{\text{in.}}$) in hydrogen. At 144 K (-200 F), the average K_{IC} values were $41 \text{ MN/m}^2 \sqrt{\text{m}}$ (37 ksi $\sqrt{\text{in.}}$) in helium and $37 \text{ MN/m}^2 \sqrt{\text{m}}$ (34 ksi $\sqrt{\text{in.}}$) in hydrogen.

The specimens were loaded to pop-in and the cracks allowed to arrest. The stress intensities at crack arrest were about the same in both helium and hydrogen environments and on an average equal to K_{IC} in helium regardless of environment. That is, the average K_{TH} values in helium and hydrogen were 32 to $33 \text{ MN/m}^2 \sqrt{\text{m}}$ (29 to 30 ksi $\sqrt{\text{in.}}$) at ambient temperature and $40 \text{ MN/m}^2 \sqrt{\text{m}}$ (36 ksi $\sqrt{\text{in.}}$) at 144 K (-200 F). There was, therefore, no indication of a hydrogen environmental effect on sustained-load crack growth for 2219-T87 Al alloy.

The yield strength of 2219-T87 Al alloy was not exceeded during any of the tests conducted on 2219-T87 Al alloy.

OFHC Copper

Crack extension did not occur in the OFHC copper specimens tested at ambient temperature in helium and hydrogen environments. Loading above the 5-percent secant intercept caused arm bending without crack extension for the specimens tested in both environments. The stress intensities computed at the 5-percent secant intercept were not valid K_{IC} values because the specimens were not sufficiently thick, but more important, because there was no measurable crack extension. They do, however, represent the stress intensities above which there is gross plastic deformation at the crack front. This is confirmed by calculation of the stress by means of Eq. 7 which showed that the stress at 5-percent secant intercept corresponded to about 117 MN/m^2 (17 ksi), which is the yield strength of copper at ambient temperature.

A small amount of crack extension did occur during the 144 K (-200 F) tests conducted in both environments. The 5-percent secant intercept stress intensity was $18 \text{ to } 19 \text{ MN/m}^2 \sqrt{\text{m}}$ (16 to 17 ksi $\sqrt{\text{in.}}$). This was slightly above the $17 \text{ MN/m}^2 \sqrt{\text{m}}$ (15 ksi $\sqrt{\text{in.}}$) maximum stress intensity allowed for plane strain conditions in 0.0254 m (1.0 in.) thick copper specimens at this temperature. The yield stress was not exceeded and, although ASTM requirements were not completely met, the K_Q values obtained should be close to actual K_{IC} values.

Three of the four specimens yielded between K_{IC} and the maximum stress intensity. Although there was some load decrease after reaching the maximum load, compliance indicated very little crack extension. Therefore, the load dropoff appeared due to creep-type relaxation phenomenon rather than to crack extension. At any rate, the final stress intensity was more indicative of the maximum stress intensity than it was of an intrinsic K_{TH} value and K_{TH} of copper at 144 K (-200 F) was, therefore, not obtained.

Sustained-Load Crack Propagation in Hydrogen

Hydrogen-induced, sustained-load crack propagation resulted from exposure to 34.5 MN/m^2 (5000 psi) hydrogen for Inconel 718 in both heat treatment conditions at ambient and 144 K (-200 F), and for Ti-5Al-2.5 Sn ELI and A-286 stainless steel at ambient temperature. Crack growth followed by blunting occurred with each loading increment in AISI 321 stainless steel and in Inconel 625 when tested in hydrogen at ambient temperature.

Except for A-286 stainless steel, these results are consistent with the influence of hydrogen on the tensile properties of these metals. Embrittlement of tensile specimens involves crack initiation followed by sustained-load crack growth, while in the precracked WOL specimens, embrittlement is strictly environment enhanced crack growth. For the most severely embrittled metals, very little plastic strain is needed for surface crack initiation, and crack growth continues in a straight line until failure. Sustained-load crack extension without any form of blunting certainly occurred in the Inconel 718 and Ti-5Al-2.5 Sn ELI specimens tested in hydrogen.

Hydrogen-induced crack growth also occurred at 144 K (-200 F) in Inconel 718, particularly in the 1214, 991 - 894 K (1725, 1325 - 1150 F) heat treatment condition. The main effect of decreasing temperature was an extremely large reduction of crack growth rate for a given stress intensity or for a given relative stress intensity (K/K_{TH}).

Sustained-load crack growth of A-286 stainless steel initiated at stresses above the materials yield strength and crack propagation was very slow. Hydrogen-induced crack growth in this material would not have been predicted from tensile test data, but is not in conflict with the tensile results. Hydrogen-induced surface crack initiation in A-286 stainless steel tensile specimens evidently requires considerable plastic deformation. Once a crack has initiated, there is very little time remaining for crack growth before the ultimate strength has been reached. The

very slow sustained-load crack growth of A-286 in hydrogen would preclude any significant reduction of tensile properties. The same reasoning can be used to predict very little embrittlement of smooth specimens subjected to low-cycle fatigue in hydrogen. At elevated temperatures, the tensile and low-cycle fatigue properties of A-286 stainless steel would be predicted to be affected by a high-pressure hydrogen environment because of increasing crack growth kinetics. In this light, Harris and Van Wanderham (Ref. 21) have shown a reduction of stress rupture strength and low-cycle fatigue strength of A-286 stainless steel from exposure to 34.5 MN/m^2 (5000 psi) hydrogen at 950 K (1250 F).

An important aspect of embrittlement of A-286 is that it is a stable austenitic stainless steel. Therefore, the lack of hydrogen-environment embrittlement observed until now in austenitic stainless steel is not evidently an intrinsic property of these steels, but instead is probably a matter of crack growth kinetics and possibly crack blunting by the ductile austenite structure.

Questions still unanswered from the tests on A-286 are whether: (1) gross yielding is necessary for hydrogen environment-induced, sustained-load crack growth of this material; and (2) hydrogen-induced crack extension will occur in plane strain as well as mixed mode fracture.

The AISI 321 stainless steel and Inconel 625 specimens showed hydrogen-induced, sustained-load crack growth but blunting followed each increment of crack growth. Blunting was in the form of rounding of the crack in AISI 321 stainless steel. Brittle crack initiation probably occurred in the strain-induced martensite followed by blunting in the austenite matrix.

Blunting of cracks in the Inconel 625 specimens was traced to crack branching in one of the specimens tested. For the other specimen, crack extension was considerably greater along the sides of the specimen instead of in the plane strain region in the middle, as observed for all of the other materials tested in hydrogen. Crack growth along the sides suggests crack nucleation in the side grooves as the result of plastic strain, but this was followed by crack blunting either by rounding of the crack front or microscopic branching as the crack extended.

Crack growth in OFHC copper and 2219-T87 Al alloy was not influenced by the hydrogen environment. Crack extension without blunting occurred in hydrogen and helium at ambient and 144 K (-200 F) in 2219-T87 Al alloy but there was no indication of greater crack growth in hydrogen.

Arm bending, rather than crack growth, occurred exclusively in OFHC copper specimens tested at ambient temperature. There was a small amount of crack growth in OFHC copper at 144 K (-200 F), but this was also accompanied by considerable plastic deformation.

PHASE III. ACOUSTIC EMISSION MONITORING OF CRACK GROWTH IN HYDROGEN

This phase consisted of developing a method for monitoring hydrogen-induced sub-critical, sustained-load crack growth. An accelerometer was attached to the ram (Fig. 8) outside the pressure vessel during several of the Phase II threshold stress intensity measurements.

In general, satisfactory correlation was obtained between the rate of acoustic emissions and the rate of load change. One very important finding emerged from the acoustic emission data: crack growth in Ti-5Al-2.5 Sn ELI, 2219-T87 Al alloy, and A-286 stainless steel (all exposed to hydrogen) proceeded discontinuously. None of the helium tests was monitored acoustically. Figure 14 shows a simultaneous plot of acoustic emission (cumulative count)/applied load versus elapsed time for the first of two K_{TH} tests conducted on A-286 stainless steel. As evident in Fig. 14, seven discrete crack growth increments were observed during the first 2.376×10^5 seconds (66 hours). A tendency for the rate of crack growth to decrease as the crack continues to grow in. entally is also apparent. (A faster counting rate is assumed to reflect a faster crack growth rate. The constant counting rates obtained between crack growth increments are assumed to be background rates.) Not enough load data were recorded to evaluate the correlation between acoustic emission and load in more detail. The A-286 stainless steel was the only material to be monitored in more than one test. The reproducibility of results could not be evaluated owing to amplifier problems in the second test.

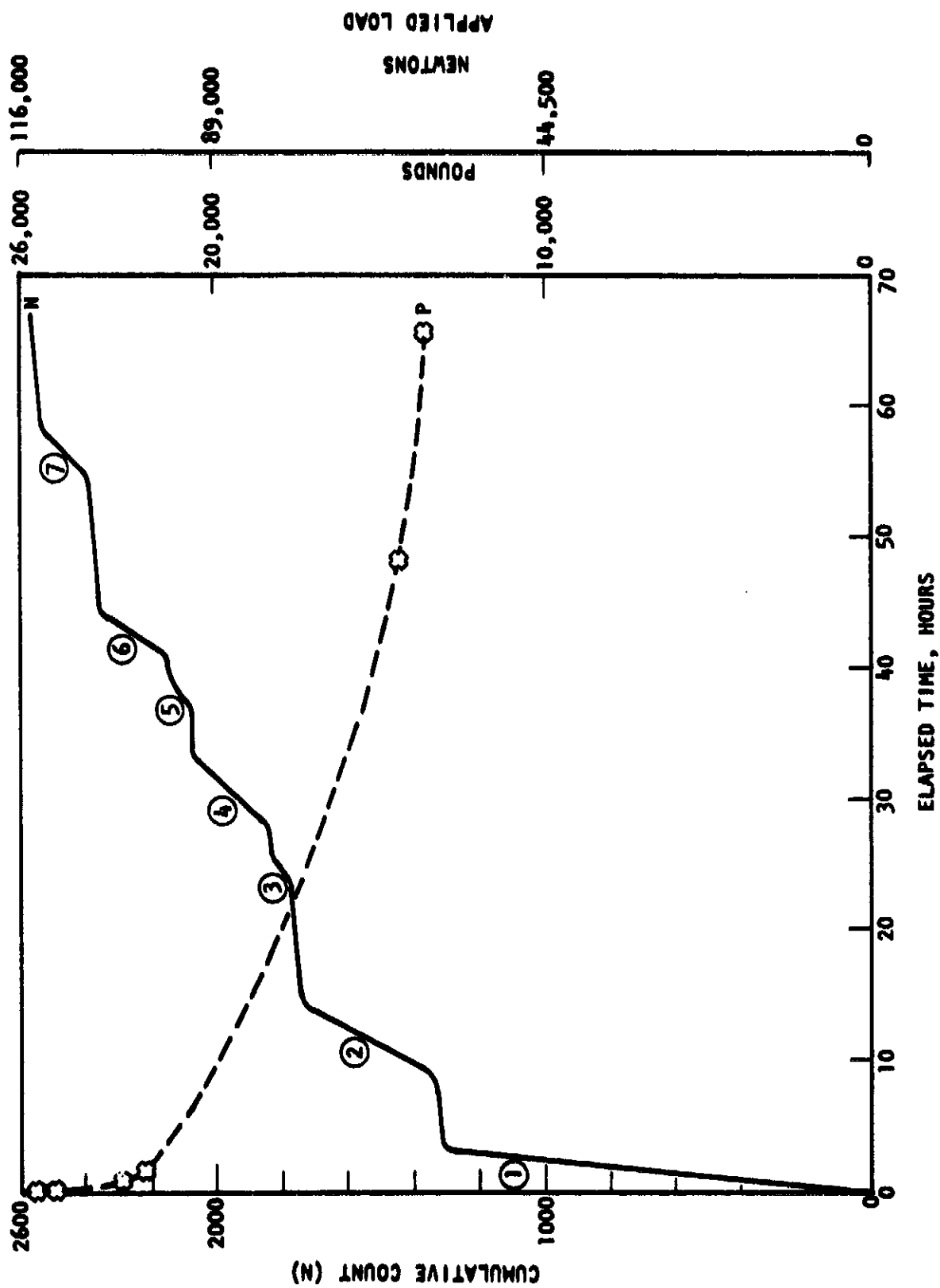


Figure 14. Changes in Acoustic Emission and Applied Load With Time During a KTH Test Conducted on A-286 Steel in 34.5 MN/m² (5000 psi), Ambient Temperature Hydrogen

PHASE IV. VARIATION OF HYDROGEN-ENVIRONMENT EMBRITTLEMENT OF INCONEL 718 WITH MATERIAL CONDITION

Tensile Tests of Notched Inconel 718 Specimens

Tensile tests were performed on notched Inconel 718 specimens fabricated from the three forms, rolled bar, forging, and plate, shown in Table 1. Notched specimens were also fabricated from a weldment made in the Inconel 718 plate with the notches located in the weld and in the weld heat affected zone (HAZ). Each of these five material conditions were tested in the A, B, and C heat treatment conditions listed in Table 5. The three material forms were also tested in the heat treatment E condition, which consisted of a 1297 K (1875 F) anneal for 600 seconds (10 minutes) followed by the standard 1033 - 922 K (1400 - 1200 F) age. The annealing treatment was selected as being sufficient to place the Ni_3Cb phase into solution, but sufficiently short to prevent significant grain growth. Thus, heat treatment E differs from C in that the annealing treatment in E was performed at a lower temperature and shorter time duration. In addition, specimens were tested in the 1297 K (1875 F) annealed condition (D) without subsequent aging.

The specimens were tested in 34.5 MN/m^2 (5000 psi) hydrogen and in 34.5 MN/m^2 (5000 psi) helium at ambient temperature. Table 11 contains the average test results and the individual specimen data are presented in Appendix C.

Consider first the results of the specimens without welds in the A, B, and C heat treatment conditions. The least hydrogen environment embrittlement, i.e., the highest $N_{\text{H}_2}/N_{\text{He}}$ ratio (0.86), occurred with the A and B heat treatments of the plate. On the other hand, the greatest embrittlement ($N_{\text{H}_2}/N_{\text{He}} = 0.54$ to 0.39) resulted from the A heat treatment of the rolled bar and forging and the B heat treatment of the forging. Intermediate embrittlement ($N_{\text{H}_2}/N_{\text{He}} = 0.70$ to 0.77) resulted from the C heat treatment of all three starting materials and from the B heat treatment of the rolled bar. Of the three heat treatments, the C heat treatment gave the most

TABLE 11. EFFECT OF 34.5 MN/m^2 (5000 PSI) HYDROGEN AT ROOM TEMPERATURE
ON THE AVERAGE PROPERTIES OF NOTCHED SPECIMENS OF
INCONEL 718 IN VARIOUS CONDITIONS

Heat Treatment Condition	Material	Environment	Notched Properties			
			Strength		N_{H_2} / N_{He}	Reduction of Area Percent
			MN/m^2	ksi		
A	Rolled Bar	He	1950	283	--	2.9
		H_2	1050	152	0.54	0.9
	Forging	He	2000	290	--	3.0
		H_2	1170	170	0.59	1.1
	Plate	He	1980	287	--	3.0
		H_2	1700	246	0.86	2.0
	Plate, Weld Metal	He	1420	206	--	1.4
		H_2	1120	163	0.79	1.0
B	Rolled Bar	He	1830	265	--	1.8
		H_2	1160	168	0.63	0.7
	Forging	He	1650	240	--	2.9
		H_2	1160	168	0.70	1.8
	Plate	He	1740	253	--	2.2
		H_2	990	144	0.57	1.2
	Plate, Weld Metal	He	1730	251	--	2.7
		H_2	1500	217	0.86	2.1
C	Rolled Bar	He	1240	180	--	2.1
		H_2	965	140	0.78	0.6
	Forging	He	1390	202	--	1.4
		H_2	1050	152	0.75	1.1
	Plate	He	2220	322	--	5.0
		H_2	1590	230	0.71	1.7
	Plate, Weld Metal	He	2340	339	--	4.6
		H_2	1780	258	0.76	1.8
D	Rolled Bar	He	2210	320	--	3.7
		H_2	1700	247	0.77	2.3
	Plate	He	1850	268	--	2.6
		H_2	1040	151	0.56	0.8
	Plate, Weld Metal	He	2080	301	--	3.8
		H_2	1500	217	0.72	1.1
	Plate, Weld HAZ	He	1120	163	--	13.6
		H_2	940	136	0.83	9.0
E	Rolled Bar	He	2200	319	--	4.0
		H_2	1560	226	0.71	1.9
	Forging	He	2220	322	--	3.5
		H_2	1850	225	0.70	1.4
	Plate	He	2200	319	--	4.2
		H_2	1650	239	0.75	2.7

consistent results with N_{H_2}/N_{He} being 0.71, 0.76, and 0.77 for the rolled bar, forging, and plate, respectively. Of the three forms of material (i.e., rolled bar, forging, and plate), the plate had the lowest and most consistent hydrogen-environment embrittlement for the three heat treatment conditions.

Although the least embrittlement occurred with the plate with the A heat treatment, the notched strength in hydrogen was the same for the plate with the C heat treatment as for the plate with the A heat treatment. The lower N_{H_2}/N_{He} ratio with the C heat treatment resulted from the higher notched strength in helium. In fact, for all three forms (rolled bar, forging, and plate), the C heat treatment resulted in the highest notch strength both in helium and hydrogen.

The results of tests on the rolled bar, forging, and plate in the E heat treatment condition indicate about the same degree of embrittlement as occurred on these materials when in the C heat treatment condition. Thus, the expected reduced grain size of the E heat treatment compared to the C heat treatment did not result in lower embrittlement. The microstructural aspects of hydrogen environment embrittlement of Inconel 718 will be discussed in the Metallography section.

The test results on the rolled bar in the annealed condition (D) showed comparatively less embrittlement. The notched strength was decreased 17 percent and the notch ductility was decreased from 13.6 to 9.0 percent reduction area due to the 34.5 MN/m^2 (5000 psi) hydrogen embrittlement. This low embrittlement ranks annealed Inconel 718 among the lesser embrittled (Ref. 4) of iron- and nickel-base alloys.

The investigation of the hydrogen-environment embrittlement of Inconel 718 welds was made only with the plate which, as it turned out, was the least embrittled of the forms tested. The welds were tested only in the heat-treated after-welding condition. For all three heat treatments, the notch strength in both helium and hydrogen was lower for the weld metal and the heat-affected zone than for the parent metal.

Also, in all cases, the degree of hydrogen-environment embrittlement was greater for the weld metal and heat-affected zone than for the parent metal. The weld metal and the heat-affected zone with the B heat treatment were embrittled by hydrogen to about the same degree. For the A heat treatment, the heat-affected zone was more embrittled by hydrogen than was the weld metal while the reverse was true for the C heat treatment. The most severe hydrogen-environment embrittlement in weld specimens was for weld metal with the C heat treatment. As with the parent metal, the notch strength in helium of both the weld metal and heat-affected zone was higher with the C heat treatment than with the other two heat treatments. However, the degree of hydrogen-environment embrittlement of the weld metal was large enough for the C heat treatment that the notch strength in hydrogen was somewhat lower with that heat treatment than with the A heat treatment.

Metallography of Inconel 718

Optical and electron microscopy was performed on specimens of the Inconel 718 bar, forging, and plates in the five heat treatment conditions. Photomicrographs of Inconel 718 in the 1228 K (1750 F) annealed, as-received condition are shown for the rolled bar in Fig. 15 and for the forging and plate in Fig. 16. Since the microstructures of longitudinal and transverse sections of the plate and forging were the same for this and subsequent heat treatments, only the transverse section photomicrographs are shown for these materials. There were considerable difference among the as-received grain structure resulting from the three processing methods. The structure of the rolled bar was duplex with the larger grains elongated in the rolling direction. The grain sizes of the forging and plate were relatively uniform. The grain size of the forging was relatively large (ASTM 4-1/2). The plate was fine grained (ASTM 10).

Photomicrographs of bar, forging, and plate specimens with the A heat treatment are shown in Fig. 17 and with the B heat treatment in Fig. 18 and 19. The microstructures resulting from these heat treatments appear virtually the same as those for the 1228 K (1750 F) annealed, as-received condition.



200x

Transverse Cross Section



Figure 15. Photomicrographs of Inconel 718 Rolled Bar in the 1228 K (1750 F) Solution Annealed As-Received Condition. Etchant: 92 HCl, 3 HNO₃, 1/2 H₂SO₄



Forging

200x



Plate

200x

Figure 16. Photomicrographs of Transverse Sections of Inconel 718 Forging and Plate in 1228 K (1750 F) Solution Annealed, As-Received Condition. Etchant: 92 HCl, 3 HNO₃, 1/2 H₂SO₄



Rolled Bar

Forging

Plate

Figure 17. Photomicrographs of Transverse Sections of Inconel 718 in the A Heat Treatment Condition. Etchant: 92 HCl, 3 HNO₃, 1/2 H₂SO₄



200x

Transverse Cross Section



200x

Longitudinal Cross Section

Figure 18. Photomicrographs of Inconel 718 Rolled Bar in the B Heat Treatment Condition. Etchant: 92 HCl, 3 HNO₃, 1/2 H₂SO₄



200x

Forging



200x

Plate

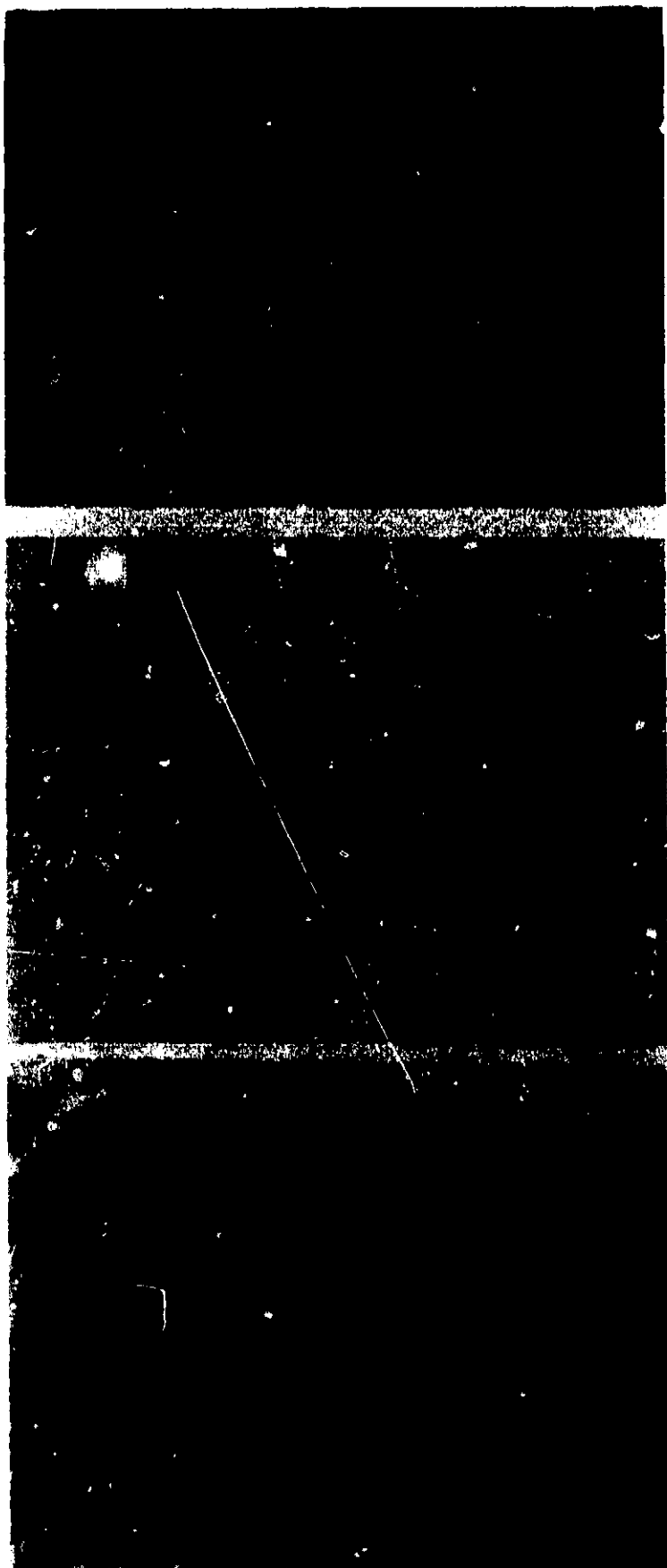
Figure 19. Photomicrographs of Transverse Sections of Inconel 718 Forging and Plate in the B Heat Treatment Condition.
Etchant: 92 HCl, 3 HNO₃, 1/2 H₂SO₄

Figure 20 shows photomicrographs of Inconel 718 bar, forging, and plate in the C heat treatment condition. Recrystallization and grain growth occurred during the heat treatment, and the microstructural appearance, including grain size, were the same for all three forms.

Electron micrographs of the bar, forging, and plate are shown in Fig. 21 for the 1228 K (1750 F) annealed, as-received condition; in Fig. 22 for the A heat treatment condition; in Fig. 23 for the B heat treatment condition; and in Fig. 24 for the C heat treatment condition. All of the electron micrographs are of transverse sections.

A second phase is evident in the 1228 K (1750 F) anneal, as-received condition, and this phase appears essentially unchanged in amount and appearance when the rolled bar, forging, and plate were subsequently given the A heat treatment. This phase(s) is believed to be either the A_2B Laves phase or the orthorhombic Ni_3Cb phase with the latter believed to be most likely.

The work of Eiselstein (Ref. 22) provides indirect evidence that the unidentified phase may be the Laves phase. Eiselstein developed a phase diagram that indicates that the Laves phase is stable for the 5-percent Cb + Ta composition in Inconel 718 at temperatures below 1310 K (1900 F), and will go into solution above that temperature. He developed a TTT diagram for Inconel 718, which was annealed at 1422 K (2100 F) for 3.6 ksec (1 hour) and water quenched, which indicated that the Laves phase would form after a 3.6 ksec (1-hour) aging treatment at 1200 to 1255 K (1700 to 1800 F), but that the Ni_3Cb phase would begin to form only after 18 ksec (5 hours) at 1200 to 1255 K (1700 to 1800 F). Eiselstein also presented a TTT diagram for Inconel 718, which was solution annealed at 1200 K (1700 F) for 7.2 ksec (2 hours), which indicates that the Ni_3Cb phase would begin to form only after 18 ksec (5 hours) to 36 ksec (10 hours) at temperatures between 1089 and 1172 K (1500 and 1650 F) and does not form in 36 ksec (10 hours) at 1200 K (1700 F). Unfortunately, Laves phase formation was not included in this TTT diagram. There is no indication from these two TTT diagrams that the Ni_3Cb phase would form during the 1228 K (1750 F), 3.6 ksec (1-hour) anneal given the as-received Inconel 718 in

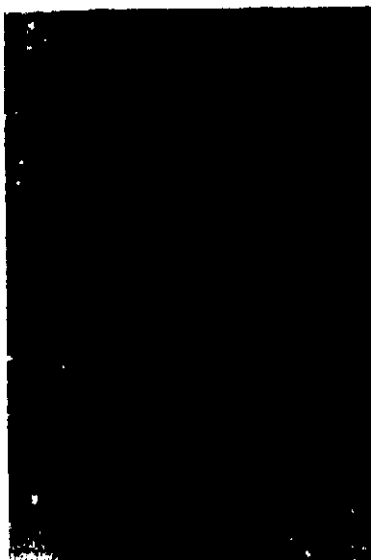


Plate

Forging

Rolled Bar

Figure 20. Photomicrographs of Transverse Sections of Inconel 718
in the C Heat Treatment Condition. Etchant: 92 HCl,
3 HNO₃, 1/2 H₂SO₄ (200X)



Rolled
Bar

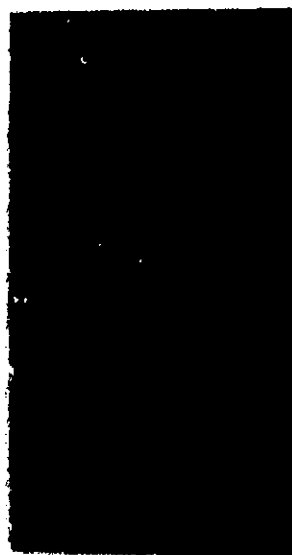


Forging

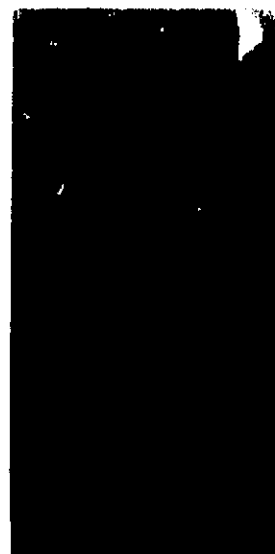


Plate

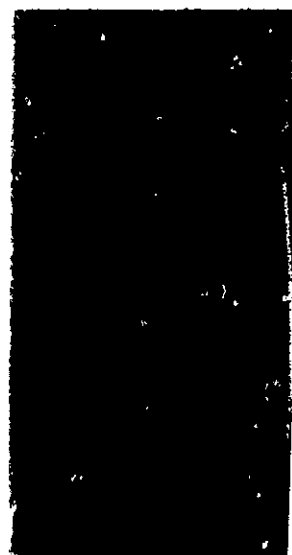
Figure 21. Electron Micrographs of Inconel 718 in the 1228 K (1750 F) Annealed, As-Received Condition. Etchant: 92 HCl, 3 HNO₃, 1/2 H₂SO₄ (3000 X)



Rolled
Bar

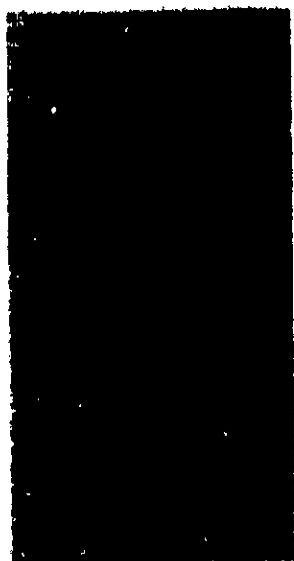


Forging



Plate

Figure 22. Electron Micrographs of Inconel 718 in the A Heat Treatment Condition. Etchant: 92 HCl, 3 HNO₃, 1/2 H₂SO₄ (3000X)



Rolled
Bar



Forging



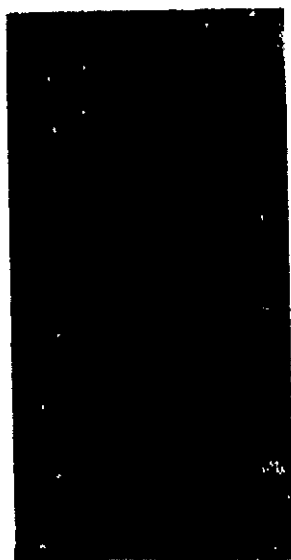
Plate

Figure 23. Electron Micrographs of Inconel 718 in the B Heat Treatment Condition. Etchants: 92 HCl, 3 HNO₃, 1/2 H₂SO₄ (3000X)



Rolled
Bar

Forging



Plate

Figure 24. Electron Micrographs of Inconel 718 in the C Heat Treatment Condition. Etchant: 92 HCl, 3 HNO₃, 1/2 H₂SO₄

this program, but there is some indication that the Laves phase would form during this anneal. Finally, Eiselstein indicated that the Laves phase appears as a flat, irregular precipitate while the Ni_3Cb phase typically appears as a needle-shaped precipitate in a Widmanstätten pattern.

Evidence that the second phase in Fig. 21 and 22 is Ni_3Cb comes from Muzyka and Maniar (Ref. 23). They annealed Inconel 718 for 3.6 ksec (1 hour) at various temperatures between 1214 and 1283 K (1725 and 1850 F) followed by a 991-894 K (1325-1150 F) aging treatment. The resulting microstructures appears similar those shown in Fig. 21 and 22. Muzyka and Maniar used selected area electron diffraction and identified a precipitate similar to the one in Fig. 21 and 22 as being Ni_3Cb . They made no mention of the Laves phase; it is presumed that the Laves phase was not present or was there to a much smaller extent than the Ni_3Cb phase.

The phase in question is assumed to be the orthorhombic Ni_3Cb phase, and it will be so identified for the remainder of the discussion.

Examination of Fig. 21 and 22 shows that the Ni_3Cb was somewhat discontinuous in the rolled bar, nearly continuous in the forging, and is dispersed in the plate. Thus, the as-received condition of the: (1) rolled bar is duplex with somewhat discontinuous Ni_3Cb , (2) forging is large grained with nearly continuous Ni_3Cb , and (3) plate is fine grained with discontinuous Ni_3Cb .

During the 991-894 K (1325-1150 F) aging treatment, coherent precipitates of γ' and γ'' form throughout the structure and are not resolved at the magnifications used. Thus, the microstructures appear about the same in the A condition as in the 1228 K (1750 F) annealed, as-received condition.

Figure 23 shows the electron microscopy of the bar, forging, and plate in the B heat treatment condition. Overaging caused coarsening and loss of coherency of the γ' and γ'' precipitates, and these phases are resolved in the electron micrographs shown in Fig. 23. Coarsening of the Ni_3Cb phase in all three electron micrographs is also evident.

Figure 24 shows the electron micrographs for the C heat treatment condition. Recrystallization, grain growth, and dissolution occurred during the heat treatment, and the resulting microstructures of the bar, forging, and plate are all virtually the same. Figure 24 shows that the Ni_3Cb went into solution during the 1325 K (1925 F) solution anneal. A thin, intergranular, carbide film together with isolated carbide particles formed during the heat treatment.

Solution of the Ni_3Cb phase is consistent with Muzyka and Maniar (Ref. 23) who showed that the phase they identified as Ni_3Cb disappeared completely during a 1311 K (1900 F) anneal. Both Muzyka and Maniar (Ref. 24) and Eisenstein (Ref. 23) showed that a carbide film formed during solution annealing at 1311 K (1900 F) and at 978-1089 K (1300-1500 F). On the other hand, Eisenstein showed that the carbide film would not form during aging after a 1200 K (1700 F) solution anneal.

The electron microscopy of Inconel 718 in the 1297 K (1875 F) annealed condition (heat treatment D) and in the 1297 K (1875 F) annealed and aged condition (heat treatment E) is shown in Fig. 25 through 28. Figures 25 and 26 show the metallography of the rolled bar in the D and E heat treatment conditions, respectively. The annealing treatment was sufficient to recrystallize the material and place the Ni_3Cb phase into solution. Carbide particles were observed in the electron micrographs.

Figures 27 and 28 show the microstructures of the Inconel 718, 0.038 m (1-1/2 in.) forging and 0.013 m (1/2 in.) plate in the 1297, 1033-922 K (1875, 1400-1200 F) condition. There was a small amount of the Ni_3Cb phase present in the forging and a trace of Ni_3Cb present in the plate. Comparison of Fig. 25 through 28 with Fig. 20 indicates that finer grain size resulted from the 1297 K (1875 F) 600 seconds (10 minutes) anneal than was obtained from the 1325 K (1925 F) 1200 seconds (20 minutes) anneal.

The microstructures of the weld and heat affected zones of the Inconel 718 plate weldments are shown in Fig. 29 for the A heat treatment condition, in Fig. 30 for the B heat treatment, and in Fig. 31 for the C heat treatment condition. A dendritic,



200x



3000x

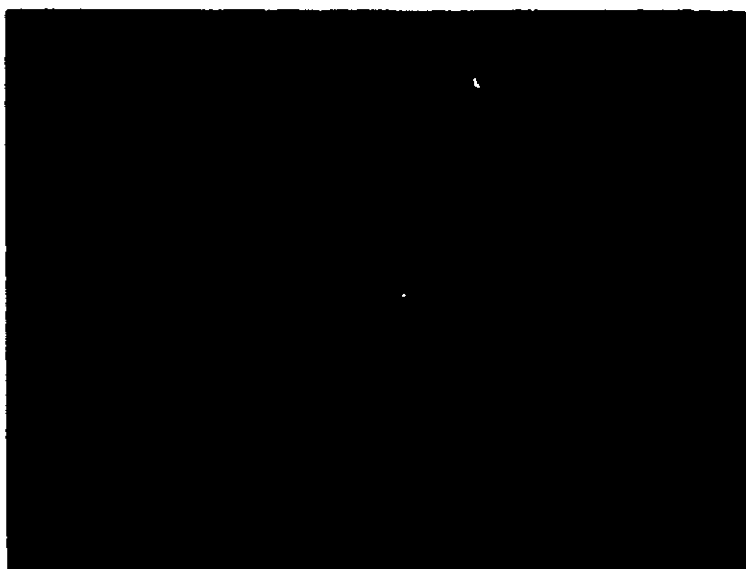
TRANSVERSE CROSS SECTION



200x

LONGITUDINAL CROSS SECTION

Figure 25. Optical and Electron Micrographs of Inconel 718 Rolled Bar in the 1297 K (1875 F) Solution Annealed Condition (Heat Treatment D). Etchant: 92 HCl, 3 HNO₃, 1/2 H₂SO₄



200x



3000x

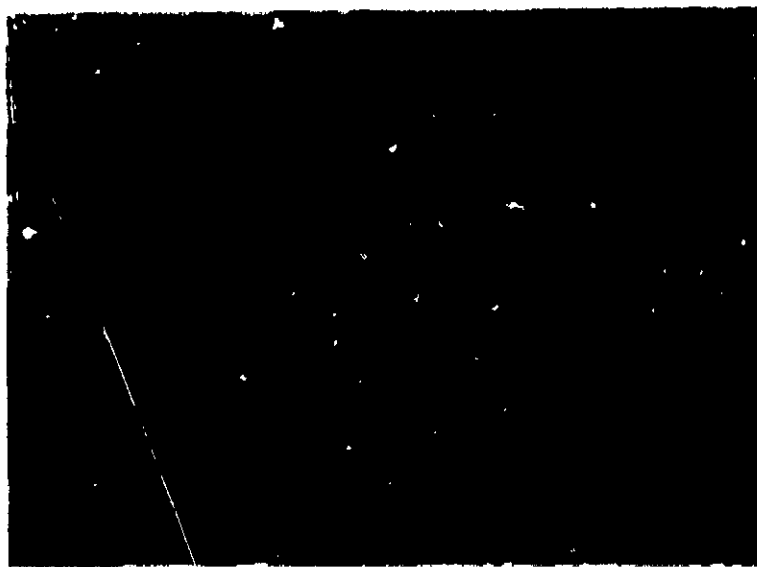
TRANSVERSE CROSS SECTION



200x

LONGITUDINAL CROSS SECTION

Figure 26. Optical and Electron Micrographs of Inconel 718 Rolled Bar in the E Heat Treatment Condition. Etchant: 92 HCl, 3 HNO₃, 1/2 H₂SO₄



200x



3000x

TRANSVERSE CROSS SECTION



200x

LONGITUDINAL CROSS SECTION

Figure 27. Optical and Electron Micrographs of Inconel 718 Forging in the E Heat Treatment Condition. Etchant: 92 HCl, 3 HNO₃, 1/2 H₂SO₄



200x



3000x

TRANSVERSE CROSS SECTION



200x

LONGITUDINAL CROSS SECTION

Figure 28. Optical and Electron Micrographs of Inconel 718 Plate in the E Heat Treatment Condition. Etchant: 92 HCl, 3 HNO₃, 1/2 H₂SO₄



200x



3000x

Heat Affected Zone



200x



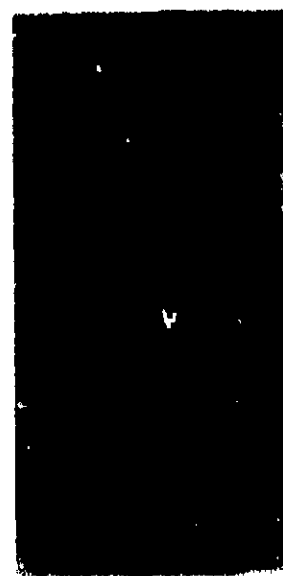
3000x

Weld Metal

Figure 29. Optical and Electron Micrographs of Welded Inconel 718 Plate in the A Heat Treatment Condition. Etchant: 92 HCl, 3 HNO₃, 1/2 H₂SO₄

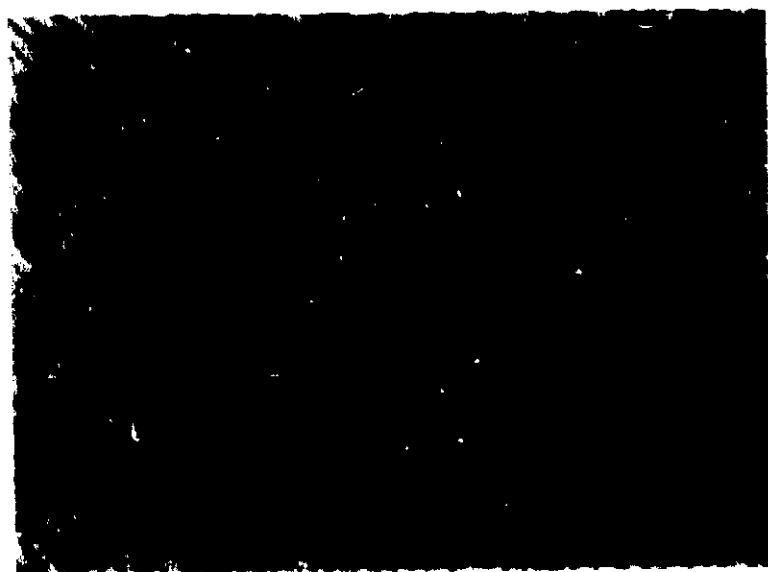


200x



3000x

Heat-Affected Zone



200x



3000x

Weld Metal

Figure 30. Optical and Electron Micrographs of Welded Inconel 718 Plate in the B Heat Treatment Condition. Etchant: 92 HCl, 3 HNO₃, 1/2 H₂SO₄

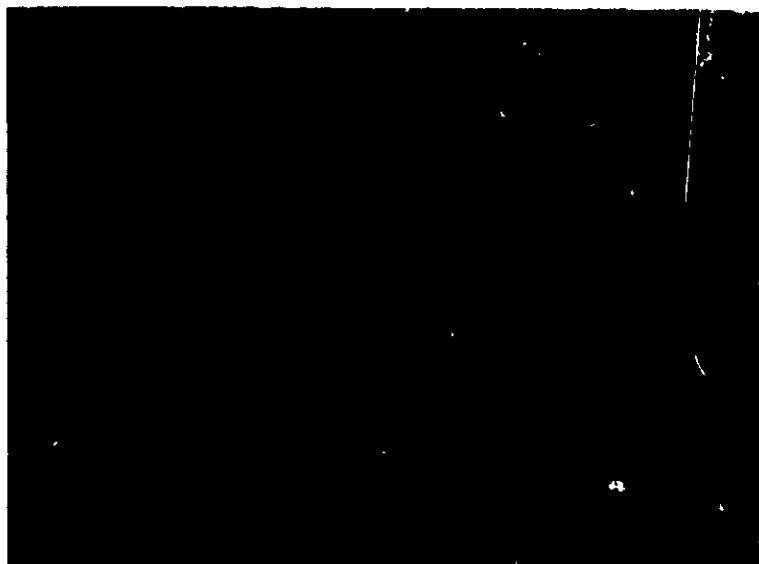


200x



3000x

Heat-Affected Zone



200x



3000x

Weld Metal

Figure 31. Optical and Electron Micrographs of Welded Inconel 718
Plate in the C Heat Treatment Condition. Etchant: 92 HCl,
3 HNO₃, 1/2 H₂SO₄

cored structure is evident in the weld when in the A and B heat treatment conditions. The microstructures of the weld in the C heat treatment condition appears similar to that for the parent metal but with somewhat smaller grain size and remnants of dendritic segregation.

The electron micrographs of the weld metal with the A and B heat treatments show an almost continuous array of the phase assumed to be Ni_3Cb . This phase can also be seen in the electron micrographs of the heat-affected zone of specimens with these same heat treatments and it is coarser and more continuous than in the parent metal. The heat-affected zone also contained Ni_3Cb needles in the typical Widmanstätten pattern.

Electron micrographs of parent metal, weld metal, and heat-affected zone all appear similar for weld specimens with the C heat treatment. Intergranular carbide films and isolated carbide particles can be seen.

Electron fractography examination was performed on Inconel 718 WOL specimens tested in high-pressure hydrogen environments in Phases II and V. The results of this examination are given in this section rather than in the Phase II and V sections because of their pertinence to the extensive microscopy in this section.

Figure 32 shows the fracture of an Inconel 718 WOL specimen tested in the A heat treatment condition. The fracture is complex but it is evident that the primary failure mode is transgranular cleavage. A small percentage of the fracture appears to be intergranular cleavage and some secondary cracking is present, which also appears to be intergranular. Large cleavage facets such as that shown in the lower right fractograph in Fig. 32 were shown to have higher than average bulk concentrations of columbium by energy dispersive X-ray analysis. The high concentration of columbium suggests that these areas are Ni_3Cb .

The fractography of an Inconel 718 WOL specimen tested in hydrogen in the F heat treat condition is shown in Fig. 33. This fracture is completely intergranular with virtually no indication of ductility. The F heat treatment is the same as the C heat treatment except that the solution anneal was extended for a longer period to develop a larger grain size (ASTM 3-1/2) in order to simulate the grain size expected in the SSME Inconel 718 forgings.

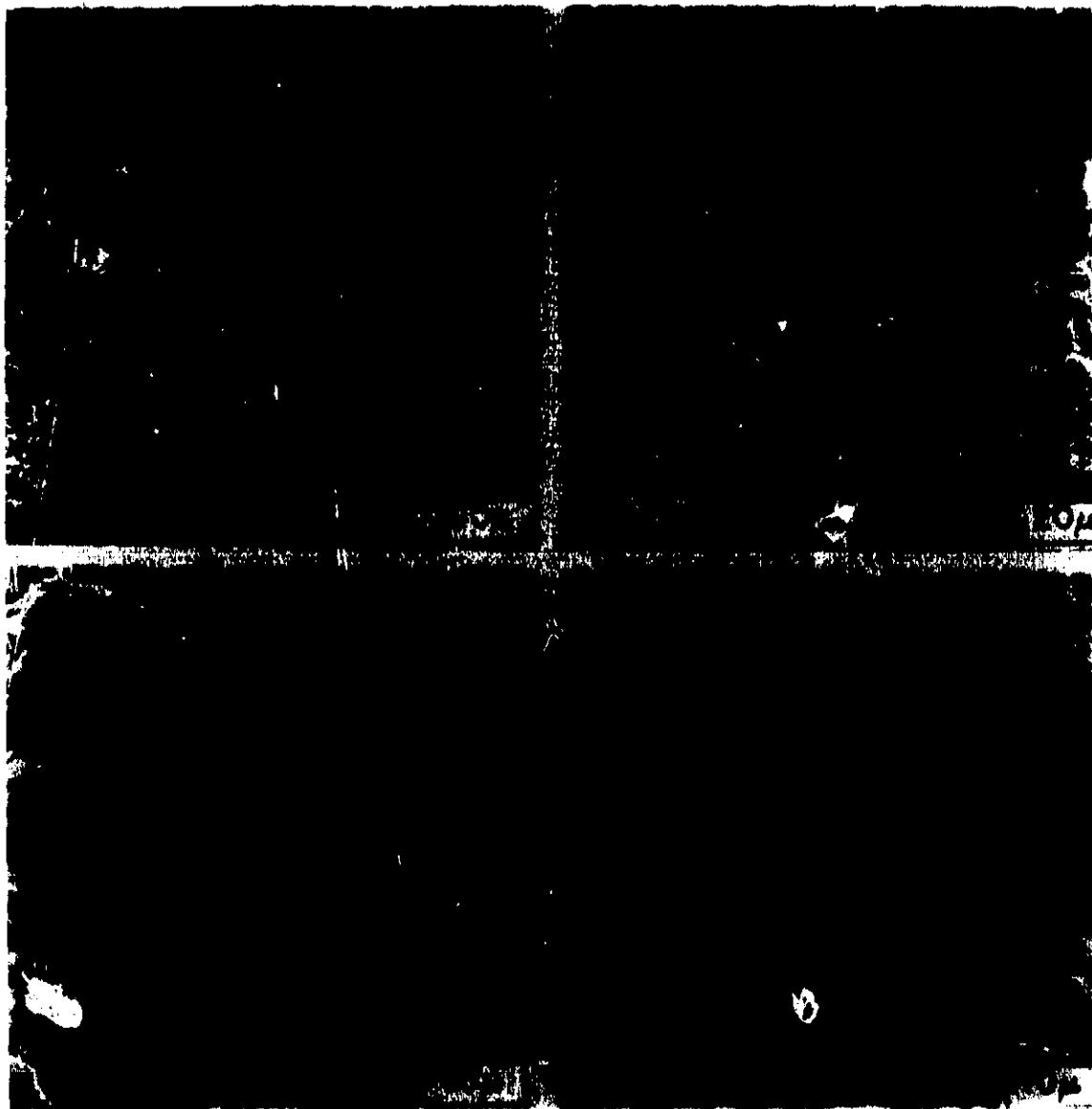


Figure 32. Scanning Electron Fractography of Inconel 718 WOL
Specimen Tested in 34.5 MN/m^2 (5000 psi) Hydrogen
in the A Heat Treatment Condition

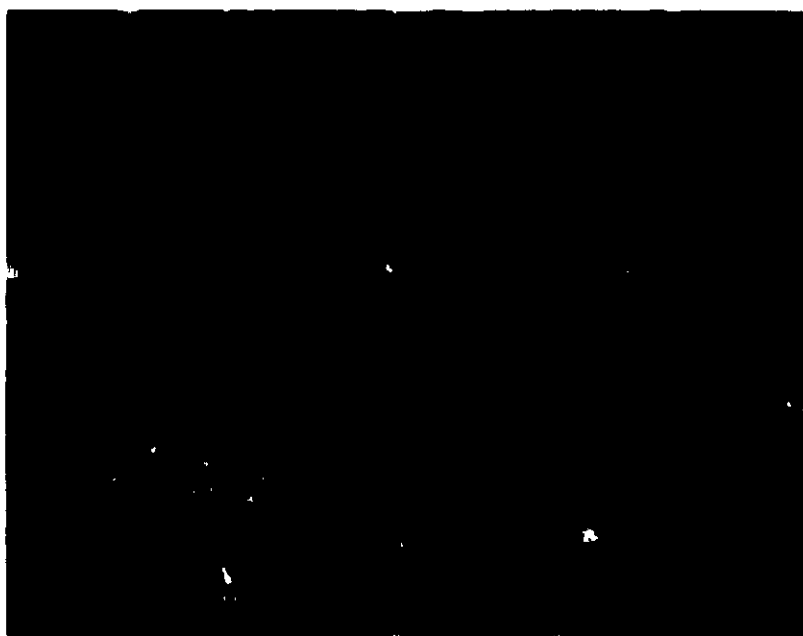


Figure 33. Scanning Electron Fractograph of an Inconel 718 WOL Specimen Tested in 68.9 MN/m² (10,000 psi) Hydrogen in the F Heat Treatment Condition *

The characteristic differences, discussed above, among the microstructures of the Inconel 718 rolled bar, forging, and plate with the various heat treatments can be related, at least qualitatively, to the degree of embrittlement by the high-pressure hydrogen environment. The least embrittled microstructure (i.e., the plate with the A heat treatment) was fine grained with discontinuous particles of the phase tentatively identified as Ni₃Cb. The most embrittled microstructure (i.e., the rolled bar and forging with the A heat treatment) was either relatively large grained or a duplex structure of small and large grains with, in both cases, semicontinuous mainly intergranular Ni₃Cb in the structure. Electron fractography examination also suggests that the fracture in hydrogen largely follows the Ni₃Cb phase.

The C heat treatment resulted in a large grain size, the elimination of Ni₃Cb, the presence of carbide particles and intermetallic films and intermediate embrittlement for the rolled bar, the forging, and the plate. The B overaging heat treatment

coarsened the Ni_3Cb and the age hardening precipitate but did not significantly change embrittlement from that for the A heat treatment. This lack of sensitivity of embrittlement to overaging indicates that the degree of hydrogen-environment embrittlement is not strongly influenced by the age hardening precipitate size, morphology, or coherency.

It thus appears that the least embrittled microstructure is one that is fine grained with dispersed Ni_3Cb . A fine-grained structure can be achieved only by severe working of the ingot and is not always feasible in large forgings. It is not clear which is the most important, dispersed Ni_3Cb or fine grain size. Removal of the Ni_3Cb phase by the C heat treatment decreased embrittlement of the relatively large grained material. Increasing the grain size while removing the Ni_3Cb phase increased embrittlement of the fine-grained material. It could, therefore, be postulated that the optimum heat treatment may be the lowest time-temperature anneal to place the Ni_3Cb into solution and avoid grain growth.

On this basis, specimens were solution annealed at 1297 K (1875 F) for 600 seconds (10 minutes) followed by the standard 1033-922 K (1400-1200 F) aging treatment (heat treatment E). Table 12 summarizes the results of the metallography examination and tensile properties of these three Inconel 718 forms when in the C and E heat treatment conditions. Grain size comparison with the 1325 K (1925 F) 1200-second (20 minutes) annealed and aged specimens shows that grain growth was certainly minimized by the 1297 K (1875 F) 600-second (10 minutes) anneal. As indicated above, the 1297 K (1875 F) 600-second (10 minutes) anneal was not successful for complete elimination of Ni_3Cb in the forging and plate.

Examination of the results in Table 12 indicates that the finer grain size resulting from E heat treatment had little or no effect on the hydrogen-environment embrittlement. For the forging material, the slightly greater hydrogen-environment embrittlement with the E heat treatment may have been caused by the presence of Ni_3Cb . The results of this study suggest that the benefit of fine-grain size for the 0.013 m (1/2 in.) plate in the A condition occurred because of the comparatively very fine-grain size of this material.

TABLE 12. AVERAGE NOTCHED TENSILE PROPERTIES OF INCONEL 718
IN 34.5 MN/m² (5000 psi) H₂ AND He

Material	Environment	Test Results											
		1297 (600 seconds) 1033-922 K (1875, 1400-1200 F)						1325 (1200 seconds) 1033-922 K (1925, 1400-1200 F)					
		Grain Size *	Ni ₃ Al Present	Notch Strength		Strength Ratio H ₂ /He	Reduction of Area, percent	Grain Size *	Ni ₃ Al Present	Notch Strength		Strength Ratio H ₂ /He	Reduction of Area, percent
				ksi	MM/m ²					ksi	MM/m ²		
0.032 x 0.07 m (1-1/4 x 2-3/4 in.) Rolled Bar	He	7.0		2200	319	--	4.0			2220	322	--	5.0
	H ₂		None	1560	226	0.71	1.9		None	1590	230	0.71	1.7
0.038 m (1-1/2 in.) Forging	He	7.0		2220	322	--	3.5	4.5		2340	339	--	4.6
	H ₂		Yes	1550	225	0.70	1.4		None	1780	258	0.76	1.8
0.013 m (1/2 in.) Plate	He	8.0		2200	319	--	4.2	5.0		2210	320	--	3.7
	H ₂		Trace	1650	239	0.75	2.7		None	1700	247	0.77	2.3

*Measured by the grain intercept method on a 200x photomicrograph

PHASE V. FRACTURE CHARACTERISTICS OF INCONEL 718 IN HYDROGEN AS A FUNCTION OF TEST VARIABLES

The effect of temperature and hydrogen pressure on the fracture mechanics properties of Inconel 718 were determined with the following measurements: (1) K_{IC} and K_{TH} at ambient temperature in 0.069 MN/m^2 (10 psi) and 69 MN/m^2 (10,000 psi) hydrogen and K_{TH} at 200 K (-100 F) in 34.5 MN/m^2 (5000 psi) hydrogen, and (2) cyclic load crack growth rate as a function of stress intensity (da/dN versus K_{II}) at ambient temperature in 0.069 MN/m^2 (10 psi), 34.5 MN/m^2 (5000 psi) and 69.9 MN/m^2 (10,000 psi) hydrogen and in 34.5 MN/m^2 (5000 psi) helium environments and at 200 K (-100 F) in 34.5 MN/m^2 (5000 psi) hydrogen. The ambient-temperature K_{IC} and K_{TH} measurements were performed on compact tension specimens (Fig. 2). The ambient-temperature cyclic crack growth measurements were performed on TDCB specimens (Fig. 4). The cryogenic-temperature K_{TH} and cyclic crack growth measurements were performed on WOL specimens (Fig. 3). The specimens were all fabricated from the 0.041 m (1-5/8 in.) Inconel 718 forging (Table 1) and were in the F heat treatment condition.

The results of the ambient-temperature K_{IC} and K_{TH} measurements are tabulated in Table 13. The ASTM K_{IC} (Ref. 14) requirements were not met for these tests because K_{max} was $>1.1 K_Q$. The very high value of $222 \text{ MN/m}^2 \sqrt{m}$ (202 ksi $\sqrt{in.}$) obtained at K_{max} on specimen No. T2 was due to crack branching immediately at onset of crack growth in the 69 MN/m^2 (10,000 psi) hydrogen environment. The average value, $103 \text{ MN/m}^2 \sqrt{m}$ (94 ksi $\sqrt{in.}$), or K_Q obtained in 69 MN/m^2 (10,000 psi) hydrogen was about the same as the $110 \text{ MN/m}^2 \sqrt{m}$ (100 ksi $\sqrt{in.}$) value obtained in Phase II in 34.5 MN/m^2 (5000 psi) hydrogen. The values of K_Q obtained in 0.069 MN/m^2 (10 psi) hydrogen were, however, greater than the value of K_Q , $119 \text{ MN/m}^2 \sqrt{m}$ (108 ksi $\sqrt{in.}$), obtained in 34.5 MN/m^2 (5000 psi) helium. The small side groove in the WOL specimens used in the Phase II tests may account for the lower stress intensity value at K_Q .

TABLE 13. RESULTS OF AMBIENT TEMPERATURE FRACTURE
ON INCONEL 718 COMPACT TENSION SPECIMENS

Specimen No.	Test Environment			K _{IC}						K _{max}			Crack Lengths Measured Directly	
	Type	Pressure		K _I		Meets ASTM Requirement			Nominal Stress Less Than σ _{ys}	MN/m ² √m	ksi √IN.	Nominal Stress Less Than σ _{ys}	MN/m ² √m	ksi √IN.
		MN/m ²	psi			2.8 (K/σ _{ys}) ²	K _Q Requirements	Crack Uniformity						
T-1	H ₂	69	10,000	98	89	yes	no	yes	yes	168	153	no	133	121
T-2	H ₂	69	10,000	104	98	yes	no	yes	yes	222	202	no	48	44
T-3	H ₂	0.069	10	-	--	--	--	yes	--	176	160	no	117	106
T-5	H ₂	0.069	10	130	118	no	yes	yes	no	147	134	no	154	140
T-6	H ₂	0.069	10	145	132	no	yes	yes	no	157	143	no	156	142

*Yield strength Inconel 718 = 1120 MN/m^2 (162 ksi) K for Plane Strain 110 $MN/m^2 \sqrt{m}$ (100 ksi $\sqrt{in.}$)

FOLDOUT FRAME

AMBIENT TEMPERATURE FRACTURE MECHANICS MEASUREMENTS
 ONEL 718 COMPACT TENSION SPECIMENS

		K Final								Nominal Stress Less Than σ_{ys}	R_{SC} $\sigma_{K_{max}}/\sigma_{ys}$	Remarks
ksi $\sqrt{in.}$	Nominal Stress Less Than σ_{ys}	Crack Lengths Measured Directly		Crack Lengths Measured by Compliance		Time Under Load		Meets ASTM Requirements				
		MN/m ² \sqrt{m}	ksi $\sqrt{in.}$	MN/m ² \sqrt{m}	ksi $\sqrt{in.}$	Seconds $\times 10^{-4}$	Hours	2.5 (K/ σ_{ys}) ²	Crack Uniformity			
153	no	133	121	--	--	8.64	24	no	no	no	1.8	{Crack extended to within 0.002 m (0.1 in.) from specimen end
202	no	48	44	--	--	8.28	23	yes	yes	yes	2.3	
160	no	117	106	90	82	5.76	16	yes	no	no	1.9	
134	no	154	140	119	108	8.64	24	no	no	yes	1.6	
143	no	156	142	117	106	25.2	70	no	no	no	1.6	

FOLDOUT FRAME

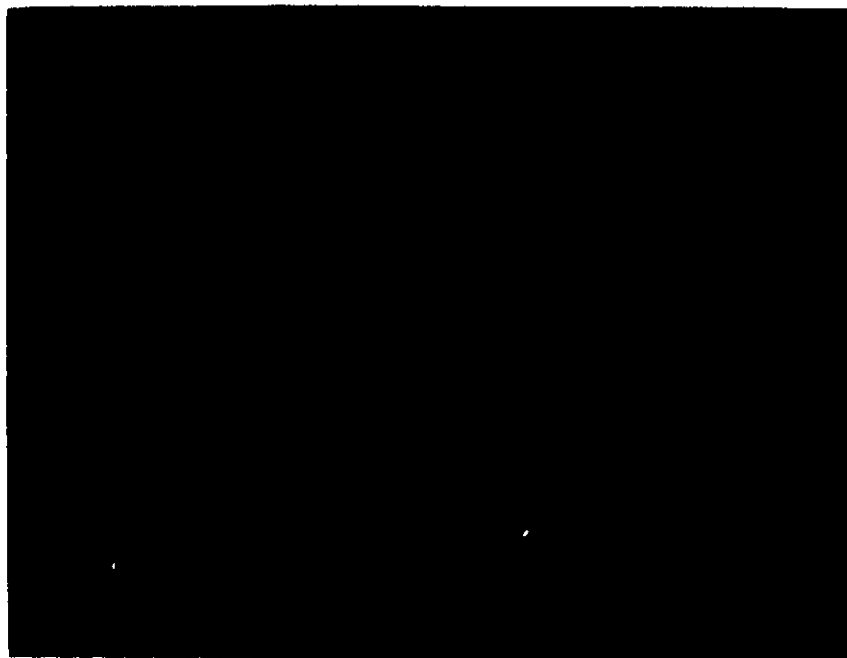
2

After the maximum "failure" load (see page 14) was reached, each specimen was held under COD control and the crack allowed to propagate until the crack arrested at K_{TH} . Crack growth was very rapid during the sustained-load part of the tests conducted in 69 MN/m^2 (10,000 psi) hydrogen. A K_{TH} value of $48 \text{ MN/m}^2 \sqrt{\text{m}}$ ($44 \text{ ksi} \sqrt{\text{in.}}$) was obtained for one of the specimens tested in this environment. The crack length of the second specimen was too long and close to the specimen end for an accurate K_{TH} measurement. The one K_{TH} value obtained is slightly higher than the $41 \text{ MN/m}^2 \sqrt{\text{m}}$ ($38 \text{ ksi} \sqrt{\text{in.}}$) value previously reported for K_{TH} in 34.5 MN/m^2 (5000 psi) hydrogen environment. The K_{TH} at various hydrogen pressures was more exactly determined in Phase VIII of this program.

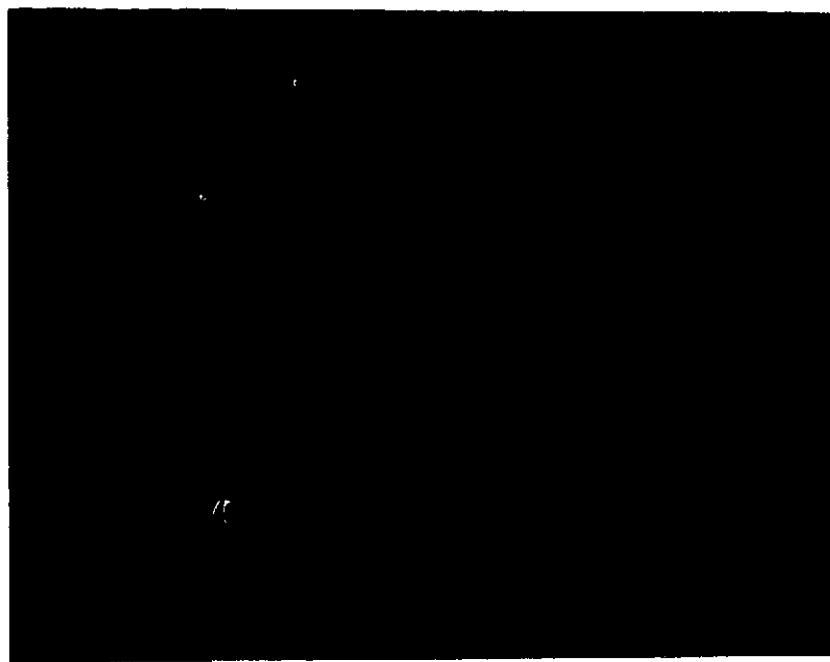
Figure 34 shows the fracture of a specimen tested in 0.069 MN/m^2 (10 psi) hydrogen. Sustained load crack growth was very slow and restricted to the inner portion of these specimens. the dark color of the sustained-load crack growth region is characteristic of fractures severely embrittled by hydrogen. Scanning electron fractography, however, showed the fracture to be predominately ductile. Because of the very irregular shape of the crack front and the long crack lengths at K final, the accuracy of the K_{TH} values obtained in 0.069 MN/m^2 (10 psi) hydrogen are questionable.

Threshold stress intensity measurements performed on Inconel 718 WOL specimens exposed to 34.5 MN/m^2 (5000 psi) helium and hydrogen environments at 200 K (-100 F) are tabulated in Table 14. The specimen tested in helium was loaded to above the 5-percent secant intercept, but below the point at which the load declines with increasing crack opening displacement. There was a small load decline soon after the specimen was loaded which may have been more the result of stress relaxation at the crack tip than crack extension. The stress intensity at the 5-percent secant offset was $150 \text{ MN/m}^2 \sqrt{\text{m}}$ ($136 \text{ ksi} \sqrt{\text{in.}}$), which is above the maximum stress intensity that meets ASTM plane strain conditions for 0.0254 m (1.0 in.) thick specimens.

Very slow sustained-load crack extension occurred in the Inconel 718 specimens exposed to hydrogen at 200 K (-100 F). The threshold stress intensity was not obtained because of the very slow rate of crack extension and because the stress intensity did not decrease during the long period that specimen T2 was under load, although there was some crack extension during the hold period. Therefore, K_{TH}



1.5x



200x

Figure 34. Scanning Electron Fractographs of an Inconel 718 WOL Specimen Tested in 0.069 MN/m^2 (10 psi) Hydrogen

TABLE 14. RESULTS OF FRACTURE MECHANICS MEASUREMENTS
TESTED IN 34.5 MN/m^2 (5000 PSI) H_2 AND He

Specimen No.	Test Environment	K_{Ic}						K_{max}				
		K_Q		Meets ASTM Requirements			Nominal Stress Less Than σ_{ys}			Nominal Stress Less Than σ_{ys}		
		$\frac{\text{MN}}{\text{m}^2} \sqrt{\text{m}}$	$\text{KSI} \sqrt{\text{in.}}$	$2.5 \left(\frac{K}{\sigma_{ys}}\right)^2$	K_Q Requirements	Crack Uniformity					$\frac{\text{MN}}{\text{m}^2} \sqrt{\text{m}}$	KSI
T3	Helium	149	136	no	no	yes	yes	164	149	yes	160	14
T1	Hydrogen	---	---	--	--	yes	---	63	57	yes	51	4
T2	Hydrogen	---	---	--	--	yes	---	47	43	yes	47	4

FOLDOUT FRAME

MECHANICS MEASUREMENTS ON INCONEL 718 WOL SPECIMENS
 1000 PSI) H₂ AND He AT 200 K (-100 F)

	K Final						Remarks	
Nominal Stress Less Than σ_{ys}	$\frac{MN}{m^2} \sqrt{m}$	KSI $\sqrt{in.}$	Time Under Load "		Meets ASTM Requirements			Nominal Stress Less Than σ_{ys}
			Seconds $\times 10^{-4}$	Hours	$2.5 \left(\frac{K}{\sigma_{ys}}\right)^2$	Crack Uniformity		
yes	160	146	7.38	20.5	no	yes	yes	The crack extended 0.0065 m (0.255 in) during this period but the crack growth was not accompanied by reduction of stress intensity
yes	51	46	69.1	192	yes	yes	yes	
yes	47	43	95.0	264	yes	yes	yes	

for Inconel 718 at 200 K (-100 F) in 34.5 MN/m^2 (5000 psi) hydrogen must be less than $47 \text{ MN/m}^2 \sqrt{\text{m}}$ (43 ksi $\sqrt{\text{in.}}$). This is near the K_{TH} value, $42 \text{ MN/m}^2 \sqrt{\text{m}}$ (38 ksi $\sqrt{\text{in.}}$), for Inconel 718 exposed to 34.5 MN/m^2 (5000 psi) hydrogen at ambient temperature. Thus, K_{TH} may be nearly the same at 200 K (-100 F) as it is at ambient temperature, but the rate of crack extension is considerably slower at 200 K (-100 F) than it is at ambient temperature. K_{TH} at 144 K (-200 F) was shown in Phase II to be $125 \text{ MN/m}^2 \sqrt{\text{m}}$ (112 ksi $\sqrt{\text{in.}}$) for Inconel 718 in the same heat treatment condition and exposed to 34.5 MN/m^2 (5000 psi) hydrogen. This large increase of measured K_{TH} from 200 K (-100 F) to 144 K (-200 F) may be partly the result of decreased rate of crack extension with decreasing temperature, and the real value for K_{TH} in hydrogen at 200 K (-100 F) may therefore, be lower than $125 \text{ MN/m}^2 \sqrt{\text{m}}$ (112 ksi $\sqrt{\text{in.}}$).

The results of the cyclic-load crack growth measurements performed at ambient temperature on Inconel 718 TDCB specimens are plotted in Fig. 35 for tests performed in 34.5 MN/m^2 (5000 psi) helium and 68.9 MN/m^2 (10,000 psi) hydrogen, in Fig. 36 for tests performed in 34.5 MN/m^2 (5000 psi) hydrogen, and in Fig. 37 for tests performed in 0.069 MN/m^2 (10 psi) hydrogen. For comparison purposes, the 34.5 MN/m^2 (5000 psi) helium curves are included in Fig. 36 and 37. Figure 38 summarizes the cyclic crack growth of Inconel 718 by including all of the curves (without data points) shown in Fig. 35 through 37.

The data show that the cyclic crack growth rate in Inconel 718 is faster in hydrogen than in helium. The influence of hydrogen on the cyclic crack growth rate increased with increasing hydrogen pressure. Even the 1.0-cps data obtained in 0.069 MN/m^2 (10 psi) hydrogen indicate a measurable increase of crack growth rate compared to that in helium. Comparison of the curves in Fig. 38 shows that the hydrogen environments had the greatest effect on the cyclic crack growth rate in Inconel 718 when the tests were performed at 0.1 cycle/sec compared to the standard cyclic rate of 1.0 cycles/sec used in this program. The crack growth rate per cycle at 0.1 cycle/sec was about five times faster in 0.069 MN/m^2 (10 psi) hydrogen and about 25 times faster in 68.9 MN/m^2 (10,000 psi) hydrogen compared to helium at 34.5 MN/m^2 (5000 psi) for the lowest stress intensity range, $55 \text{ MN/m}^2 \sqrt{\text{m}}$ (50 ksi $\sqrt{\text{in.}}$), tested at this cyclic rate.

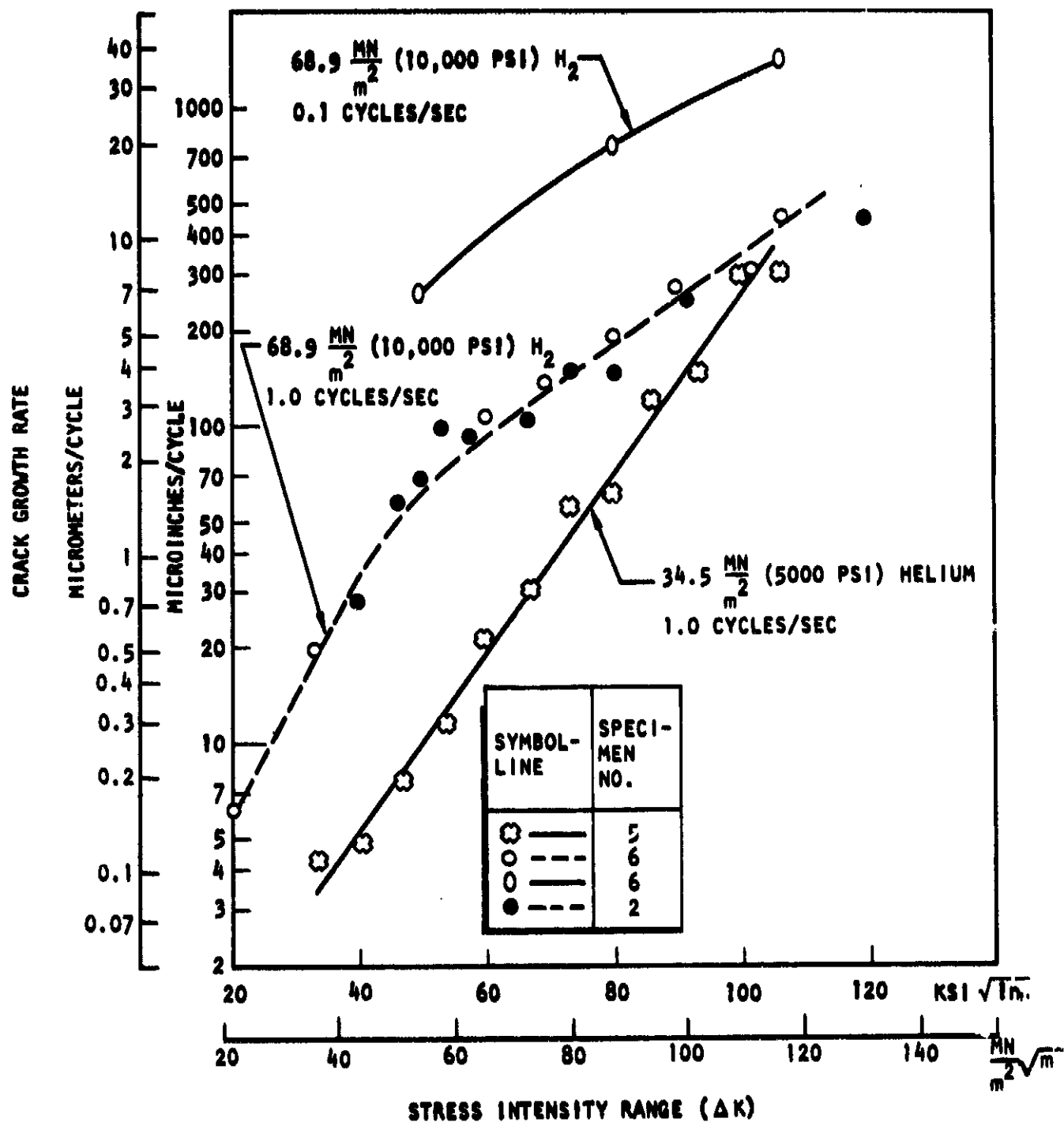


Figure 35. Cyclic Crack Growth Rate as a Function of Stress Intensity Range for Inconel 718 Exposed to 34.5 MN/m^2 (5000 psi) Helium and 68.9 MN/m^2 (10,000 psi) Hydrogen Ambient Temperature Environments

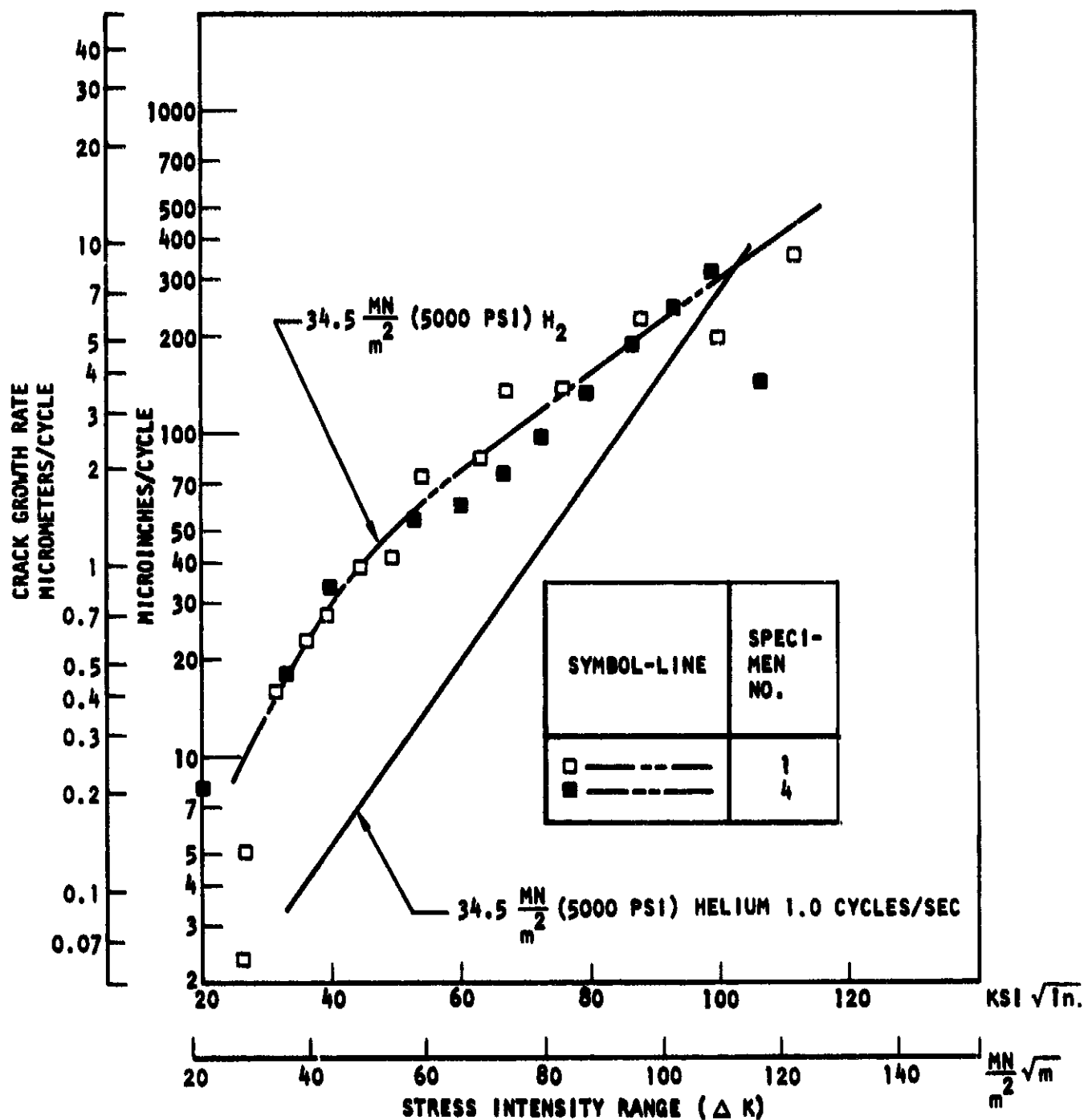


Figure 36. Cyclic Crack Growth Rate as a Function of Stress Intensity Range for Inconel 718 Exposed to 34.5 MN/m^2 (5000 psi) Helium and 34.5 MN/m^2 (5000 psi) Hydrogen Ambient Temperature Environments

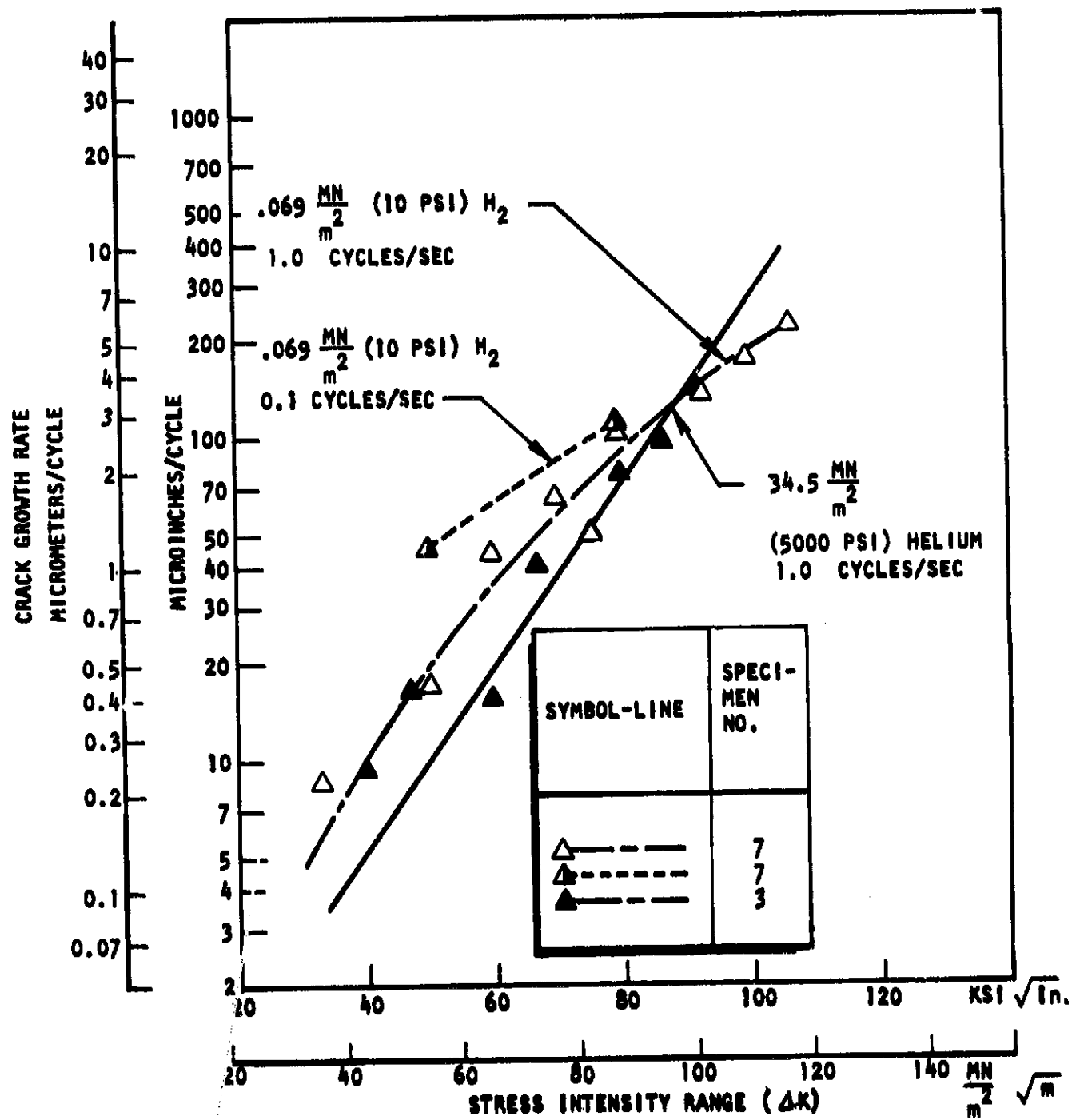


Figure 37. Cyclic Crack Growth Rate as a Function of Stress Intensity Range for Inconel 718 Exposed to 34.5 MN/m^2 (5000 psi) Helium and 0.069 MN/m^2 (10 psi) Hydrogen Ambient Temperature Environments

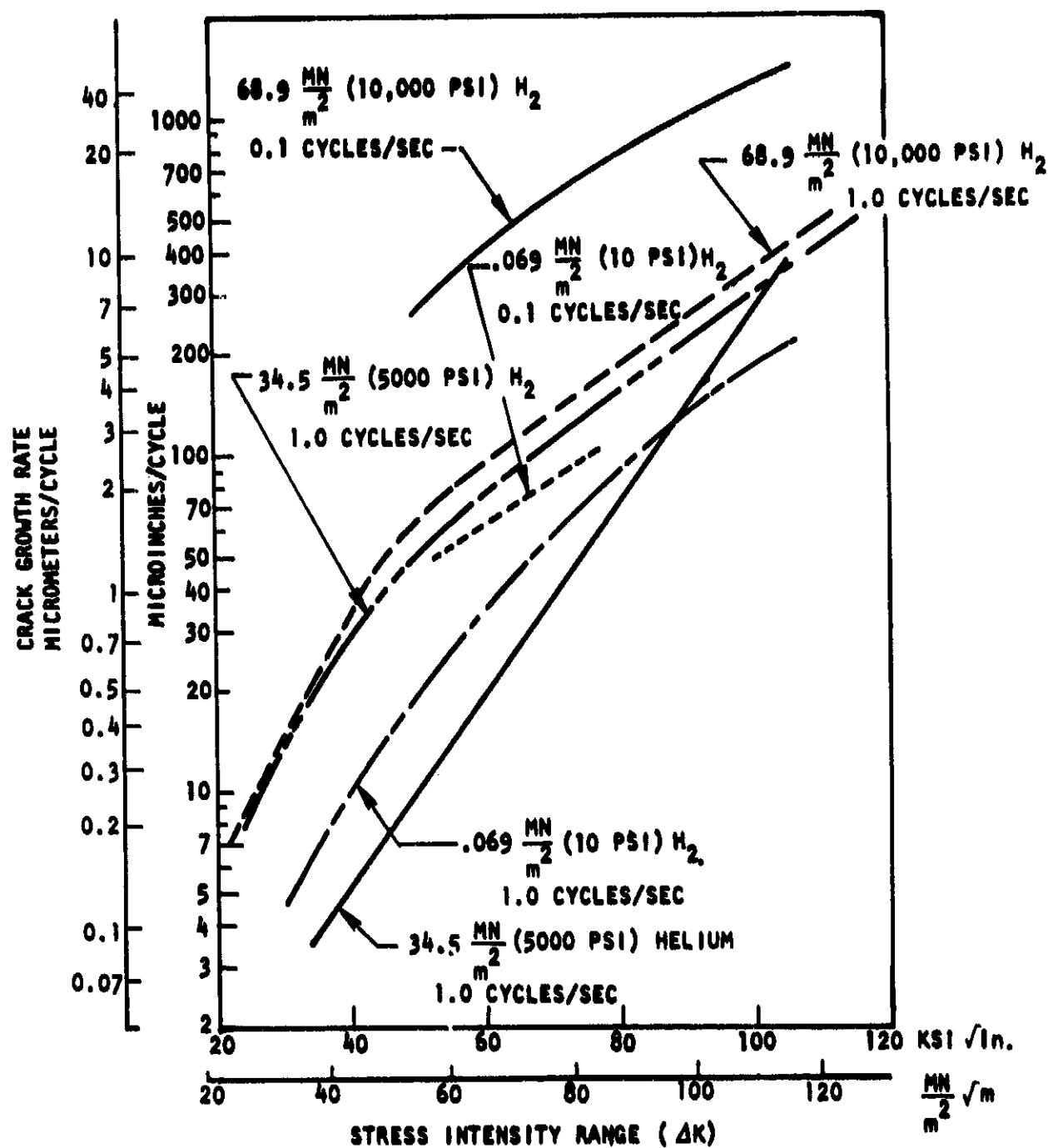


Figure 38. Cyclic Crack Growth Rate as a Function of Stress Intensity Range for Inconel 718 Exposed to 34.5 MN/m^2 (5000 psi) Helium and 0.069 MN/m^2 (10 psi), 34.5 MN/m^2 (5000 psi), and 68.9 MN/m^2 (10,000 psi) Hydrogen Ambient Temperature Environments

The increase of cyclic crack growth rate due to the hydrogen environments decreased with increasing stress intensity for all hydrogen pressures and cyclic rates tested. Above $110 \text{ MN/m}^2 \sqrt{\text{m}}$ ($100 \text{ ksi } \sqrt{\text{in.}}$) stress intensity range, the crack growth rate was less than or equal to the crack growth rate in helium when the tests were conducted at 1.0 cycle/sec. At 0.1 cycle/sec, there was still a sizeable effect of 68.9 MN/m^2 (10,000 psi) hydrogen environment on the crack growth rate at a stress intensity range of $117 \text{ MN/m}^2 \sqrt{\text{m}}$ ($106 \text{ ksi } \sqrt{\text{in.}}$). For the 0.069 MN/m^2 (10 psi) tests, the cyclic crack growth rate was about the same at 1.0 and 0.1 cycles/sec when cycled at $88 \text{ MN/m}^2 \sqrt{\text{m}}$ ($80 \text{ ksi } \sqrt{\text{in.}}$) stress intensity range.

Figure 39 is a plot of the crack growth rates in Inconel 718 exposed to 68.9 MN/m^2 (10,000 psi) hydrogen and cycled at 1.0, 0.75, 0.50, 0.25, and 0.1 cycles/sec at $54.7 \text{ MN/m}^2 \sqrt{\text{m}}$ ($49.7 \text{ ksi } \sqrt{\text{in.}}$) stress intensity range. The crack growth rate in 34.5 MN/m^2 (5000 psi) helium at $54.7 \text{ MN/m}^2 \sqrt{\text{m}}$ ($49.7 \text{ ksi } \sqrt{\text{in.}}$) stress intensity range is also included for comparison purposes. The data in Fig. 39 show that the crack growth rate increases with the time per cycle and that the cyclic crack growth rate in 68.9 MN/m^2 (10,000 psi) hydrogen would approach the rate in helium at cyclic rates greater than 1 cycle per second.

Recently, Wei and co-workers (Ref. 24) measured the cyclic crack growth rate at 5 cycles per second in Inconel 718 in 0.133 MN/m^2 (10^{-3} torr, 19.3 psia) hydrogen at 576, 296, and 221 K (577, 73 and -62 F), and in argon at 297 K (75 F), and showed no hydrogen effect on the cyclic crack growth rate. Their specimens were fabricated from 0.0032 m (1/8 in.) plate and were in the 1255, 991-894 K (1800, 1325-1150 F) heat treatment condition which is essentially equivalent to heat treatment A (Table 5). The lack of embrittlement observed by Wei and co-workers is probably due to the combination of low hydrogen pressure and high cyclic test rate.

The data in Fig. 39 show that the function between time per cycle and crack growth rate is complex, and could not be expressed as the summation of the cyclic crack growth rate in helium and the sustained-load crack growth rate in 68.9 MN/m^2 (10,000 psi) hydrogen. This summation theory has been proposed by Wei and Landes (Ref. 25) to explain cyclic load crack growth in reactive environments.

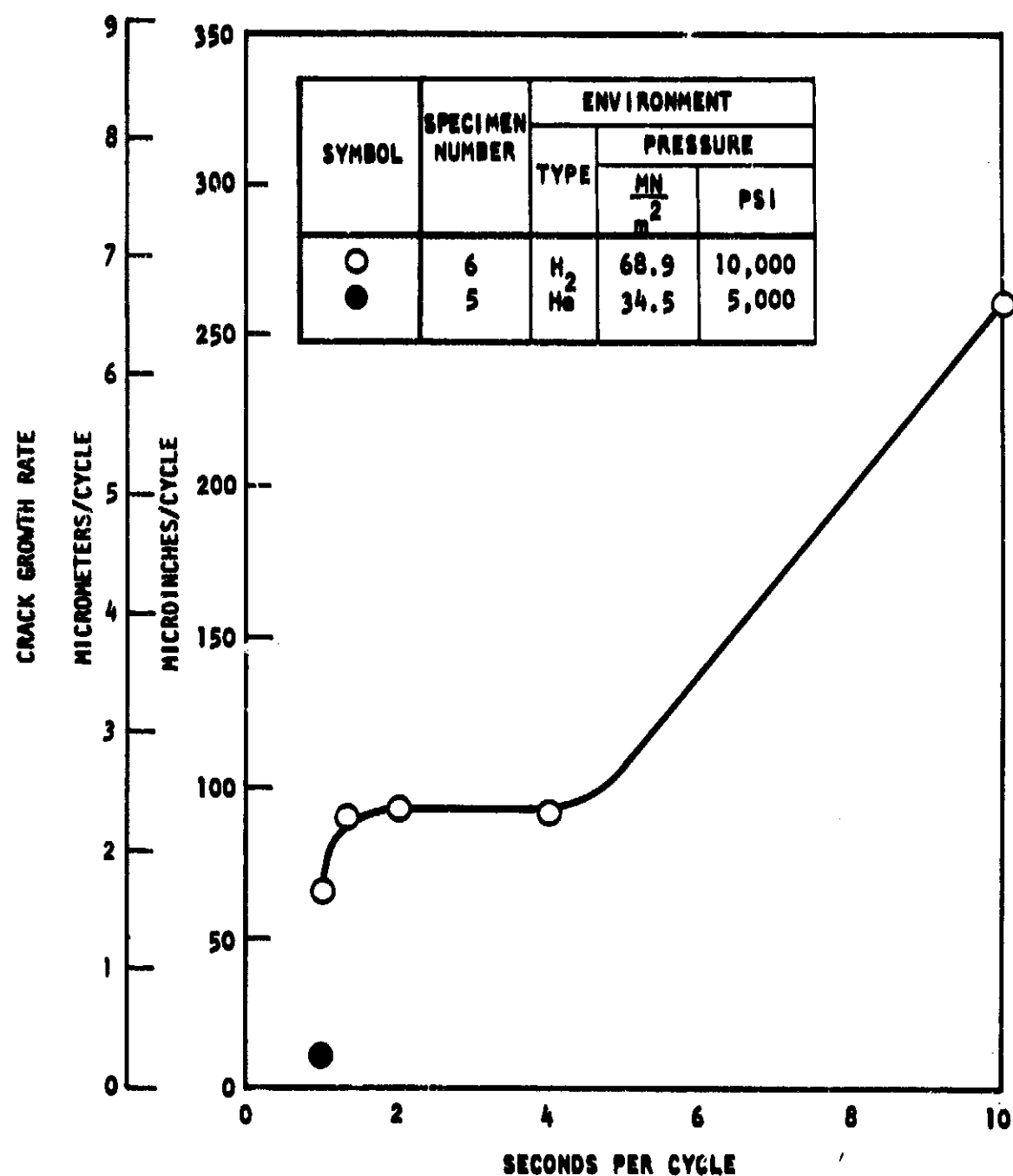


Figure 39. Ambient Temperature Cyclic Crack Growth Rate as a Function of Cyclic Rate for Inconel 718 Specimen No. 6 Exposed to 68.9 MN/m^2 (10,000 psi) Hydrogen at Stress Intensity Range of $54.7 \text{ MN/m}^2 \sqrt{m}$ ($49.7 \text{ ksi} \sqrt{\text{in.}}$)

Wei and Landes proposed that cyclic crack growth in an aggressive environment is equal to the sum of the rate of fatigue crack growth in an inert environment and sustained-load crack growth in the aggressive environment. Gallagher (Ref. 26) showed that Wei and Landes summation theory adequately described fatigue crack propagation of AISI 4340 in salt water. Recently, Nelson, Tetelman, and Williams (Ref. 27) showed that the crack growth rate in Ti-5Al-2.5 Sn in 0.101 MN/m^2 (1-atmosphere-pressure) hydrogen can be expressed as the sum of sustained-load crack growth rate in hydrogen and cyclic load crack growth rate in 0.133 NM/m^2 (10^{-3} torr) vacuum.

Quantitative sustained-load crack growth rates are not available for Inconel 718 exposed to high-pressure hydrogen environments. Comparison with the sustained-load crack growth during K_{TH} measurements (Phase VIII below) would, however, indicate that the sustained-load crack growth rate of Inconel 718 in 34.5 MN/m^2 (5000 psi) hydrogen is considerably faster than would be indicated by the data shown in Fig. 37, assuming Wei and Landis summation theory to be applicable.

The results of the cyclic-load crack growth measurements performed on Inconel 718 WOL specimens exposed to 34.5 MN/m^2 (5000 psi) hydrogen at 200 K (-100 F) are plotted in Fig. 40. The data shows a greater degree of scatter than was obtained at ambient temperatures on Inconel 718 TDCB specimens. The difference in data scatter is probably the result of the different specimen types. For the WOL specimens, the stress intensity increases continuously with increasing crack length and for each cyclic increment, the average stress intensity during that period is assumed. For the TDCB specimen, the stress intensity remained constant with crack length and the cyclic crack growth rate can be well established before proceeding to a higher stress intensity.

Comparison of the crack growth rates in Fig. 38 and 40 shows that the rate of crack extension was about the same in 34.5 MN/m^2 (5000 psi) hydrogen at 200 K (-100 F) as in 34.5 MN/m^2 (5000 psi) helium at ambient temperature. The cyclic crack growth measurements performed by Wei and co-workers (Ref. 24) showed that the cyclic crack growth rate decreased with decreasing temperature in Inconel 718. Thus, the similarity between the cyclic crack growth rates in hydrogen at 200 K (-100 F) and in

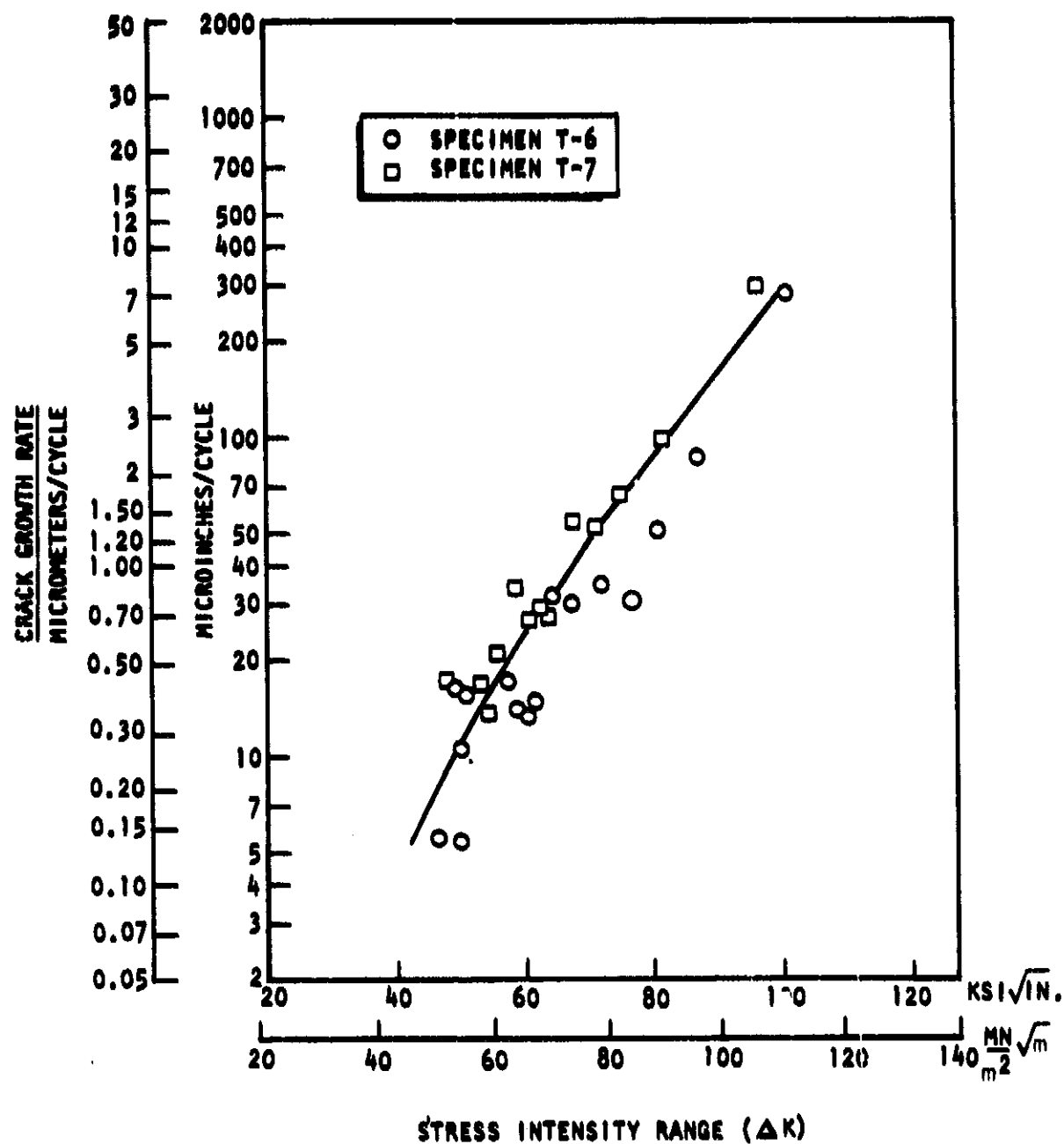


Figure 40. Cyclic Crack Growth Rate as a Function of Stress Intensity Range for Inconel 718 Exposed to 34.5 MN/m^2 (5000 psi) Hydrogen at 200 K (-100 F)

helium at ambient temperature does not necessarily mean that there was no hydrogen environmental effect on crack growth at 200 K (-100 F) since the crack growth rate in helium may be slower at 200 K (-100 F) than at ambient temperatures.

PHASE VI. FRACTURE MECHANICS PROPERTIES OF A PRESSURE VESSEL STEEL IN HIGH-PRESSURE HYDROGEN

The tensile properties, K_{IC} , K_{TH} , and rate of crack extension during cyclic loading was determined for ASTM A-533-B steel exposed to 103.4 MN/m² (15,000 psi) hydrogen and helium environments. The fracture mechanics testing was performed with 0.0254 m (1 in.) thick compact tension specimens for the K_{IC} and K_{TH} measurements and with TDCB specimens for the cyclic loading crack growth rate measurements.

The tensile test results are tabulated in Table 15. The degree of embrittlement of the notched specimen is consistent with the H₂/He notch strength ratio of 0.78 obtained previously (Ref. 28) in 68.9 MN/m² (10,000 psi) hydrogen, for ASTM A-533-B material. The reduction of unnotched specimen ductility is also about the same as obtained previously in 68.9 MN/m² (10,000 psi) hydrogen, but the strength decrease of the unnotched specimen IUH-3 was larger than expected.

The results of tests performed on A-533-B compact tension specimens in 103 MN/m² (15,000 psi) helium and hydrogen environments are tabulated in Table 16. The tests were performed in the same manner as the compact tension tests on Inconel 718 specimens discussed in Phase V. The results in Table 16 indicate that plane strain K_{IC} values were not obtained on the A-533-B specimens. That is, the 0.0254 m (1.0 in.) specimens were not sufficiently thick to meet plane strain requirements. The nominal stresses at K_Q were also higher than the yield strength of A-533-B. The stress intensities at K_{max} were greater than 1.1 times K_Q and, therefore, the recent modification of the ASTM K_Q requirement was not met for any of the tests. The cyclic crack growth measurements reported below show that 103 MN/m² (15,000 psi) hydrogen environment considerably accelerates the rate of cyclic load crack growth at stress

TABLE 15. TENSILE PROPERTIES OF ASTM A-533-B (ASTM A-302 Gr B, NICKEL MODIFIED)
STEEL IN 103.4 MN/m² (15,000 PSI) HYDROGEN AND HELIUM ENVIRONMENTS

Specimen					Strength				Ductility	
No.	Type	Stress Conc. Factor	Environ-ment	Yield		Ultimate		Strength Ratio H ₂ /He	Reduction of Area %	Elonga-tion %
				MN/m ²	KSI	MN/m ²	KSI			
1 UB-1	UN	-	Helium	703	102	786	114	-	69	20
1 UB-2	UN	-	Hydrogen	696	101	745	108	0.95	27	10
1 UB-3	UN	-	Hydrogen	-	-	593	86	0.75	33	15
1 NB-29	N	8.4	Helium	-	-	1475	214	-	-	6.8
1 NB-27	N	8.4	Hydrogen	-	-	1138	165	0.77	-	5.2
1 NB-28	N	8.4	Hydrogen	-	-	1103	160	0.75	-	4.1

TABLE 16. RESULTS OF AMBIENT TEMPERATURE FRACTURE MECHANISMS
ON ASTM A-533B COMPACT TENSION SPECIMENS

Specimen No.	Test Environment		K_{IC}							K_{max}			Crack Lengths Measured Directly	
			K_{IC}		Meets ASTM Requirement			Nominal Stress Less Than σ_{ys}	Nominal Stress Less Than σ_{ys}	Nominal Stress Less Than σ_{ys}				
	Type	Pressure			$2.5 (K/\sigma_{ys})^2$	K_{IC} Requirements	Crack Uniformity							
			MN/m ² psi	MN/m ² \sqrt{m} ksi $\sqrt{in.}$										
4	He	103 15,000	100	91	no	no	yes*	no	147	134	no	141	131	
1	H ₂	103 15,000	86	78	no	no	yes	no	129	117	no	108	98	
2	H ₂	103 15,000	80	73	no	no	yes*	no	98	89	no	95	86	
3	H ₂	103 15,000	83	75	no	no	yes*	no	128	116	no	106	96	

*Crack front along one edge $< 1.27 \times 10^{-5}$ m (0.05 in.) from machined notch and thus the precrack does not meet all ASTM requirements

**Yield strength A-533-B = 689 MN/m² (100 ksi) K for plane strain ≤ 43 MN/m² \sqrt{m} (63 ksi $\sqrt{in.}$)

FOLDOUT FRAME

IENT TEMPERATURE FRACTURE MECHANICS MEASUREMENTS
3B COMPACT TENSION SPECIMENS

		K Final									R _{SC} $\sigma_{K_{max}}/\sigma_{ys}$	Remarks
		Crack Lengths Measured Directly		Crack Lengths Measured by Compliance		Time Under Load		Meets ASTM Requirements		Nominal Stress Less Than σ_{ys}		
						Seconds $\times 10^{-4}$	Hours	2.5 (K/ σ_{ys}) ²	Crack Uniformity			
i	Nominal Stress Less Than σ_{ys}	MN/m ² \sqrt{m}	ksi $\sqrt{in.}$	MN/m ² \sqrt{m}	ksi $\sqrt{in.}$	$\times 10^{-4}$	Hours	2.5 (K/ σ_{ys}) ²	Crack Uniformity	Than σ_{ys}		
134	no	144	131	135	123	7.62	46	no	no	no	2.1	Specimen was loaded to 10% Secant intercept-which was less than the failure load
117	no	108	98	64	58	7.62	46	yes	no	no	1.9	
89	no	95	86	91	83	3.96	11	no	no	no	1.5	
116	no	106	96	99	90	25.9	72	no	no	no	1.8	

FOLDOUT FRAME

2

intensities as low as $22 \text{ MN/m}^2 \sqrt{\text{m}}$ ($20 \text{ ksi } \sqrt{\text{in.}}$). Thus, it would be expected that crack extension accompanied plastic deformation at the K_Q values obtained during the 103 MN/m^2 ($15,000 \text{ psi}$) hydrogen-environment tests. The K_Q values obtained in hydrogen were significantly less than the value obtained in helium, which tends to indicate that hydrogen induced crack extension at K_Q did occur.

Sustained load crack growth of A-533-B in hydrogen occurred predominately at the inner region of the specimen, and there was very little, if any, crack extension along the sides. One possibility is that the excess plastic deformation present at K_{max} blunted the crack, thus inhibiting crack extension except at the inner high triaxial restraint region. To confirm this, specimen No. 2 was loaded to the 10-percent secant intercept, rather than to the failure load, and then placed in COD control to crack arrest. The crack extended only an average of $3.7 \times 10^{-6} \text{ m}$ (0.014 in.) during the test, and it would, therefore, seem that the excessive plastic deformation at K_{max} does not account for the lack of sustained-load crack growth at the specimen sides.

The greatest sustained-load crack extension occurred on specimen No. 2, but there was virtually no crack growth along the specimen sides and the deviation of crack length from the average crack length was 38 percent. K_{TH} of specimen No. 1 determined from compliance measured crack length was $64 \text{ MN/m}^2 \sqrt{\text{m}}$ ($58 \text{ ksi } \sqrt{\text{in.}}$). This difference is due to the irregularity of the crack front and the compliance determined crack length should better represent the effective crack length.

It would, therefore, appear that appreciable sustained-load crack growth occurs in ASTM A-533-B in hydrogen only under plane strain conditions and K_{TH} can be measured only on specimens that are appreciably thicker than the 0.025 m (1.0 in.) compact tension specimens.

The strength ratio R_{SC} is the ratio of the nominal stress at K_{max} to the material's yield strength, and according to ASTM E-399 is to be computed whenever the K_Q plane strain requirement is not met. The stress at K_{max} was almost twice yield for all but specimen No. 2, which was not loaded to the "failure" load.

The cyclic load crack growth rates obtained on ASTM A-533-B specimens exposed to 103.4 MN/m^2 (15,000 psi) hydrogen and 103.4 MN/m^2 (15,000 psi) helium environments at ambient temperature are plotted in Fig. 41. Comparison of the two curves in Fig. 41 indicates that the hydrogen environment considerably accelerates the cyclic crack growth rate in ASTM A-533-B steel. The crack growth rates were about 20 times faster in hydrogen than in helium over the entire stress intensity range for which testing was performed.

PHASE VII. CYCLIC CRACK GROWTH IN HY100 STEEL IN HIGH-PRESSURE HYDROGEN

The effect of high-pressure hydrogen environments at ambient temperature on cyclic crack growth rates was determined for the HY100 steel. Two series of tests were performed to determine cyclic crack growth rates as a function of stress intensity in 51.7 MN/m^2 (750 psi) helium and hydrogen environments. A third series of tests were performed at one stress intensity range, $54.7 \text{ MN/m}^2 \sqrt{m}$ (49.7 ksi $\sqrt{in.}$), while the specimen was exposed to hydrogen at pressures ranging from 0.101 MN/m^2 (1 atmosphere) to 103.4 MN/m^2 (15,000 psi).

Figure 42 shows the results of the cyclic-load crack growth measurements performed on HY100 specimens. Specimens No. 1 and 2 were tested in both hydrogen and helium environments, with the tests conducted in helium first. For specimen No. 1, the data obtained in hydrogen progressed from the higher stress intensity ranges to lower stress intensity ranges. Because of the rapid crack extension in hydrogen, the overload condition existing at the beginning of testing at each stress intensity range was quickly eliminated. It was observed, however, that the load range could be reduced only a limited amount, $5.5\text{-}11 \text{ MN/m}^2 \sqrt{m}$ (5-10 ksi $\sqrt{in.}$) for the crack to extend immediately at the beginning of each reduced stress intensity series.

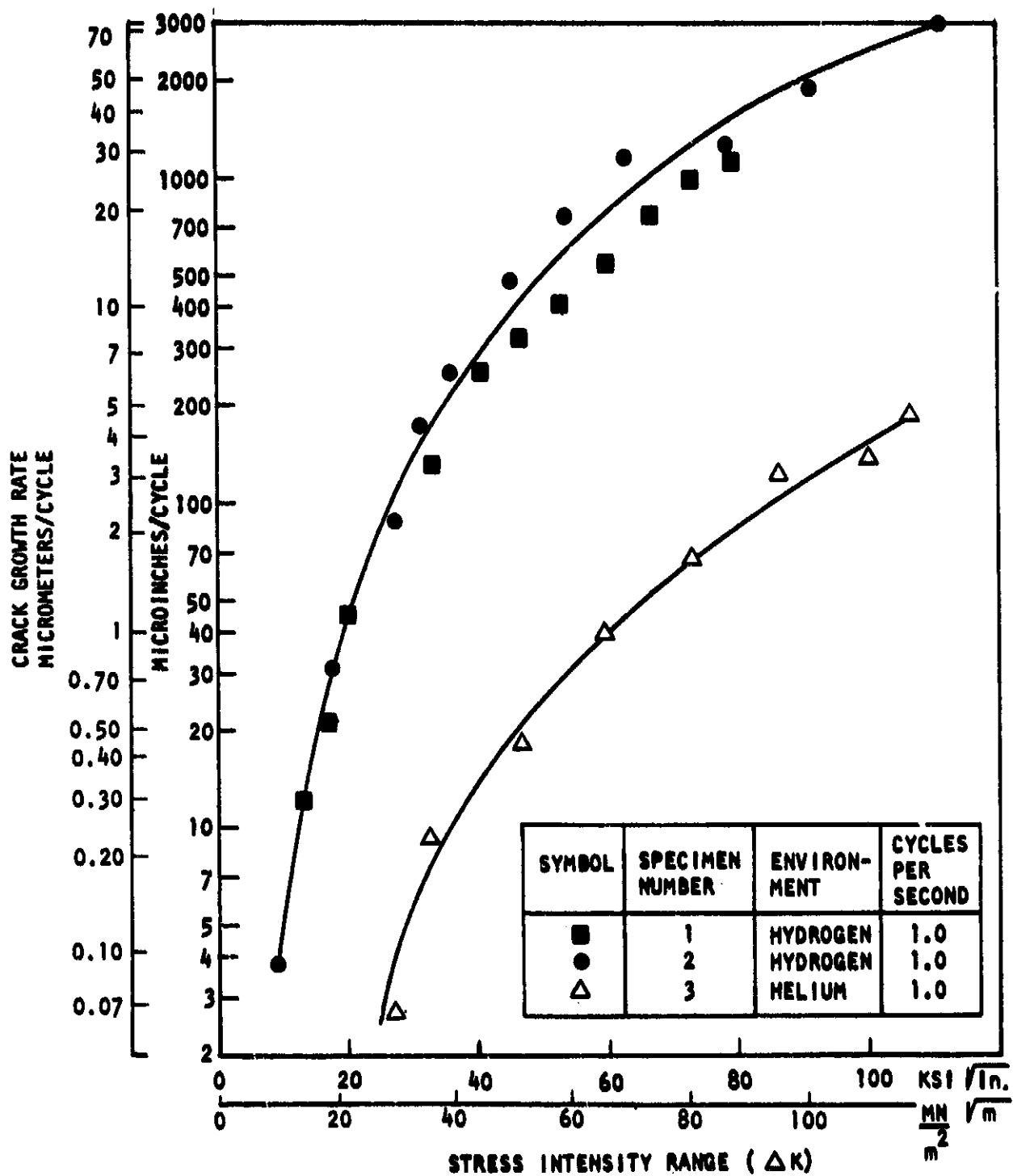


Figure 41. Cyclic Crack Growth Rate as a Function of Stress Intensity for ASTM A-533-B Exposed to 103.4 MN/m^2 (15,000 psi) Helium and 103.4 MN/m^2 (15,000 psi) Hydrogen Ambient Temperature Environments

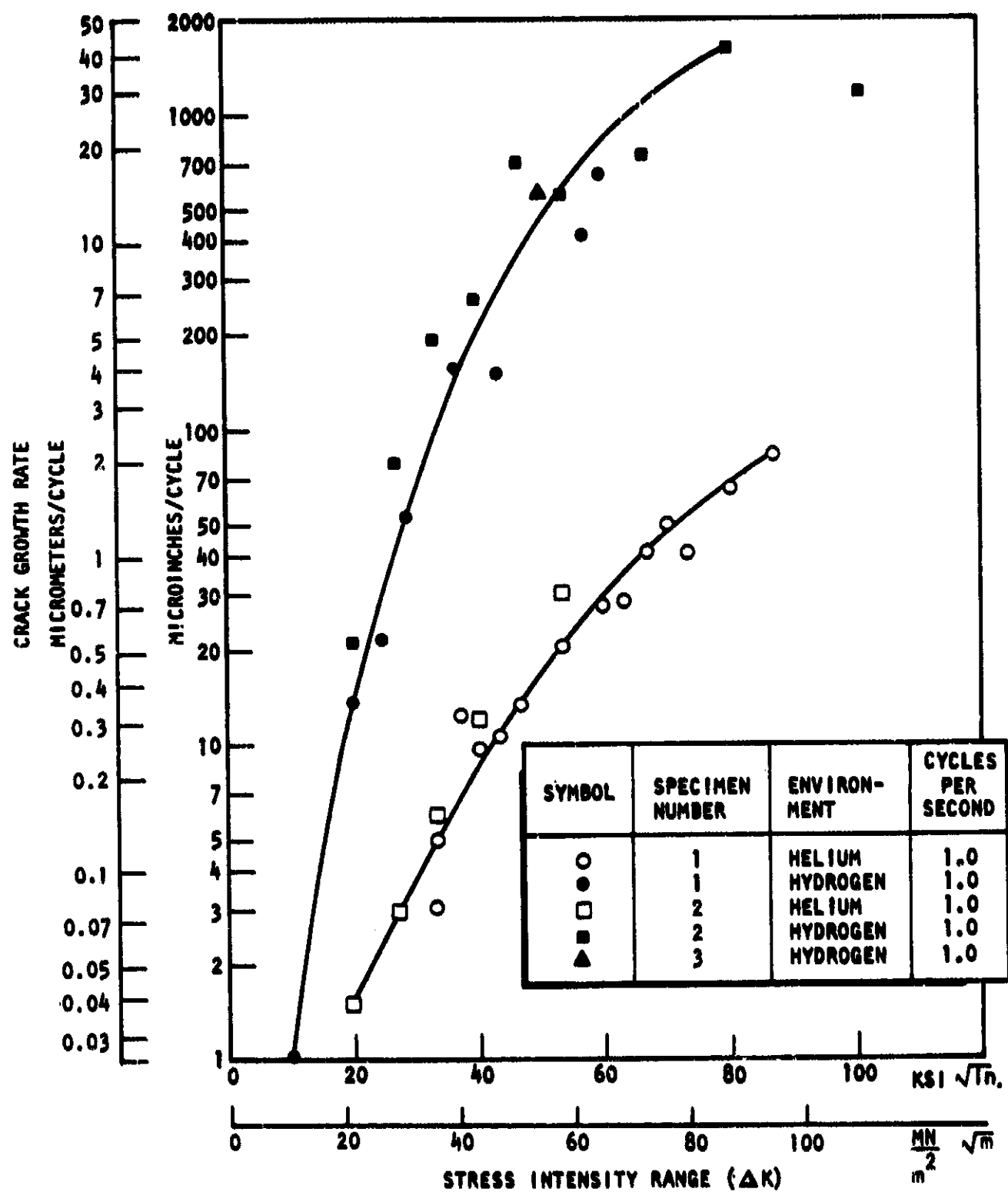


Figure 42. Cyclic Crack Growth Rate as a Function of Stress Intensity Range for HY100 Exposed to 51.7 MN/m² (7500 psi) Helium and 51.7 MN/m² (7500 psi) Hydrogen Ambient Temperature Environments

After completing the cyclic-load crack growth measurements in helium on specimen No. 2, the crack was extended by cycling in hydrogen at a stress intensity less than the lowest stress intensity for crack growth measurements. Thus, all of the hydrogen data on specimen No. 2 were obtained in the usual manner by load cycling at progressively higher stress intensities.

The results of the cyclic-load crack growth measurements indicate that the 51.7 MN/m^2 (7500 psi) hydrogen environment considerably increases the crack growth rate over the entire range of stress intensities at which measurements were made. The cyclic-load crack growth curves shown in Fig. 41 for HY100 are similar to those shown in Fig. 40 for ASTM A-533-B. The cyclic-load crack growth rate is about 20 times faster in hydrogen than it is in helium at the higher stress intensity ranges.

Figure 43 shows the effect of hydrogen pressures ranging from 0.101 MN/m^2 (1 atm) to 103.4 MN/m^2 (15,000 psi) on the cyclic crack growth rate in HY100 when cycled at $54.7 \text{ MN/m}^2 \sqrt{\text{m}}$ (49.7 ksi $\sqrt{\text{in.}}$) stress intensity range. The cyclic crack growth rates increased with increasing hydrogen pressure with no indication of leveling out at the higher hydrogen pressures. Plotting the data on log-log or as square roots did not result in straight-line curves.

The hydrogen environment appeared to increase the cyclic crack growth rate even at the lowest hydrogen pressures tested. The cyclic crack growth rate in 51.7 MN/m^2 (7500 psi) helium was about 0.38 micrometers/cycle (15 microinches/cycle) (Fig. 42) when cycled at $54.7 \text{ MN/m}^2 \sqrt{\text{m}}$ (49.7 ksi $\sqrt{\text{in.}}$) stress intensity range. This is considerably lower than the cyclic crack growth rate obtained in hydrogen at 0.101 MN/m^2 (1-atmosphere pressure).

An attempt was made to determine the sustained-load threshold stress intensity in 51.7 MN/m^2 (7500 psi) hydrogen. On completion of the cyclic load testing in hydrogen, specimen No. 1 was loaded to $140 \text{ MN/m}^2 \sqrt{\text{m}}$ (127 ksi $\sqrt{\text{in.}}$) stress intensity and significant sustained-load crack extension did not occur. The specimen was then unloaded and reloaded to $147 \text{ MN/m}^2 \sqrt{\text{m}}$ (134 ksi $\sqrt{\text{in.}}$) and sustained-load

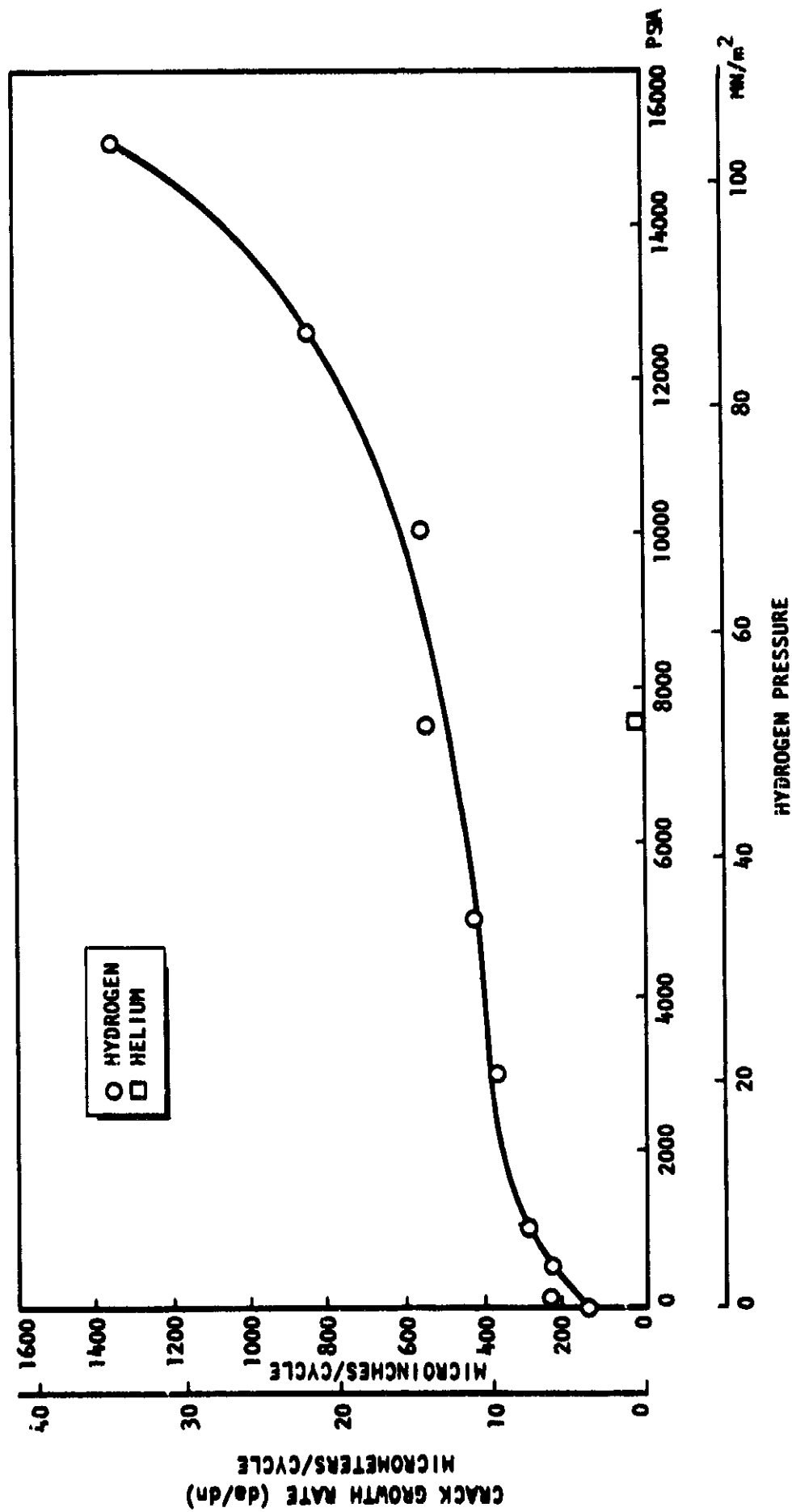


Figure 43. Ambient-Temperature Cyclic Crack Growth Rate as a Function of Hydrogen Pressure for HY100 at Stress Intensity Range of $54.7 \text{ MN/m}^2 \sqrt{\text{in.}}$ ($49.7 \text{ ksi} \sqrt{\text{in.}}$) (Cyclic Rate: 1.0 cycles/sec)

crack growth occurred for about 4680 seconds (80 minutes), at which time it was evident that crack growth had stopped at a stress intensity of $133 \text{ MN/m}^2 \sqrt{\text{m}}$ ($121 \text{ ksi } \sqrt{\text{in.}}$). During this period, the crack extended an average of 0.0076 m (0.3 in.). Examination of the fracture showed that sustained-load crack extension was not uniform across the fracture and was about 0.0160 m ($5/8 \text{ in.}$) along the edges and 0.0032 m ($1/8 \text{ in.}$) in the middle. There was a discontinuity perpendicular to the plane of the fracture in this region and that may have inhibited sustained-load crack growth in the center of the fracture.

A comparative K_{TH} test was not performed on ASTM A-533-B TDCB specimen, but as was reported in Phase VI, sustained-load crack extension in ASTM A-533-B compact tension specimen was almost entirely in the inner region with almost no growth along the specimen sides. The side grooves in the HY100 TDCB specimen would increase the plane strain restraint along the edges and, therefore, may account for the greater crack extension at the edges. However, the apparent discontinuity at the specimen center would seem to offer a more likely explanation for the predominant crack growth along the fracture edges.

PHASE VIII. MECHANISM OF HYDROGEN-ENVIRONMENT EMBRITTLEMENT

Crack arrest measurements (K_{TH}) were performed on Inconel 718 and AISI 4340 low alloy steel specimens exposed to hydrogen at various pressures. Crack arrest measurements were selected for this investigation because at crack arrest, equilibrium exists between the hydrogen in the gas phase, at the crack tip, and the hydrogen adsorbed on the metal surface or absorbed in the affected surface layer. Thus, equilibrium crack extension measurements in hydrogen should be independent of the transport processes involved in the transfer of hydrogen from the gas phase to the embrittling location on or in the metal. The change of stress intensity at crack arrest due to the hydrogen environment is, therefore, a measure of the embrittling condition and is independent of the reactions involved with obtaining this condition.

Mechanisms that have been postulated (Ref. 12) for explaining hydrogen-environment embrittlement of metals are: (1) reduction of strain energy needed to initiate and propagate a crack by the energy evolved during adsorption of hydrogen on the metal surface, (2) reduction of the bond strength of the metal lattice because of the presence of absorbed hydrogen, and (3) reduction of surface ductility because of the presence of adsorbed or absorbed hydrogen.

The relationship between K_{TH} and hydrogen pressure should clarify the role of adsorbed and absorbed hydrogen on hydrogen-environment embrittlement. Beeck et al. (Ref. 29) and Porter and Tompkins (Ref. 30) have shown that a saturated chemisorbed surface hydrogen layer is obtained on nickel and iron surfaces exposed to hydrogen at pressures considerably less than 0.101 MN/m^2 (1 atm). On the other hand, the solubility (Ref. 31) of hydrogen in iron and nickel increases with increasing hydrogen pressure according to Sievert's square root of pressure relationship. Therefore, the stress intensity at crack arrest should be virtually independent of hydrogen pressure for a hydrogen-adsorption-dependent mechanism and would increase as the square root of hydrogen pressure for a hydrogen-absorption-dependent mechanism.

The K_{TH} measurements were performed on AISI 4340 WOL specimens and Inconel 718 WOL and TDCB specimens. The Inconel 718 specimens were in the F heat treatment condition, and were fabricated from the 0.0041 m (1-5/8 in.) forging. The AISI 4340 specimens were tested in the vessel shown in Fig. 8, using either the loading column described in Fig. 9 or electrohydraulic control to maintain a constant COD. The Inconel 718 WOL and TDCB specimens were tested in the vessel shown in Fig. 7 with electrohydraulic control maintaining a constant COD.

AISI 4340

The initial tests on AISI 4340 were performed such that each specimen was exposed to only one hydrogen pressure. The results of these tests are tabulated in Table 17. Examination of the data in Table 17 indicates that for a given set of test conditions, there was a greater difference of K_{TH} between specimens than between repeated tests on the same specimens.

TABLE 17. RESULTS OF CRACK ARREST MEASUREMENTS ON AISI 4340 MOL SPECIMENS
TESTED IN HYDROGEN AT AMBIENT TEMPERATURE AT VARIOUS PRESSURES

Specimen No.	Pressure		K Arrest				Meets ASTM Requirements (2.5) $\left(\frac{K}{\sigma_{ys}}\right)^2$	Nominal Stress Less Than σ_{ys}	Remarks
	MN/m^2	psi	Crack Lengths Measured Visually		Crack Lengths Measured By Compliance				
			$MN/m^2 \sqrt{m}$	$ksi \sqrt{in.}$	$MN/m^2 \sqrt{m}$	$ksi \sqrt{in.}$			
203	0.069	10	--	--	14.3 13.6	13.0 12.4	Yes	Yes	1
206	0.069	10	11.3	10.3	12.9	11.7	Yes	No	2
205	0.69	100	12.6	11.5	12.4	11.3	Yes	No	
204	6.9	1000	11.1	10.1	11.6	10.6	Yes	No	
201	34.5	5000	--	--	--	--	Yes	Yes	3
207	34.5	5000	--	--	--	--	Yes	Yes	3
202	34.5	5000	--	--	7.7 7.5 8.8	7.0 6.8 8.0	Yes	Yes	1
208	34.5	5000	10.1	9.2	10.1	9.2	Yes	No	Yes

Remarks: 1 - Repeated Tests Using Compliance to Indicate Crack Length
2 - Crack Grew Only Along One Side
3 - Crack Extended Too Near Specimen End for Accurate K Measurement

Subsequent testing was then conducted by performing repeated crack arrest measurements on the same specimen at various pressures until the crack length was too long for accurate measurements. These test results are plotted in Fig. 44. It can be seen from these results that the stress intensity at crack arrest decreases slightly with increasing hydrogen pressure. The data indicate the stress intensity at crack arrest is approximately proportional to hydrogen pressure to the 0.076 power.

Crack arrest was assumed to occur when the load versus time strip chart recording became horizontal (no further decrease of load with time). The rate of crack growth approaching crack arrest for one of the specimens is plotted in Fig. 45. To conserve the specimens, they were loaded to stress intensities only slightly above K_{TH} , thus relatively few data points were obtained at each pressure. It is evident, however, that the crack growth rates decrease much more rapidly with decreasing stress intensity at the higher hydrogen pressures than at the lower hydrogen pressures. Extrapolation of the crack growth rate data indicates that the curves would meet at a crack growth rate of approximately 4.2 nm/s (10 μ in./min) and a stress intensity of approximately $9.9 \text{ MN/m}^2 \sqrt{\text{m}}$ (9 ksi $\sqrt{\text{in.}}$).

The purging treatment for the series of tests shown in Fig. 44 consisted of a series of evacuations to <20 microns and backfillings to the lowest test pressure. Prior to performing each subsequent test at pressures greater than 0.34 MN/m^2 (50 psia), the vessel was pressurized-depressurized between the next test pressure and about 0.34 MN/m^2 (50 psia). It could be postulated that because the purging treatments at the higher pressures were more effective, the impurities (air) present in the hydrogen were less concentrated at the higher hydrogen pressures and this, in turn, resulted in a lower K_{TH} at the higher hydrogen pressures. To test this, crack arrest measurements were performed on specimen No. 14 at 0.34 MN/m^2 (50 psi) and 0.034 MN/m^2 (5 psi) hydrogen pressures following the series of increasing pressure tests to 34.5 MN/m^2 (5000 psi). The results are contained in Fig. 44 and 45. There was no difference in the stress intensity at crack arrest between the increasing and decreasing pressure tests, but the crack growth rates just preceding crack arrest were somewhat slower for the decreasing pressure tests than for the increasing pressure tests.

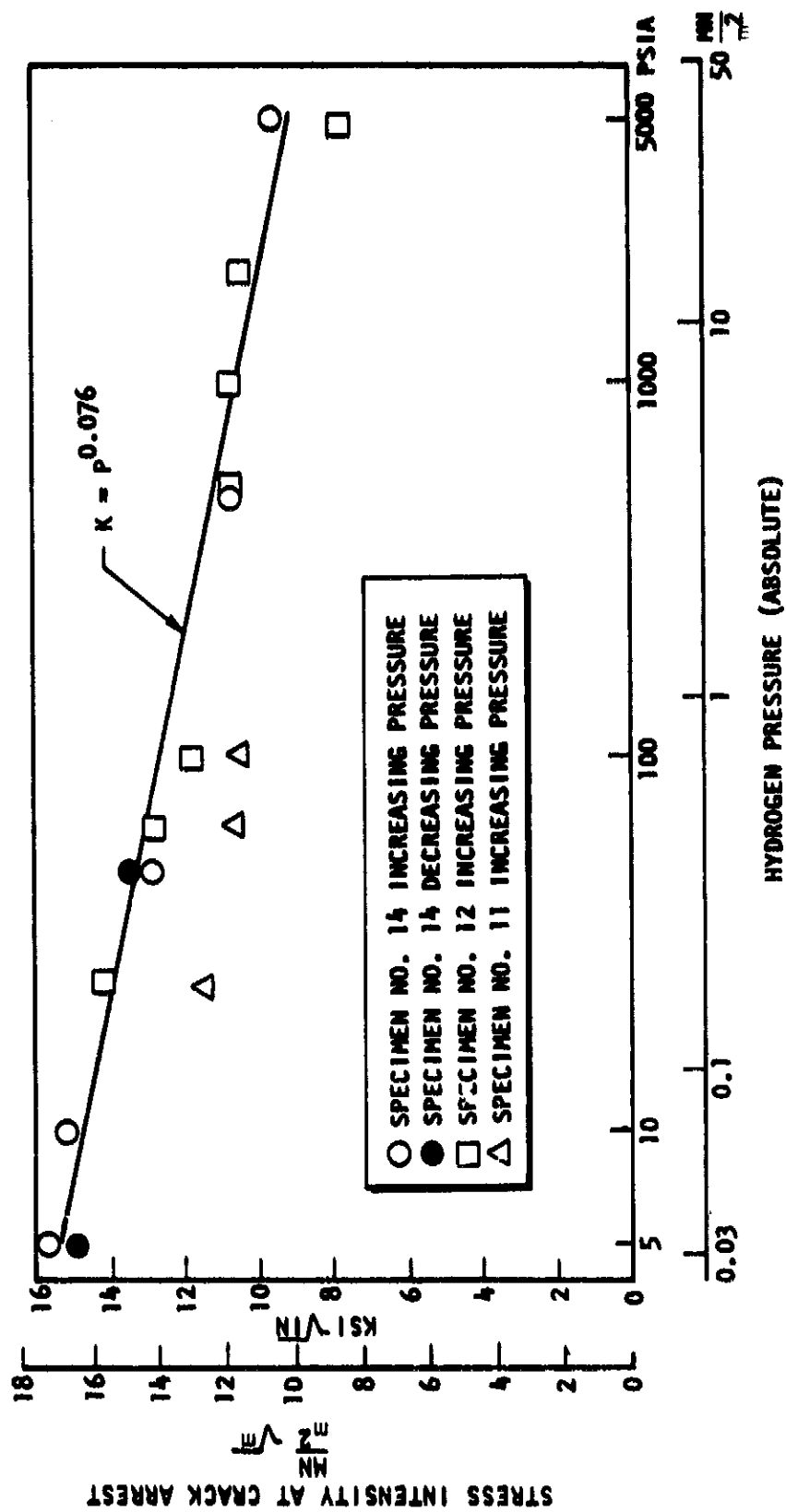
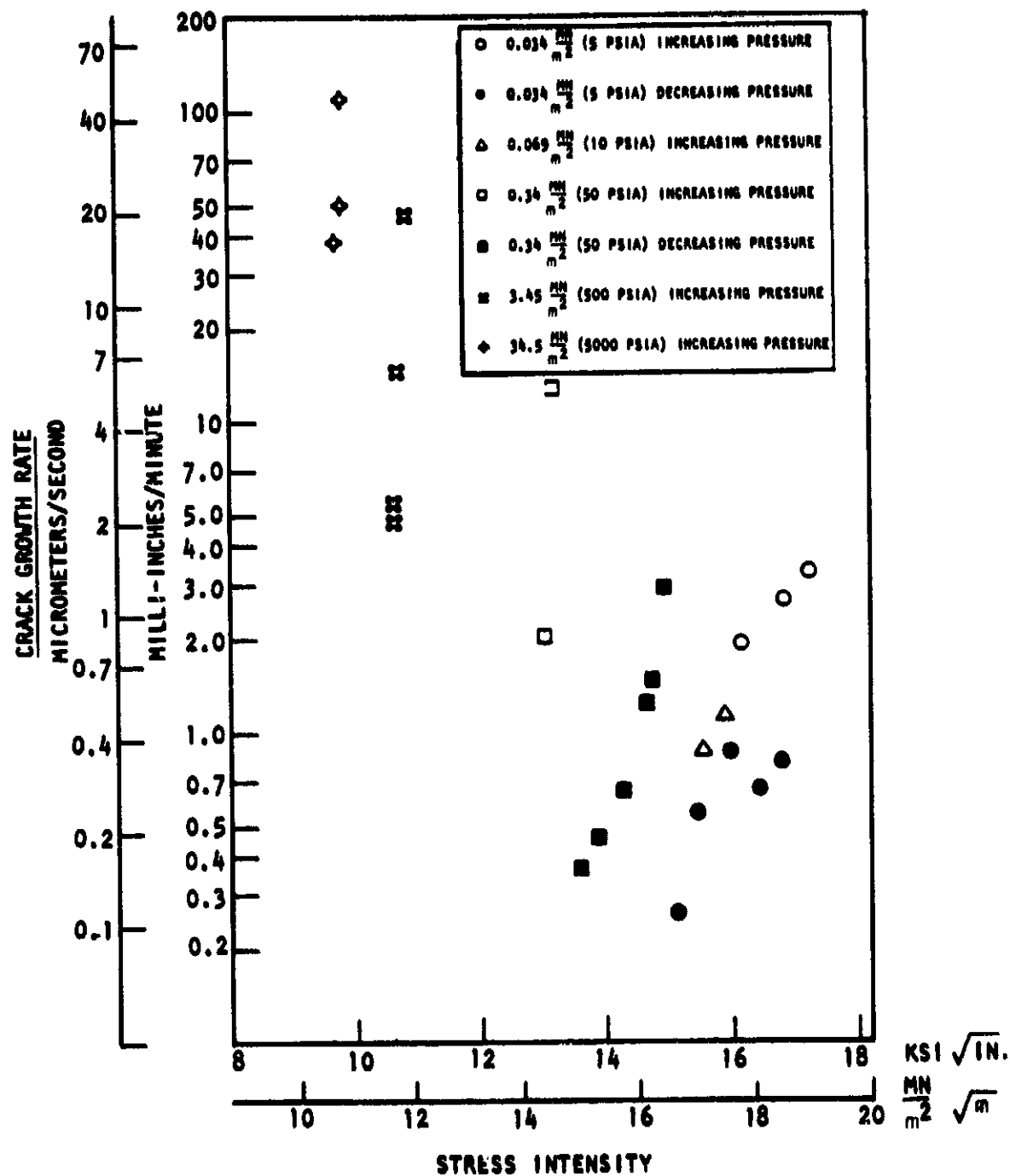


Figure 44. Stress Intensity at Crack Arrest for AISI 4340 WOL Specimens at Ambient Temperature as a Function of Hydrogen Pressure



Nelson and Williams (Ref. 32) have performed an extensive series of sustained-load crack extension measurements on AISI 4130 steel in low-pressure hydrogen environments at various temperatures. Their tests were performed on TDCB specimens, heat treated to Rc 47, which is the same hardness as the AISI 4340 WOL specimens in this program. They performed ambient-temperature (297 K, 75 F) measurements at 0.0025, 0.0112, 0.03333, and 0.0773 MN/m² (0.36, 1.62, 4.8, and 11.2 psia) hydrogen pressures at crack growth rates from 10⁻⁴ to 10⁻⁸ m/s (236 to 0.023 x 10⁻³ in./min). Thus, the test conditions for the tests performed by Nelson and Williams were similar to those in this program. The stress intensity at the lowest crack growth rate measured by Nelson and Williams was about 19 MN/m² √m (17 ksi √in.) at 0.0773 MN/m² (11.2 psia) hydrogen pressure and about 21 MN/m² √m (19 ksi √in.) at 0.0333 MN/m² (4.8 psia) hydrogen pressure. Thus, the K_{TH} stress intensities were about 5 MN/m² √m (4.5 ksi √in.) higher for the AISI 4130 steel than for the AISI 4340 steel. The stress intensity at a crack growth rate of 1 x 10⁻⁶ m/sec (2.36 x 10⁻³ in./min) was proportional to $P_{H_2}^{0.2}$.

The quantitative agreement between the data obtained on AISI 4130 in low-pressure hydrogen and on AISI 4340 in high-pressure hydrogen is poor. The pressure exponents in the K_{TH} equations of 0.076 for AISI 4340 and 0.2 for AISI 4130 steel are not particularly close, and the K_{TH} values obtained were significantly higher for AISI 4130 than for AISI 4340. In general, further investigations are needed to determine the influence of hydrogen pressure on crack arrest for low-alloy steels in hydrogen.

Inconel 718

Crack arrest measurements were performed on Inconel 718 WOL and TDCB specimens in the F heat treatment condition, and the test results are tabulated in Table 18. K_{TH} is plotted versus P_{H_2} in Fig. 46 and versus square root of P_{H_2} in Fig. 47. There was very good correlation of test results between the WOL and TDCB specimens.

The results indicate that at lower hydrogen pressures, below approximately 20.7 MN/m² (3000 psi), K_{TH} is a function of pressure, but at higher pressures it is independent of pressure. At the lower pressures, K_{TH} is approximately proportional

TABLE 18. RESULTS OF CRACK ARREST MEASUREMENTS ON INCONEL 718 WOL AND TDCB
SPECIMENS TESTED IN HYDROGEN AT ROOM TEMPERATURE AT VARIOUS PRESSURES

Specimen		Hydrogen Pressure		K Arrest		Meets ASTM Requirements		Nominal Stress Less Than OYS	Remarks
		MN/m ²	psi	MN/m ² √m	ksi√in.	2.5 (K/σ _{YS}) ²	Crack Uniformity		
No.	Type								
8	TDCB	3.45	500	89	81	--	--	Yes	
8	TDCB	6.89	1,000	70	64	--	--	Yes	
T-13	MOL	6.89	1,000	68	62	Yes	Marginal	Yes	
9	TDCB	17.2	2,500	46	42	--	--	Yes	
9	TDCB	34.5	5,000	38	35	--	--	--	
T-5	MOL	34.5	5,000	43	39	Yes	Yes	Yes	
T-4	MOL	34.5	5,000	41	37	Yes	Yes	Yes	
B-10	MOL	34.5	5,000	41	37	Yes	Yes	Yes	
T-14	MOL	68.9	10,000	49	45	Yes	Yes	Yes	Crack arrest not obtained
9	TDCB	68.9	10,500	42	38	--	--	--	

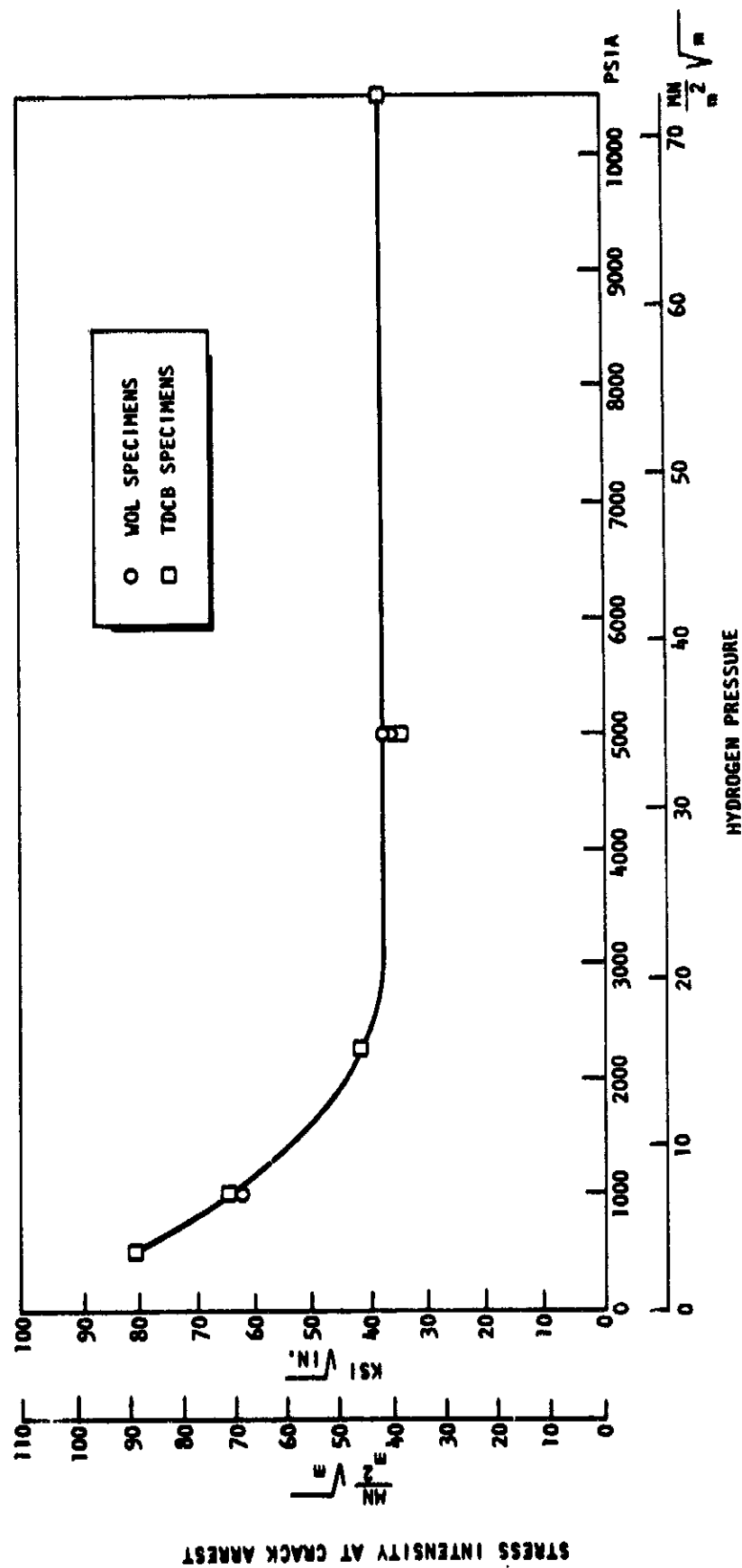


Figure 46. Stress Intensity at Crack Arrest for Inconel 718 at Ambient Temperature as a Function of Hydrogen Pressure

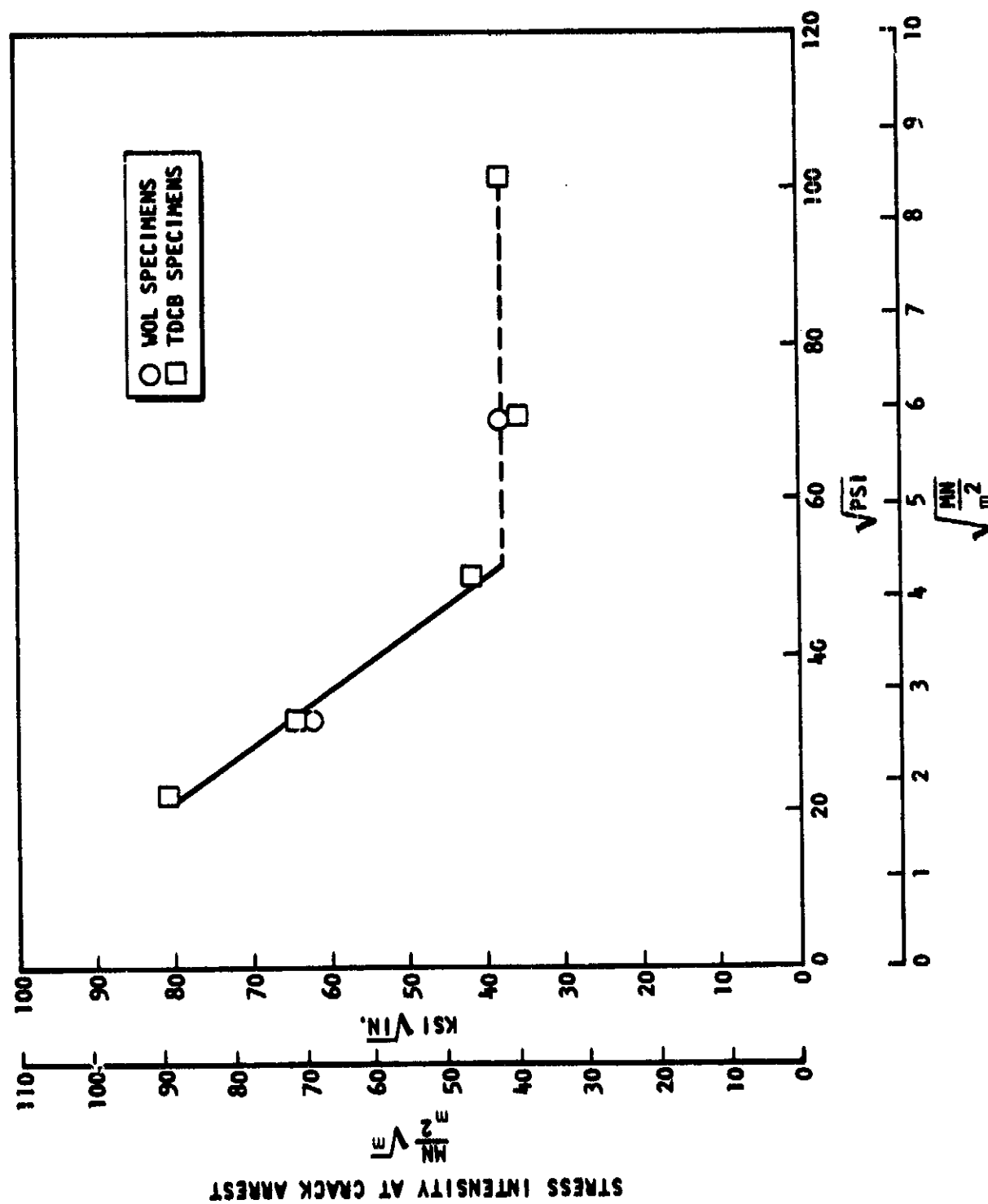


Figure 47. Stress Intensity at Crack Arrest for Inconel 718 at Ambient Temperature as a Function of Square Root of Hydrogen Pressure

to $P_{H_2}^{0.43}$. The exponent is sufficiently close to 0.5 to suggest that K_{TH} may be proportional to the square root of pressure and a plot of K_{TH} versus $\sqrt{P_{H_2}}$ (Fig. 47) shows a reasonable straight-line relationship.

The sustained-load crack growth rates preceeding crack arrest are plotted in Fig. 48. Crack propagation preceeding crack arrest is about 2 orders of magnitude slower in Inconel 718 than in AISI 4340. The tests were terminated when there was no measureable load decline during a 1- to 2-day period. The rate of crack extension did not appear to be uniform with time, and the lack of apparent crack growth over a 1- to 2-day period did not necessarily mean that a crack arrest had occurred. In fact, it is not likely that true crack arrest was obtained at the lower pressures, although crack arrest may have been closely approached.

It is evident that the rate of crack growth decreases less rapidly with decreasing stress intensity at the lower hydrogen pressures than at the higher hydrogen pressures. The data for the lower pressures extrapolates to $42 \text{ MN/m}^2 \sqrt{\text{m}}$ ($38 \text{ ksi } \sqrt{\text{in.}}$) stress intensity at a crack growth rate of about $7 \times 10^{-11} \text{ m/s}$ ($1 \times 10^{-6} \text{ in./hour}$).

There are two suggested interpretations of the results on Inconel 718. One is that crack arrest was not obtained at hydrogen pressures less than 21 MN/m^2 (3000 psi) and that the $\sqrt{P_{H_2}}$ relationship in this region is fortuitous. On this assumption, true crack arrest was obtained only at hydrogen pressures above 21 MN/m^2 (3000 psi), and K_{TH} is independent of hydrogen pressure as predicted if the embrittlement is purely a surface effect and thus depends only on adsorption.

A second interpretation is that crack arrest was achieved at the lower pressures, and the stress intensity at crack arrest is proportional to the square root of hydrogen pressure at these pressures because it is a function of the amount of hydrogen in solution in the surface layers, and this is equal to the solubility under equilibrium conditions. The lack of a hydrogen pressure effect above 21 MN/m^2 (3000 psi) would have to be explained on the basis that increasing the hydrogen in solution above a certain limit (the equilibrium solubility of hydrogen in Inconel 718 in contact with 21 MN/m^2 (3000 psi) hydrogen at ambient temperature) does not further decrease K_{TH} (increase embrittlement).

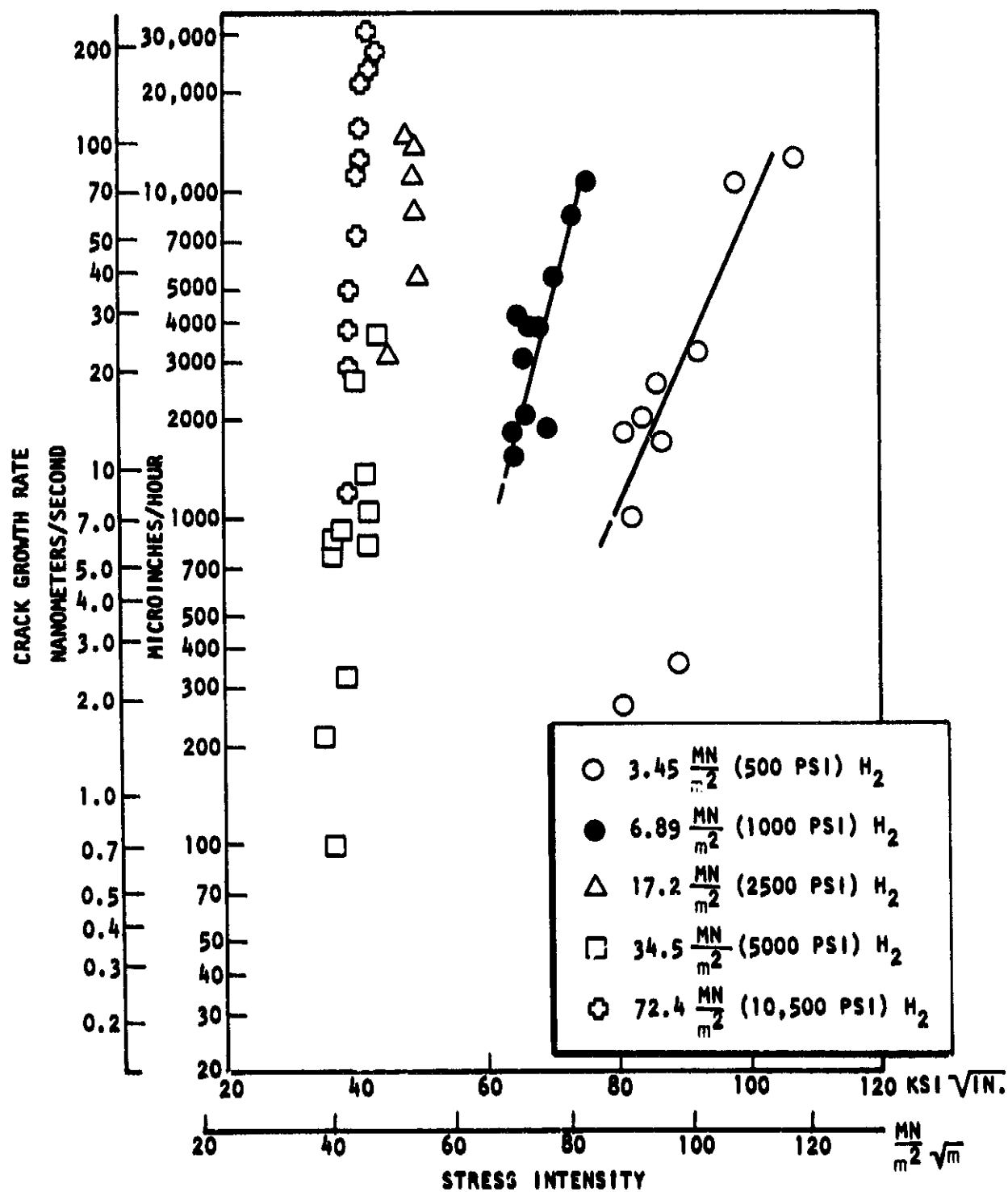


Figure 48. Sustained Load Crack Growth Rate in Inconel 718 TDCB Specimens as a Function of Stress Intensity at Various Hydrogen Pressures

The determination of the relationship between the stress intensity at crack arrest and pressure for Inconel 718 in the F heat treatment condition would require additional, longer-time testing at the lower pressures. The determination of this relationship for nickel-base materials could be more easily achieved by testing a material in which crack growth rates are more rapid, and crack arrest would be more rapidly obtained. Examples of such materials would be electroformed nickel or Inconel 718 in the A heat treatment condition.

DISCUSSION AND SUMMARY

To correlate the results of the eight different phases, the results will be summarized, for the most part, by material.

INCONEL 718

The degree of hydrogen-environment embrittlement of Inconel 718, as measured by reduction of notch tensile strength at ambient temperature in 34.5 MN/m^2 (5000 psi) hydrogen, was found to be a function of both forming operation and heat treatment.

The least hydrogen embrittlement, i.e., the highest N_{H_2}/N_{He} ratio occurred with the plate in the A and B (Table 5) heat treatment conditions. The corresponding microstructure was one which was fine grained, with Ni_3Cb being very dispersed. On the other hand, the greatest embrittlement resulted from the A heat treatment on the rolled bar and forging. The corresponding most embrittled microstructure was one which was coarse grained and contained an almost continuous network of Ni_3Cb . For all three forms (rolled bar, forging, and plate), the C heat treatment gave the most consistent results and the highest notch strength in helium and hydrogen. The C heat treatment consisted of a 1325 K (1925 F) anneal and 1033 to 922 K (1400 to 1200 F) age. The high-temperature anneal placed the Ni_3Cb into solution, but also increased the grain size. Removal of the Ni_3Cb phase decreased embrittlement of the relatively large-grained rolled bar and forging materials, but the increase of grain size increased embrittlement of the fine-grained plate although the Ni_3Cb phase was eliminated.

Heat treatment E, designed to place the Ni_3Cb into solution but avoid grain growth, resulted in the same degree of embrittlement as the C heat treatment. Grain growth was minimized by the E heat treatment, but complete solution of Ni_3Cb occurred only in the rolled bar and not in the forging and plate. The results indicated that a very fine grain size, ASTM 10, is needed to significantly improve the resistance to hydrogen-environment embrittlement of Inconel 718.

With respect to hydrogen-environment embrittlement of the welded Inconel 718 specimens, the weld metal with C heat treatment was the most severely embrittled condition. As with the parent metal, the notch strength in helium of both the weld metal and heat-affected zone was higher with the C heat treatment than with the other two heat treatments. However, the degree of hydrogen-environment embrittlement of the weld metal was large enough so that the C heat treatment that the notch strength in hydrogen was somewhat lower with that heat treatment than with the A heat treatment. Therefore, the fine dendritic weld structure of the A condition was less embrittled by the hydrogen environments than the equiaxed recrystallized structure of the C heat treatment.

For the parent metal and weld metal, the B overaging heat treatment did not significantly change embrittlement from that for the A heat treatment. This lack of sensitivity of embrittlement to overaging indicates that the degree of hydrogen-environment embrittlement is not strongly influenced by the age-hardening precipitate size, morphology, or coherency.

There are three distinct fracture stages during the testing in hydrogen of non-precracked specimens of embrittled materials: crack initiation, subcritical crack growth, and ductile fast rupture. Crack initiation occurs at the surface after a critical amount of the plastic deformation. The strain at crack initiation was measured in a company-sponsored program on unnotched Inconel 718 specimens exposed to 48.2 MN/m^2 (7000 psi) hydrogen. The strain-to-crack initiation was the same (about 3 percent) for the specimens in the A and C heat treatment conditions, indicating that the degree of embrittlement was a function of subcritical crack growth rate rather than the strain at crack initiation.

The influence of hydrogen on the sustained-load, subcritical crack growth (K_{TH}) of Inconel 718 was determined. The results showed a considerably lower critical stress intensity for hydrogen-environment induced crack growth for specimens in the A condition than in the C condition. The rolled bar in the A condition tested in 34.5 MN/m^2 (5000 psi) hydrogen had the lowest K_{TH} value, $14 \text{ MN/m}^2 \sqrt{\text{m}}$ (13 ksi $\sqrt{\text{in.}}$), of all the materials that were tested. Hydrogen-induced crack growth was intergranular in the C condition and predominantly transgranular in the

A condition. The flat transgranular cleavage of the A condition contained a higher-than-average columbium concentration, indicating the presence of Ni_3Cb . Thus, hydrogen-induced crack extension evidently occurred more readily through the Ni_3Cb phase, when present, than intergranularly. If this is true, the subcritical crack growth rate in the A heat treatment condition would be determined by the continuity of the Ni_3Cb phase. Thus, the fine-grained plate with dispersed Ni_3Cb was less embrittled than the coarse-grained bar and forging with relatively continuous Ni_3Cb .

K_{TH} for subcritical sustained-load crack growth in Inconel 718 in the F heat treatment condition was found to be approximately proportional to the square root of hydrogen pressure at pressures less than 21 MN/m^2 (3000 psi) and independent of hydrogen pressure at pressures greater than 21 MN/m^2 (3000 psi). K_{TH} was apparently independent of temperature between ambient temperature and 200 K (-100 F). K_{TH} at 144 K (-200 F) was apparently not reduced by the 34.5 MN/m^2 (5000 psi) hydrogen environment when in the C heat treatment condition. There was, however, a small decrease of K_{TH} for Inconel 718 in the A heat treatment condition when exposed to 34.5 MN/m^2 (5000 psi) hydrogen at 144 K (-200 F).

The cyclic crack growth rate in Inconel 718 also increased with increasing hydrogen pressure. The crack growth rate for ΔK around K_{IC} ($\sim 110 \text{ MN/m}^2 \sqrt{\text{m}}$ (100 ksi $\sqrt{\text{in.}}$)) was about the same in hydrogen as in helium. Decreasing the cyclic frequency from 1.0 cycle/sec to 0.1 cycle/sec considerably increased the cyclic crack growth rate at 0.69 MN/m^2 (10 psi) and at 68.9 MN/m^2 (10,000 psi) hydrogen pressures. A series of measurements performed between 1.0 cycle/sec and 0.1 cycle/sec showed that the crack growth rate increased as a complex function of the time per cycle.

The suggestion (Ref. 25 through 27) that cyclic crack growth in an aggressive environment is equal to the sum of the sustained-load crack growth in the aggressive environment and the inert environment cyclic crack growth does not appear to hold

true for Inconel 718 in hydrogen. The cyclic crack growth rate for Inconel 718 in hydrogen was slower than the sum of cyclic crack growth rate in helium and sustained-load crack growth rate in hydrogen at high ΔK levels. The opposite occurred at the low ΔK levels where the hydrogen environments increased the cyclic crack growth rates at stress intensities below K_{TH} .

It has been observed frequently that there is a delay before sustained load crack extension occurs when loaded immediately after cyclic loading in hydrogen. Thus, the lack of significant increase of cyclic crack growth rate as the cycling rate decreased from 1.0 to 0.25 cycles/sec may be the result of this delay. It was shown that fracture of the Inconel 718 specimens was intergranular when tested under sustained load in hydrogen. It is likely that cyclic crack growth in hydrogen is transgranular and the delay between cyclic and sustained-load crack growth may be the transfer from transgranular to intergranular crack growth.

Cyclic crack growth measurements also were performed on Inconel 718 at 200 K (-100 F) in 34.5 MN/m^2 (5000 psi) hydrogen, and the rates were about the same as obtained in 34.5 MN/m^2 (5000 psi) helium at ambient temperature.

ASTM A-533-B

ASTM A-533-B is embrittled by hydrogen as shown by the formation of surface cracks, reduction of notched tensile strength, sustained-load crack growth, and increased rate of cyclic crack growth when tested in high-pressure hydrogen environments.

The reduction of tensile properties in 103.4 MN/m^2 (15,000 psi) hydrogen was similar to the reduction of tensile properties obtained previously (Ref. 27) in 68.9 MN/m^2 (10,000 psi) hydrogen on a different heat of material. In the earlier program, it was shown that ASTM A-533-B was severely embrittled by high-pressure hydrogen environments.

Fracture mechanics tests were performed on 0.0254 m (1.0 inch) thick specimens. This thickness was found insufficient to meet ASTM plane strain fracture toughness requirements for the K_{IC} and K_{TH} values obtained. The K_Q values obtained during

the fracture toughness tests in 103 MN/m^2 (15,000 psi) hydrogen were significantly less than the values obtained in helium, and it appears that sustained-load crack growth did initiate in hydrogen at about $80 \text{ MN/m}^2 \sqrt{\text{m}}$ (73 ksi $\sqrt{\text{in.}}$) stress intensity.

The sustained-load crack growth during the K_{TH} measurements in hydrogen was limited to the inner region of the specimens, but was appreciable in that region despite the restraint of the edges at which the cracks did not propagate. Thus, it would appear that sustained-load crack growth occurs in ASTM A-533-B in hydrogen only under plane strain conditions.

Cyclic crack growth rates were considerably accelerated by 103.4 MN/m^2 (15,000 psi) hydrogen over the entire stress intensity range for which testing was performed.

The tensile and fracture toughness measurements on ASTM A-533-B indicate that the degree of embrittlement is determined largely by crack blunting. Under plane strain conditions, crack blunting is prevented, and sustained-load crack growth extended until it was held up by the lack of crack extension at the edges. Cyclic loading continually resharpened the crack, and the resulting cyclic crack growth rate was 20 times faster in hydrogen than in helium. Therefore, both cyclic and sustained-load crack growth must be considered carefully in the design of thick-wall hydrogen pressure vessels constructed of ASTM A-533-B steel. The minimum stress intensity for hydrogen-accelerated cyclic crack growth is below $11 \text{ MN/m}^2 \sqrt{\text{m}}$ (10 ksi $\sqrt{\text{in.}}$). The minimum stress intensity for hydrogen-induced, sustained load crack growth was unfortunately not measured because of the lack of crack extension along the edges of the specimens.

HY100

The cyclic-load crack growth measurements on HY100 showed that high-pressure hydrogen appreciably increased the cyclic crack growth rate. The increase in rate in hydrogen occurred over the entire stress intensity range of the measurements in 51.7 MN/m^2 (7500 psi) hydrogen, and the crack growth rates were very similar to those obtained in 103.4 MN/m^2 (15,000-psi hydrogen) on ASTM A-533-B.

The influence of hydrogen on the cyclic crack growth rate increased with increasing hydrogen pressure, but was significant even at 1-atmosphere pressure.

The influence of hydrogen on HY100 has been investigated to a considerably smaller extent than it has for ASTM A-533-B. Both are pressure vessel steels and have similar mechanical properties. The data obtained in this program indicate that hydrogen-induced subcritical crack growth in HY100 would be similar to that in ASTM A-533-B. Thus, the plane strain conditions present in thick-wall pressure vessels would likely prevent crack blunting during hydrogen-induced sustained load crack growth. Therefore, both cyclic and sustained load crack growth must be carefully considered in the design of thick-wall hydrogen pressure vessels constructed of HY100 steel.

INCONEL 625

The ductility of unnotched Inconel 625 specimens was considerably reduced, and the strength and ductility of notched specimens was moderately reduced in 34.5 MN/m^2 (5000 psi) hydrogen compared to 34.5 MN/m^2 (5000 psi) helium at room temperature. Even the ultimate strength of unnotched specimens was somewhat reduced in hydrogen at room temperature. The unnotched specimens tested in hydrogen contained surface cracks in the necked-down region which were rather large and deep. The effect of 34.5 MN/m^2 (5000 psi) hydrogen on the tensile properties of Inconel 625 at 144 K (-200 F) was insignificant, and no surface cracking was observed at that temperature.

The threshold stress intensity (K_{TH}) measurements in high-pressure hydrogen were affected by branching or blunting at the crack tip. At ambient temperature, hydrogen-induced, sustained-load crack growth was followed by blunting with each load increment. At 144 K (-200 F), crack arrest occurred in hydrogen and helium at stress intensities which appeared to be a function of the maximum load only rather than an intrinsic value. Thus, crack blunting also appeared to have a dominant effect on crack extension during the 144 K (-200 F) tests. There was no sustained-load crack extension in helium at ambient temperature. Crack extension in helium at 144 K (-200 F) was about the same as in hydrogen.

Crack branching was probably an important factor determining the tensile as well as fracture toughness properties of Inconel 625 in hydrogen. The fact that there were several fairly large surface cracks formed on the unnotched specimens is an indication of crack branching. Crack branching in tensile specimens can cause the crack to change direction toward the tensile axis, reduce the stress at the crack tip, cause the crack to cease propagating, and give other surface cracks an opportunity to form.

AISI 321 STAINLESS STEEL

The ductility of AISI 321 stainless steel was reduced in 34.5 MN/m^2 (5000 psi) hydrogen at ambient temperature and 144 K (-200 F). The reduction of ductility correlated with the nature of the surface cracks formed. At ambient temperature, the cracks were shallow and blunt. At 144 K (-200 F), the cracks were considerably sharper and deeper than at ambient temperature, and there was a corresponding greater embrittlement at 144 K (-200 F) than at ambient temperature. Hydrogen-induced surface cracking in the metastable austenitic stainless steels has been attributed (Ref. 4 and 5) to reaction of hydrogen with strain-induced martensite.

The results of the K_{TH} experiments were similar to those for Inconel 625. When specimens were loaded in 34.5 MN/m^2 (5000 psi) hydrogen at ambient temperature and 144 K (-200 F), crack growth followed by blunting and arrest occurred at each load increment, and the crack arrest stress intensity was higher after each load increment.

A-286 STAINLESS STEEL

Tensile tests were conducted on A-286 stainless steel in 68.9 MN/m^2 (10,000 psi) hydrogen, at ambient temperature in a previous program (Ref. 4), and the data showed a slight (~2-1/2 percent) reduction of notched strength and no reduction of notched or unnotched specimen ductility.

The results of K_{TH} measurements on A-286 WOL specimens therefore were somewhat surprising because of hydrogen-enhanced, sustained-load crack growth at ambient

temperature. The crack growth rate was quite slow in comparison with the other metals tested, and there was no indication of crack blunting. K_{TH} in hydrogen was not established but it was below $113 \text{ MN/m}^2\sqrt{\text{m}}$ ($103 \text{ ksi}\sqrt{\text{in.}}$). A-286 stainless steel had the highest fracture toughness of any material tested, and all of the crack extension occurred above the materials yield strength. Since crack arrest was not obtained, it was not ascertained whether (1) gross yielding is necessary for hydrogen-environment-induced crack growth in this material, and (2) hydrogen-induced crack extension will occur in plane strain as well as mixed mode fracture.

There was almost no measureable crack extension in the specimens tested in hydrogen and helium environments at 144 K (-200 F) although the specimens were loaded to a stress intensity of approximately $198 \text{ MN/m}^2\sqrt{\text{m}}$ ($180 \text{ ksi}\sqrt{\text{in.}}$).

Ti-5 Al-2.5 Sn ELI

Tensile tests conducted in a previous program (Ref. 4), on Ti-5 Al-2.5 Sn ELI showed that 68.9 MN/m^2 (10,000 psi) hydrogen reduced the notched tensile strength 20 percent at ambient temperature. Tensile tests conducted in the current program at 144 K (-200 F) in 34.5 MN/m^2 (5000 psi) hydrogen showed that there was no reduction of tensile properties and no surface cracks were observed.

Sustained load crack growth without crack branching or blunting occurred in Ti-5 Al-2.5 Sn ELI WOL specimens tested in 34.5 MN/m^2 (5000 psi) helium and hydrogen environments at ambient and 144 K (-200 F). The ambient-temperature, K_{TH} values were $69 \text{ MN/m}^2\sqrt{\text{m}}$ ($63 \text{ ksi}\sqrt{\text{in.}}$) in helium, and $34 \text{ MN/m}^2\sqrt{\text{m}}$ ($31 \text{ ksi}\sqrt{\text{in.}}$) in hydrogen. The average stress intensity at 144 K (-200 F) was $60 \text{ MN/m}^2\sqrt{\text{m}}$ ($55 \text{ ksi}\sqrt{\text{in.}}$) in helium, and 58 MN/m^2 ($53 \text{ ksi}\sqrt{\text{in.}}$) in hydrogen. There was, therefore, a considerable hydrogen environmental reduction of K_{TH} at ambient temperature but there does not appear to be a hydrogen environmental influence on K_{TH} at 144 K (-200 F).

2219-T87 ALUMINUM ALLOY

The tensile properties of 2219-T87 aluminum alloy have not been measured in high-pressure hydrogen. In a previous program (Ref. 4), it was shown that 1100-0 aluminum, and 7075 T-73 and 6061 T-6 aluminum alloys were negligibly embrittled when tensile tested in 68.9 MN/m^2 (10,000 psi) hydrogen at ambient temperature. Thus, very little, if any, reduction of tensile properties of 2219-T87 aluminum would be expected from exposure to high-pressure hydrogen.

Quantitative fracture mechanics data were obtained on 2219-T87 aluminum alloy at ambient and at 144 K (-100 F). The stress intensity values at crack arrest were about the same in both helium and hydrogen environments and, on an average, equal to K_{IC} in helium regardless of environment. That is, the average K_{TH} was about $33 \text{ MN/m}^2 \sqrt{\text{m}}$ (30 ksi $\sqrt{\text{in.}}$) at ambient temperature, and about $41 \text{ MN/m}^2 \sqrt{\text{m}}$ (37 ksi $\sqrt{\text{in.}}$) at 144 K (-200 F) in both 34.5 MN/m^2 (5000 psi) hydrogen and 34.5 MN/m^2 (5000 psi) helium.

OFHC COPPER

The tensile and fracture toughness properties of OFHC copper were unaffected by 34.5 MN/m^2 (5000 psi) hydrogen at ambient and 144 K (-200 F). Arm bending rather than crack growth occurred during the ambient-temperature fracture toughness tests. There was, however, a small amount of crack growth accompanying considerable plastic deformation during the 144 K (-200 F) fracture mechanics measurements. No K_{TH} values were obtained on OFHC copper.

ACOUSTIC EMISSION MONITORING OF CRACK GROWTH

Crack growth rates in some of the K_{TH} tests were monitored using acoustic emission circuitry designed and developed at Rocketdyne. The gross correlation obtained between crack growth rates monitored by acoustic emission and by reduction in applied load was satisfactory despite instrumentation problems. Discontinuous crack growth was indicated acoustically in Ti-5 Al-2.5 Sn ELI, A-286 stainless steel, and 2219-T87 aluminum. The results obtained for A-286 alloy were especially detailed and interesting.

MECHANISM OF HYDROGEN-ENVIRONMENT EMBRITTLEMENT

A series of crack arrest (K_{TH}) measurements were performed on AISI 4340 and Inconel 718 to clarify the mechanism of hydrogen-environment embrittlement. Crack arrest measurements have the advantage of being independent of rate processes and thus are indicative of the actual embrittlement process. The results of the measurements on AISI 4340 indicated that the stress intensities at crack arrest were proportional to $(P_{H_2})^{0.076}$ for hydrogen pressures between 0.034 MN/m^2 (5 psia) and 34.5 MN/m^2 (5000 psi). The Inconel 718 results showed that K_{TH} was approximately proportional to the square root of hydrogen pressure for pressures between 3.4 MN/m^2 (500 psi) and 21 MN/m^2 (3000 psi), and was independent of hydrogen pressure for pressures from 21 MN/m^2 (3000 psi) to 72.4 MN/m^2 (10,500 psi). The crack growth rate of both metals decreased less rapidly with decreasing stress intensity at the lower hydrogen pressures than at the higher hydrogen pressures. It appeared from extrapolation of the crack growth rate data that the stress intensity at crack arrest may be independent of hydrogen pressure for both alloys.

If hydrogen-environment embrittlement were determined by the reduction of strain energy resulting from hydrogen adsorption at the crack tip, K_{TH} would be predicted to be independent of hydrogen pressure. This is because the concentration of chemisorbed hydrogen is essentially independent of hydrogen pressure for both metals over the pressure range of these measurements. On the other hand, if embrittlement were due to hydrogen absorbed into the metal, K_{TH} would be predicted to be a function of hydrogen solubility, which is a function of the square root of hydrogen pressure. The small effect of hydrogen pressure on K_{TH} of both alloys indicates that hydrogen-environment embrittlement results from a hydrogen adsorption dependency mechanism.

REFERENCES

1. Walter, R. J., and W. T. Chandler: Effect of High-Pressure Hydrogen on Metals, paper presented at 1968 Materials Engineering Congress, Detroit, Michigan, October 1968. ASM Report No. D8-14.2, ASM Report System, Metals Park, Ohio.
2. Walter, R. J., and W. T. Chandler: Effect of High-Pressure Hydrogen on Storage Vessel Materials, paper presented at WESTEC Conference, Los Angeles, California, March 1968. ASM Report No. W8-2.4, ASM Report System, Metals Park, Ohio.
3. Steinman, J. B., H. C. Van Ness, and G. S. Ansell: "The Effect of High-Pressure Hydrogen Upon the Notch Tensile Strength and Fracture Mode of 4140 Steel," Welding Journal, May 1965, pp. 221s-224s.
4. Walter, R. J., and W. T. Chandler: Effects of High-Pressure Hydrogen on Metals at Ambient Temperatures, Final Report on Task 7 of NASA Contract NAS8-19, Rocketdyne, a Division of Rockwell International, Canoga Park, California, Report No. R-7780-1, -2, -3, February 1969.
5. Benson, R. B., Jr., R. K. Dann, and L. W. Roberts, Jr.: "Hydrogen Embrittlement of Stainless Steel," Trans. AIME, 242, pp. 2199, 1968.
6. Hofmann, V. W., and W. Rauls: "Ductility of Steel Under the Influence of External High-Pressure Hydrogen," Welding Journal, May 1965, pp. 225s-230s.
7. Cavett, R. H., and H. C. Van Ness: "Embrittlement of Steel by High Pressure Hydrogen Gas," Welding Journal, July 1963, pp. 316s-319s.
8. Vennett, R. M., and G. S. Ansell: "The Effect of High-Pressure Hydrogen Upon the Tensile Properties and Fracture Behavior of 304L Stainless Steel," Trans. ASM, 60, pp. 242, 1967.
9. Lorenz, P. M.: Effect of Pressurized Hydrogen Upon Inconel 718 and 2219 Aluminum, paper presented at WESTEC Conference, Los Angeles, California, March 1969, ASM Report No. W9-13.2, ASM Report System, Metals Park, Ohio.

10. Walter, R. J., and W. T. Chandler: "Effect of Hydrogen Environments on Inconel 718 and Ti-6Al-4V (STA)," paper presented at AIME Meeting, Las Vegas, Nevada, 11-14 May 1970.
11. Vennett, R. M., and G. S. Ansell: "A Study of Gaseous Hydrogen Damage in Certain FCC Metals," Trans. Quart. ASM, 62, pp 1007, 1969.
12. Walter, R. J., R. P. Jewett, and W. T. Chandler: "On the Mechanism of Hydrogen Environment Embrittlement of Iron and Nickel-Base Alloys," Materials Science and Engineering, Vol. 5, 99, February 1969.
13. Peterson, R. E.: Stress Concentration Design Factors, John Wiley & Sons, New York, 1953.
14. "Standard Method of Test for Plane-Strain Fracture Toughness of Metallic Materials," ASTM Standards, E399-72, 1972, pp 955-974.
15. Vroman, G. A., J. Halchak, and M. Cohn: Progress Report ITP Fracture Mechanics Project Task V Data Compilation Criteria and Applications, Publication 572-K-1 Rocketdyne, a Division of Rockwell International, Canoga Park, California, January 1972.
16. Novak, S. R., and S. T. Rolfe: "Modified WOL Specimen for K_{ISCC} Environmental Testing," Journal of Materials, 4, No. 3, 1969, 701.
17. "Tentative Method of Test for Plane-Strain Fracture Toughness of Metallic Materials," ASTM Standards, E399-70T, 1971, pp. 919-935.
18. Mostovoy, S., P. P. Crosley, and E. J. Ripling: "Use of Crack-Line Loaded Specimens for Measuring Plane-Strain Fracture Toughness," J. of Materials, Vol. 2, No. 3, pp. 661, (1967).
19. Demonet, R. J.: Compliance Calibration of TDCB Specimens for Rocketdyne, Laboratory Test Report LR 9745-4045 on IDWA R7600 Space Division, Rockwell International, October 1972.
20. Bixler, W. D.: Flaw Growth of Inconel 718 and 5Al-2.5Sn (ELI) Titanium in a High-Purity Gaseous Hydrogen Environment, Boeing Document D180-10142-1, prepared for Aerojet General Corporation, Sacramento, California, Contract L-80076, The Boeing Company, Seattle, Washington, September 1970.

21. Harris, J. A., and M. C. VanWanderham: Properties of Materials in High Pressure Hydrogen at Cryogenic, Room, and Elevated Temperatures, Annual Report PWA FR-4566, Contract NAS8-2619, Pratt & Whitney Aircraft, West Palm Beach, Florida, 30 June 1971.
22. Eiselstein, H. L.: "Metallurgy of a Columbium-Hardened Nickel-Chromium-Iron Alloy," from Advances in the Technology of Stainless Steels and Related Alloys, Special Technical Publication No. 369, American Society for Testing Materials, 1965.
23. Muzyka, D. R., and G. N. Maniar: "Effects of Solution Treating Temperature and Microstructure on the Properties of Hot Rolled 718 Alloy," Metals Engineering Quarterly, 9, No. 4, November 1969, 23.
24. Wei, R. P., K. Klier, G. W. Simmons, and E. Chornet: Hydrogen Adsorption and Diffusion, and Subcritical-Crack Growth in High-Strength Steels and Nickel Base Alloys, Annual Report on NASA Contract NGR 39-007-067 Lehigh University IFSM-72-32.
25. Wei, R. P., and J. D. Landes: "Correlation Between Sustained-Load and Fatigue Crack Growth in High-Strength Steels," Materials Research and Standards, MTRSA, Vol. 9, No. 7, 1966, pp. 25.
26. Gallagher, J. P.: "Corrosion Fatigue Crack Growth Rate Behavior Above and Below K_{ISCC} in Steels," Journal of Materials, JMLSA, Vol. 6, No. 4, Dec. 1971, pp. 941-964.
27. Nelson, H. G., A. S. Tetelman, and D. P. Williams: "The Kinetic Aspects of Corrosion Fatigue in a Gaseous Hydrogen Environment," Corrosion Fatigue, pp. 359-365, 1972.
28. Walter, R. J., and W. T. Chandler: "Influence of Hydrogen Pressure and Notch Severity on Hydrogen-Environment Embrittlement at Ambient Temperature," Materials Science and Engineering, Vol. 8 (1971), 90-97.
29. Beck, O., A. E. Smith, and A. Wheeler: Proc. Roy Soc., A177, 1940, 62.
30. Porter, A. S., and F. C. Tompkins: Proc. Roy Soc., A217, 1953, 529.

31. Smith, P.: Hydrogen in Metals, the University of Chicago Press, Chicago, Illinois, 1948.
32. Nelson, H. G., and D. P. Williams: Quantitative Observations of Hydrogen-Induced, Slow Crack Growth in a Low Alloy Steel, NASA Technical Memorandum NASA TM X-62,253 Ames Research Center, NASA Moffett Field, California 94035, March 1973.

APPENDIX A

MEASUREMENT UNITS AND CONVERSION TO INTERNATIONAL SYSTEM OF UNITS (SI)

The following are the units and conversions used for obtaining and reporting the data.

Quantity	Units in Which Measurements Made	SI Base Units	SI Symbol	To Convert to SI Units From Units in Which Measurements Were Made, multiply by
Temperature	degree Fahrenheit	degree Kelvin	°K	$^{\circ}\text{K} = \frac{^{\circ}\text{F} + 459.67}{1.8}$
Length	inch	meter	m	2.54×10^{-2}
Force	pound	newton	N	4.4482
Pressure	psi	--	N/m^2	6.8948×10^3
Stress Intensity	ksi $\sqrt{\text{in.}}$	--	$\text{N/m}^2 \sqrt{\text{m}}$	1.09885×10^6
Velocity	in./min	--	m/s	4.23×10^{-4}

SI PREFIXES USED

<u>Multiplication Factor</u>	<u>Prefix</u>	<u>SI Symbol</u>
10^6	mega	M
10^3	kilo	k
10^{-3}	milli	m
10^{-6}	micro	μ
10^{-9}	nano	n

APPENDIX B

PHASE I DATA

The following tables contain the data for the individual tensile tests performed under Phase I, Tensile Properties of Alloys In Hydrogen Environments.

TABLE B-1. TENSILE PROPERTIES OF INCONEL 625 IN VARIOUS ENVIRONMENTS

Specimen		Environment						Test Results							
		No.	Type	Stress Conc. Factor	Type	Pressure		Temperature		Strength		Reduction of Area %	Elongation %		
						MN 2 m	psig	K	F	Yield MN 2 m	ksi			Ultimate MN 2 m	ksi
I-1	UN	-	Air	0	0	295	70	660	96	1006	146	-	56	45	
I-2	↓	-	Air	0	0	↓	↓	630	91	979	142	-	51	54	
I-11	↓	-	Helium	34.5	5000	↓	↓	620	90	979	142	-	51	56	
I-12	↓	-	Helium	↓	↓	↓	↓	650	94	1006	146	-	49	54	
I-3	↓	-	Hydrogen	↓	↓	↓	↓	590	86	869	126	0.88	18	21	
I-4	↓	-	Hydrogen	↓	↓	↓	↓	640	93	917	133	0.92	21	19	
I-5	UN	-	Hydrogen	↓	↓	↓	↓	570	82	882	128	0.89	16	19	
I-21	N	8.7	Helium	↓	↓	↓	↓	-	-	1358	197	-	8.9	-	
I-22	↓	8.7	Helium	↓	↓	↓	↓	-	-	1510	219	-	9.8	-	
I-13	↓	8.9	Hydrogen	↓	↓	↓	↓	-	-	1110	161	0.77	3.9	-	
I-14	↓	8.9	Hydrogen	↓	↓	↓	↓	-	-	1062	154	0.74	5.0	-	
I-15	N	8.7	Hydrogen	↓	↓	↓	↓	-	-	1103	160	0.77	5.0	-	
I-6	UN	-	Helium	↓	↓	↓	↓	724	105	1145	166	-	52	45	
I-7	↓	-	Helium	↓	↓	↓	↓	696	101	1117	162	-	51	44	
I-8	↓	-	Hydrogen	↓	↓	↓	↓	703	102	1117	162	-	48	40	
I-9	↓	-	Hydrogen	↓	↓	↓	↓	660	95	1048	152	-	47	42	
I-10	UN	-	Hydrogen	↓	↓	↓	↓	731	106	1186	172	-	49	48	
I-16	N	8.7	Helium	↓	↓	↓	↓	-	-	1496	217	-	8.0	-	
I-17	↓	8.9	Helium	↓	↓	↓	↓	-	-	1420	206	-	8.2	-	
I-18	↓	8.9	Hydrogen	↓	↓	↓	↓	-	-	1572	228	-	7.4	-	
I-19	↓	8.9	Hydrogen	↓	↓	↓	↓	-	-	1482	215	-	6.7	-	
I-20	N	8.9	Hydrogen	↓	↓	↓	↓	-	-	1510	219	-	6.5	-	

TABLE B-2. TENSILE PROPERTIES OF AISI TYPE 321 STAINLESS STEEL
IN VARIOUS ENVIRONMENTS

Specimen			Environment					Test Results					
No.	Type	Stress Conc. Factor	Type	Pressure		Temperature		Yield	Strength		Strength Ratio, H ₂ /He	Reduction of Area, %	Elongation, %
				MN $\frac{Z}{m}$	psig	K	F		MN $\frac{Z}{m}$	ksi			
S-1	UN	-	Air	0	0	295	70	220	600	32	-	71	77
S-2	↓	-	Air	0	0	↓	↓	210	600	31	-	70	77
S-11	↓	-	Helium	34.5	5000	↓	↓	190	590	28	-	65	62
S-12	↓	-	Helium	↓	↓	↓	↓	200	570	30	-	67	64
S-4	↓	-	Hydrogen	↓	↓	↓	↓	240	590	36	-	59	63
S-6	UN	-	Hydrogen	↓	↓	↓	↓	260	590	37	-	61	64
S-21	N	8.4	Helium	↓	↓	↓	↓	-	765	111	-	6.3	-
S-22	↓	8.7	Helium	↓	↓	↓	↓	-	793	115	-	6.5	-
S-13*	↓	8.7	Hydrogen	↓	↓	↓	↓	-	696	101	0.89	1.2	-
S-14**	↓	8.7	Hydrogen	↓	↓	↓	↓	-	680	98	0.87	2.0	-
S-15	N	8.9	Hydrogen	↓	↓	295	70	-	670	97	0.86	3.6	-
S-25	UN	-	Helium	↓	↓	144	-200	-	827	120	-	67	45
S-29	↓	-	Helium	↓	↓	↓	↓	-	882	128	-	66	51
S-26	↓	-	Hydrogen	↓	↓	↓	↓	-	779	113	-	64	38
S-27***	↓	-	Hydrogen	↓	↓	↓	↓	-	814	118	-	53	39
S-28	UN	-	Hydrogen	↓	↓	↓	↓	-	924	134	-	51	51
S-16	N	8.5	Helium	↓	↓	↓	↓	-	979	142	-	14	-
S-17	↓	8.7	Helium	↓	↓	↓	↓	-	986	143	-	10	-
S-18	↓	8.7	Hydrogen	↓	↓	↓	↓	-	1000	145	-	9.6	-
S-20	N	8.7	Hydrogen	↓	↓	144	-200	-	972	141	-	14	-

*Specimen bent and straightened prior to testing.

**34.5 MN/mm² (5000 psi) hydrogen was established during test, but prior to plastic deformation.

***Leakage occurred near end of test and the final test temperature was 223 K (-50 F)

TABLE B-3. TENSILE PROPERTIES OF Ti-5Al-2.5Sn ELI IN VARIOUS ENVIRONMENTS

Specimen			Environment				Test Results									
No.	Type	Stress Conc. Factor	Type	Pressure		Temp.		Yield			Ultimate		Strength Ratio, H_u/H_e	Reduction of Area, %	Ductility	Elongation, %
				$\frac{MN}{in^2}$	psig	K	F	$\frac{MN}{in^2}$	ksi	$\frac{MN}{in^2}$	ksi					
T-1	UN	-	Air	0	0	295	70	786	114	820	119	-	30	17		
T-2	UN	-	Air	0	0	295	70	786	114	820	119	-	32	19		
T-6	UN	-	Helium	34.5	5000	144	-200	-	-	1048	152	-	26	11		
T-7	UN	-	Helium	-	5000	-	-200	-	-	1027	149	-	26	16		
T-3	UN	-	Hydrogen	-	5000	-	-200	660	95	1041	151	-	33	10		
T-4	UN	-	Hydrogen	-	5000	-	-200	800	116	1048	152	-	29	10		
T-5	UN	-	Hydrogen	-	5000	-	-200	765	111	993	144	-	28	8		
T-8	N	8.9	Helium	-	5000	-	-200	-	-	1586	230	-	1.6	-		
T-9	N	8.7	Helium	-	5000	-	-200	-	-	1551	225	-	1.7	-		
T-10	N	8.9	Hydrogen	-	5000	-	-200	-	-	1572	228	-	1.4	-		
T-11	N	8.7	Hydrogen	-	5000	-	-200	-	-	1572	228	-	1.5	-		
T-12	N	8.7	Hydrogen	34.5	5000	144	-200	-	-	1558	226	-	0.9	-		

TABLE B-4. TENSILE PROPERTIES OF OFHC COPPER IN VARIOUS ENVIRONMENTS

Specimen			Environment				Test Results							
No.	Type	Stress Conc. Factor	Type	Pressure		Temp.		Yield		Strength		Reduction of Area, %	Ductility	Elongation, %
				$\frac{\text{MN}}{\text{m}^2}$	psig	K	F	$\frac{\text{MN}}{\text{m}^2}$	ksi	$\frac{\text{MN}}{\text{m}^2}$	ksi			
C-1	UN	-	Air	0	0	295	70	100	15	190	28	84		61
C-2	UN	-	Air	0	0			120	18	190	28	83		53
C-11	UN	-	Helium	34.5	5000			75	11	190	28	81		62
C-12	UN	-	Helium		5000			83	12	185	27	88		63
C-3	UN	-	Hydrogen		5000			76	11	185	27	86		62
C-4	UN	-	Hydrogen		5000			76	11	185	27	83		65
C-5	UN	-	Hydrogen		5000			69	10	190	26	84		68
C-21	N	8.7	Helium		5000				-	300	44	25		-
C-22	N	8.8	Helium		5000				-	280	41	21		-
C-13	N	8.7	Hydrogen		5000				-	275	40	24		-
C-14	N	8.8	Hydrogen		5000				-	295	43	26		-
C-15	N	8.7	Hydrogen		5000				-	300	44	25		-
C-19	N	8.7	Helium		5000	144	-200		-	275	40	30		-
C-20	N	8.8	Helium		5000		-200		-	280	41	28		-
C-16	N	8.7	Hydrogen		5000		-200		-	280	41	30		-
C-17	N	8.6	Hydrogen		5000		-200		-	320	46	23		-
C-18	N	8.7	Hydrogen	34.5	5000	144	-200		-	310	45	20		-

APPENDIX C

PHASE IV DATA TABULATIONS

The following tables contain the data for the individual tests performed under Phase IV, Variation of Hydrogen-Environment Embrittlement With Material Condition For Inconel 718.

TABLE C-1. ROOM TEMPERATURE TENSILE PROPERTIES OF INCONEL 718
SPECIMENS FABRICATED FROM THE ROLLED BAR SUPPLIED BY ALLVAK

Heat Treatment	Specimen			Environment			Test Results						
							Strength			Ductility			
No.	Type	Stress Conc. Factor	Type	Pressure		Yield		Ultimate		Strength Ratio H ₂ /He	Reduction of Area	Percent Elongation	
				MN/m ²	psig	MN/m ²	ksi	MN/m ²	ksi				
A	IA-1	UN	--	Air	0	0	1110	161	1386	201	--	34	23
	IA-2	UN	--	Air	0	0	1140	165	1400	203	--	36	22
	IA-6	N	8.7	He	34.5	5000		--	1958	284	--	2.8	--
	IA-7	N	8.7	He		5000		--	1937	281	--	2.9	--
	IA-3	N	8.9	H ₂		5000		--	1034	150	0.53	0.8	--
C	IA-4	N	8.9	H ₂		5000		--	779	113	0.40	0.5	--
	IA-5	N	8.5	H ₂		5000		--	1323	192	0.68	1.5	--
	IB-1	UN	--	Air	0	0	1100	160	1344	195	--	36	25
	IB-2	UN	--	Air	0	0	1110	161	1344	195	--	37	26
	IB-6	N	8.5	He	34.5	5000		--	2220	322	--	4.6	--
B	IB-7	N	8.9	He		5000		--	2210	321	--	5.3	--
	IB-3	N	8.2	H ₂		5000		--	1572	228	0.71	1.9	--
	IB-4	N	8.7	H ₂		5000		--	1572	228	0.71	2.1	--
	IB-5	N	8.7	H ₂		5000		--	1610	234	0.73	1.1	--
	IC-1	UN	--	Air	0	0	876	127	1254	182	--	33	24
	IC-2	UN	--	Air	0	0	876	127	1254	182	--	31	24
	IC-6	N	8.9	He	34.5	5000		--	1689	245	--	2.9	--
	IC-7	N	8.7	He		5000		--	1613	234	--	2.9	--
	IC-3	N	8.7	H ₂		5000		--	1144	166	0.69	0.9	--
	IC-4	N	8.5	H ₂		5000		--	1207	175	0.73	1.3	--
	IC-5	N	8.9	H ₂		5000		--	1131	164	0.68	3.3	--

TABLE C-2. ROOM TEMPERATURE TENSILE PROPERTIES OF INCONEL 718
SPECIMENS FABRICATED FROM THE FORGING SUPPLIED BY
CARLTON FORGE, MILL SUPPLIER: SPECIAL METALS

Heat Treatment	Specimen		Environment				Test Results						
			Type	Pressure		Yield	Strength		Ductility				
				Stress Conc. Factor	MN/m ²		psig	MN/m ²			ksi		
												Type	MN/m ²
No.	Type	Stress Conc. Factor	Type	MN/m ²	psig	MN/m ²	ksi	Ultimate	Strength Ratio H ₂ /He	Percent Reduction of Area	Percent Elongation		
A	IG-1	UN	--	Air	0	0	1062	154	1372	199	--	29	22
	IG-2	UN	--	Air	0	0	1131	164	1358	197	--	32	21
	IG-6	N	8.7	He	34.5	5000	--	--	2020	293	--	2.4	--
	IG-7	N	8.5	He	↓	5000	--	--	1972	283	--	3.5	--
	IG-3	N	8.3	H ₂	↓	5000	--	--	1241	180	0.62	1.3	--
	IG-4	N	8.9	H ₂	↓	5000	--	--	1096	159	0.55	0.9	--
	IG-5	N	8.3	H ₂	↓	5000	--	--	1186	172	0.59	1.1	--
C	IH-1	UN	--	Air	0	0	1172	170	1379	200	--	42	26
	IH-2	UN	--	Air	0	0	1158	168	1351	196	--	39	26
	IH-6	N	8.0	He	34.5	5000	--	--	2344	340	--	3.0	--
	IH-7	N	8.3	He	↓	5000	--	--	2330	338	--	6.2	--
	IH-3	N	8.9	H ₂	↓	5000	--	--	1724	250	0.74	1.3	--
	IH-4	N	8.7	H ₂	↓	5000	--	--	1786	259	0.76	2.2	--
	IH-5	N	8.3	H ₂	↓	5000	--	--	1827	265	0.78	2.0	--
B	II-1	UN	--	Air	0	0	917	133	1262	183	--	35	24
	II-2	UN	--	Air	0	0	793	115	1193	173	--	34	26
	II-6	N	8.7	He	34.5	5000	--	--	1710	248	--	1.9	--
	II-7	N	8.5	He	↓	5000	--	--	1779	258	--	2.5	--
	II-3	N	8.8	H ₂	↓	5000	--	--	1000	145	0.57	1.3	--
	II-4	N	8.5	H ₂	↓	5000	--	--	938	136	0.54	1.0	--
	II-5	N	8.7	H ₂	↓	5000	--	--	1034	150	0.59	1.2	--

TABLE C-3. ROOM TEMPERATURE TENSILE PROPERTIES OF INCONEL 718

SPECIMENS FABRICATED FROM THE PLATE

SUPPLIED BY STELLITE DIV., CABOT CORP.

Heat Treatment	Specimen			Environment			Test Results						
							Strength				Ductility		
							Yield	Ultimate		Strength Ratio H_2/He			Percent Reduction of Area
	Type	MN/m^2	psig	MN/m^2	ksi	MN/m^2		ksi					
A	ID-1	UN	--	Air	0	0	1103	160	1420	206	--	36	22
	ID-2	UN	--	Air	0	0	1089	158	1407	204	--	36	23
	ID-6	N	8.0	He	34.5	5000		--	1910	277	--	2.0	--
	ID-7	N	8.9	He		5000		--	2041	296	--	4.0	--
	ID-3	N	8.7	H ₂		5000		--	1772	257	0.89	2.4	--
	ID-4	N	8.4	H ₂		5000		--	1606	233	0.81	2.0	--
	ID-5	N	8.3	H ₂		5000		--	1717	249	0.87	1.7	--
C	IE-1	UN	--	Air	0	0	1124	163	1407	204	--	37	25
	IE-2	UN	--	Air	0	0	1172	170	1400	203	--	39	24
	IE-6	N	8.7	He	34.5	5000		--	2199	319	--	3.6	--
	IE-7	N	8.7	He		5000		--	2213	321	--	3.8	--
	IE-5	N	8.7	H ₂		5000		--	1710	248	0.78	2.9	--
	IE-3	N	8.3	H ₂		5000		--	1696	246	0.77	2.1	--
	IE-4	N	8.5	H ₂		5000		--	1710	248	0.78	2.0	--
B	IF-1	UN	--	Air	0	0	917	133	1296	188	--	36	23
	IF-2	UN	--	Air	0	0	917	133	1303	189	--	33	25
	IF-6	N	8.7	He	34.5	5000		--	1710	248	--	3.0	--
	IF-7	N	8.1	He		5000		--	1751	254	--	2.3	--
	IF-3	N	8.9	H ₂		5000		--	1489	216	0.86	2.0	--
	IF-4	N	8.1	H ₂		5000		--	1510	219	0.87	1.5	--
	IF-5	N	8.3	H ₂		5000		--	1489	216	0.86	2.9	--

TABLE C-4. ROOM TEMPERATURE TENSILE PROPERTIES OF WELDED
SPECIMENS OF INCONEL 718 PLATE, IN THE A
HEAT TREATMENT CONDITION

Specimen			Environment			Stress Conc. Factor	Test Results						
							Strength			Ductility			
No.	Type	Type	Pressure MN/m ²	Pressure psig	Yield MN/m ²	Yield ksi	Ultimate MN/m ²	Ultimate ksi	Strength Ratio, H ₂ /He	Percent Reduction of Area	Percent Elongation		
IJW-11	UN	Weld	Air	0	0	--	1062	154	1276	185	--	1.5	6.3
IJW-12	UN	Weld	Air	0	0	--	1007	146	1110	161	--	9.2	3.4
IJW-1	N	Weld	He	34.5	5000	8.7		--	1365	198	--	1.7	--
IJW-2	N	Weld	He		5000	8.7		--	1469	213	--	1.0	--
IJW-3	N	Weld	H ₂		5000	8.7		--	1151	167	0.81	1.1	--
IJW-4	N	Weld	H ₂		5000	8.9		--	1138	165	0.80	0.8	--
IJW-5	N	Weld	H ₂		5000	8.9		--	1096	159	0.76	1.1	--
IJU-6	N	HAZ	He		5000	8.3		--	1993	289	--	2.6	--
IJW-10	N	HAZ	He		5000	8.1		--	1669	242	--	0.9	--
IJW-7	N	HAZ	H ₂		5000	8.5		--	1131	164	0.62	1.1	--
IJW-8	N	HAZ	H ₂		5000	8.5		--	1213	176	0.66	0.4	--
IJW-9	N	HAZ	H ₂		5000	8.3		--	1131	164	0.62	0.7	--

TABLE C-5. ROOM TEMPERATURE TENSILE PROPERTIES OF WELDED SPECIMENS OF
INCONEL 718 IN THE B HEAT TREATMENT CONDITION

Specimen		Environment		Stress Con. Factor	Test Results							
					Strength				Ductility			
					Type	Pressure MN/m ²	Pressure psig	Yield MN/m ² ksi	Ultimate MN/m ² ksi	Strength Ratio, H ₂ /He	Percent Reduction of Area	Percent Elongation
No.	Type											
ILN-11	UN	Weld	Air	0	0	876	127	1131	164	--	12	6.2
ILN-12	UN	Weld	Air	0	0	862	125	1158	168	--	14	8.5
ILN-1	N	Weld	He	5000	8.9		--	1282	186	--	2.1	--
ILN-2	N	Weld	He	5000	8.7		--	1200	174	--	2.0	--
ILN-3*	N	Weld	H ₂	5000	8.7		--		--	--	--	--
ILN-4	N	Weld	H ₂	5000	8.9		--	1000	145	0.81	0.8	--
ILN-5	N	Weld	H ₂	5000	8.7		--	931	135	0.75	0.4	--
ILN-6	N	HAZ	He	5000	8.7		--	1441	209	--	1.3	--
ILN-7	N	HAZ	He	5000	8.3		--	1344	195	--	1.5	--
ILN-8	N	HAZ	H ₂	5000	8.7		--	1041	151	0.75	2.0	--
ILN-9	N	HAZ	H ₂	5000	8.5		--	1027	149	0.74	0.5	--
ILN-10	N	HAZ	H ₂	5000	8.5		--	1076	156	0.77	0.9	--

*Failed during pressurization.

TABLE C-6. ROOM TEMPERATURE TENSILE PROPERTIES OF WELDED SPECIMENS OF
INCONEL 718 IN THE C HEAT TREATMENT CONDITION

Specimen			Environment		Stress Conc. Factor	Test Results							
						Strength				Ductility			
						Yield		Ultimate				Strength Ratio, H ₂ /He	Percent Reduction of Area
No.	Type	Type	MN/m ²	psig	MN/m ²	ksi	MN/m ²	ksi					
IKM-11	UN	Weld	Air	0	0	--	1145	166	1372	199	--	19	11
IKM-12	UN	Weld	Air	0	0	--	1131	164	1365	198	--	26	15
IKM-1	N	Weld	He	34.5	5000	8.7		--	1806	262	--	2.6	--
IKM-4	N	Weld	He		5000	8.7		--	1889	274	--	2.5	--
IKM-2	N	Weld	H ₂		5000	8.7		--	1020	148	0.55	0.8	--
IKM-3	N	Weld	H ₂		5000	8.7		--	1207	175	0.65	0.9	--
IKM-5	N	Weld	H ₂		5000	8.9		--	903	131	0.49	0.7	--
IKM-6	N	HAZ	He		5000	8.1		--	2137	310	--	5.0	--
IKM-7	N	HAZ	He		5000	8.9		--	1324	292	--	2.6	--
IKM-8	N	HAZ	H ₂		5000	8.7		--	1634	237	0.79	0.4	--
IKM-9	N	HAZ	H ₂		5000	8.7		--	1248	181	0.60	0.8	--
IKM-10	N	HAZ	H ₂		5000	8.7		--	1600	232	0.77	2.1	--

TABLE C-7. ROOM TEMPERATURE TENSILE PROPERTIES OF INCONEL 718
IN THE E HEAT TREATMENT CONDITION

Material	Specimen			Environment		Test Results							
	No.	Type	Stress Concentration Factor	Type	Pressure MN/m ²	Yield		Strength		Reduction of Area, percent	Ductility	Elongation percent	
						ksi	MN/m ²	ksi	Ultimate ksi				
													ksi
0.031 x 0.07 m (1-1/4 x 2-3/4 in.) Rolled Bar	IM-6	UN	-	Air	0	1140	165	1380	200	-	42	22	
	IM-7	UN	-	Air	0	1170	169	1370	199	-	41	24	
	IM-4	N	8.7	Helium	34.5	-	-	2200	319	-	4.2	-	
	IM-5	N	8.7	Helium	34.5	-	-	2190	318	-	3.7	-	
	IM-1	N	8.7	Hydrogen	34.5	-	-	1580	229	0.72	2.1	-	
	IM-2	N	8.7	Hydrogen	34.5	-	-	1600	232	0.73	2.0	-	
	IM-3	N	8.9	Hydrogen	34.5	-	-	1490	217	0.68	1.6	-	
	0.038 m (1-1/2 in.) Forging	IP-6	UN	-	Air	0	1170	169	1390	202	-	42	22
		IP-7	UN	-	Air	0	1170	169	1390	201	-	34	21
		IP-4	N	8.5	Helium	34.5	-	-	2240	325	-	4.0	-
		IP-5	N	8.5	Helium	34.5	-	-	2200	319	-	3.0	-
		IP-1	N	8.9	Hydrogen	34.5	-	-	1610	233	0.72	1.9	-
		IP-2	N	8.5	Hydrogen	34.5	-	-	1630	236	0.73	1.3	-
		IP-3	N	8.7	Hydrogen	34.5	-	-	1430	297	0.64	0.9	-
	0.013 m (1/2 in.) Plate	IO-6	UN	-	Air	0	1180	171	1430	207	-	39	22
IO-7		UN	-	Air	0	1160	168	1420	206	-	40	22	
IO-4		N	8.3	Helium	34.5	-	-	2200	319	-	4.7	-	
IO-5		N	8.7	Helium	34.5	-	-	2200	319	-	3.6	-	
IO-1		N	8.7	Hydrogen	34.5	-	-	1620	235	0.74	3.4	-	
IO-2		N	8.5	Hydrogen	34.5	-	-	1670	242	0.76	2.0	-	
IO-3		N	8.3	Hydrogen	34.5	-	-	1660	240	0.75	2.6	-	

TABLE C-8. ROOM TEMPERATURE TENSILE PROPERTIES OF NOTCHED INCONEL 718
SPECIMENS FABRICATED FROM ROLLED BAR SOLUTION ANNEALED AT
1297 K (1875 F), 600 SECONDS (D HEAT TREATMENT) AND
TESTED IN 34.5 MN/m² (5000 psi) HYDROGEN AND
HELIUM ENVIRONMENTS

Specimen		Environment	Strength			Ductility
No.	Stress Concentration Factor		Notch Strength		Strength Ratio, H ₂ /He	Reduction of Area, percent
			MN/m ²	ksi		
IR-4	8.7	Helium	1130	164	--	13.8
IR-5	8.9	Helium	1120	162	--	13.4
IR-1	8.7	Hydrogen	920	133	0.82	9.0
IR-2	8.7	Hydrogen	930	135	0.83	9.6
IR-3	8.7	Hydrogen	960	139	0.85	8.3